RMZ

MATERIALS and GEOENVIRONMENT

MATERIALI in GEOOKOLJE

RMZ – M&G, **Vol. 66**, No. 1
pp. 001–074 (2019)

Ljubljana, January 2019

RMZ – Materials and Geoenvironment
RMZ – Materiali in geookolje
ISSN 1408-7073

Old title/Star naslov
Mining and Metallurgy Quarterly/Rudarsko-metalurški zbornik
ISSN 0035-9645, 1952–1997

Published by/Izdajatelj
Faculty of Natural Sciences and Engineering, University of Ljubljana/
Naravoslovnotehniška fakulteta, Univerza v Ljubljani

Associated Publisher/Soizdajatelj
Institute for Mining, Geotechnology and Environment, Ljubljana/
Inštitut za rudarstvo, geotehnologijo in okolje
Velenje Coal Mine/Premogovnik Velenje
Slovenian Chamber of Engineers/Inženirska zbornica Slovenije

Editorial Office/Uredništvo
Technical editors/Tehnična urednika Teja Čeru and Jože Žarn
Secretary/Tajnica Nives Vukič

Editorial Address/Naslov uredništva
RMZ – Materials and Geoenvironment
Aškerčeva cesta 12, p. p. 312
1001 Ljubljana, Slovenija
Tel.: +386 (0)1 470 46 10
Fax.: +386 (0)1 470 45 60
E-mail: rmz-mg@ntf.uni-lj.si

Published/Izhajanje
4 issues per year/4 številke letno

Partly funded by Ministry of Education, Science and Sport of Republic of Slovenia./Pri financiranju revije sodeluje Ministrstvo za izobraževanje, znanost in šport Republike Slovenije.

Articles published in Journal "RMZ M&G" are indexed in international secondary periodicals and databases:/Članki, objavljeni v periodični publikaciji „RMZ M&G", so indeksirani v mednarodnih sekundarnih virih:
CA SEARCH® – Chemical Abstracts®, METADEX®, GeoRef.

Annual subscription for individuals in Slovenia: 20 EUR, for institutions: 30 EUR. Annual subscription for the rest of the world: 30 EUR, for institutions: 50 EUR/Letna naročnina za posameznike v Sloveniji: 20 EUR, za inštitucije: 30 EUR. Letna naročnina za tujino: 30 EUR, inštitucije: 50 EUR

Transaction account/Tekoči račun
Nova Ljubljanska banka, d. d., Ljubljana: UJP 01100-6030708186

VAT identification number/Davčna številka
24405388

Online Journal/Elektronska revija
www.rmz-mg.com
www.degruyter.com/view/j/rmzmag

Table of Contents

Kazalo

Historical Review

More than 90 years have passed since the University Ljubljana in Slovenia was founded in 1919. Technical fields were united in the School of Engineering that included the Geologic and Mining Division, while the Metallurgy Division was established only in 1939. Today, the Departments of Geology, Mining and Geotechnology, Materials and Metallurgy are all part of the Faculty of Natural Sciences and Engineering, University of Ljubljana.

Before World War II, the members of the Mining Section together with the Association of Yugoslav Mining and Metallurgy Engineers began to publish the summaries of their research and studies in their technical periodical Rudarski zbornik (Mining Proceedings). Three volumes of Rudarski zbornik (1937, 1938 and 1939) were published. The War interrupted the publication and it was not until 1952 that the first issue of the new journal Rudarsko-metalurški zbornik – RMZ (Mining and Metallurgy Quarterly) was published by the Division of Mining and Metallurgy, University of Ljubljana. Today, the journal is regularly published quarterly. RMZ – M&G is co-issued and co-financed by the Faculty of Natural Sciences and Engineering Ljubljana, the Institute for Mining, Geotechnology and Environment Ljubljana, and the Velenje Coal Mine. In addition, it is partly funded by the Ministry of Education, Science and Sport of Slovenia.

During the meeting of the Advisory and the Editorial Board on May 22, 1998, Rudarsko-metalurški zbornik was renamed into "RMZ – Materials and Geoenvironment (RMZ – Materiali in Geookolje)" or shortly RMZ – M&G. RMZ – M&G is managed by an advisory and international editorial board and is exchanged with other world-known periodicals. All the papers submitted to the RMZ – M&G undergoes the course of the peer-review process.

RMZ – M&G is the only scientific and professional periodical in Slovenia which has been published in the same form for 60 years. It incorporates the scientific and professional topics on geology, mining, geotechnology, materials and metallurgy. In the year 2013, the Editorial Board decided to modernize the journal's format.

A wide range of topics on geosciences are welcome to be published in the RMZ – Materials and Geoenvironment. Research results in geology, hydrogeology, mining, geotechnology, materials, metallurgy, natural and anthropogenic pollution of environment, biogeochemistry are the proposed fields of work which the journal will handle.

Editor-in-Chief

Zgodovinski pregled

Že več kot 90 let je minilo od ustanovitve Univerze v Ljubljani leta 1919. Tehnične stroke so se združile v Tehniški visoki šoli, ki sta jo sestavljala oddelka za geologijo in rudarstvo, medtem ko je bil oddelek za metalurgijo ustanovljen leta 1939. Danes oddelki za geologijo, rudarstvo in geotehnologijo ter materiale in metalurgijo delujejo v sklopu Naravoslovnotehniške fakultete Univerze v Ljubljani.

Pred 2. svetovno vojno so člani rudarske sekcije skupaj z Združenjem jugoslovanskih inženirjev rudarstva in metalurgije začeli izdajanje povzetkov njihovega raziskovalnega dela v Rudarskem zborniku. Izšli so trije letniki zbornika (1937, 1938 in 1939). Vojna je prekinila izdajanje zbornika vse do leta 1952, ko je izšel prvi letnik nove revije Rudarsko-metalurški zbornik – RMZ v izdaji odsekov za rudarstvo in metalurgijo Univerze v Ljubljani. Danes revija izhaja štirikrat letno. RMZ – M&G izdajajo in financirajo Naravoslovnotehniška fakulteta v Ljubljani, Inštitut za rudarstvo, geotehnologijo in okolje ter Premogovnik Velenje. Prav tako izdajo revije financira Ministrstvo za izobraževanje, znanost in šport.

Na seji izdajateljskega sveta in uredniškega odbora je bilo 22. maja 1998 sklenjeno, da se Rudarsko-metalurški zbornik preimenuje v RMZ – Materiali in geookolje (RMZ – Materials and Geoenvironment) ali skrajšano RMZ – M&G. Revijo RMZ – M&G upravljata izdajateljski svet in mednarodni uredniški odbor. Revija je vključena v mednarodno izmenjavo svetovno znanih publikacij. Vsi članki so podvrženi recenzijskemu postopku.

RMZ – M&G je edina strokovno-znanstvena revija v Sloveniji, ki izhaja v nespremenjeni obliki že 60 let. Združuje področja geologije, rudarstva, geotehnologije, materialov in metalurgije. Uredniški odbor je leta 2013 sklenil, da posodobi obliko revije.

Za objavo v reviji RMZ – Materiali in geookolje so dobrodošli tudi prispevki s širokega področja geoznanosti, kot so: geologija, hidrologija, rudarstvo, geotehnologija, materiali, metalurgija, onesnaževanje okolja in biokemija.

Glavni urednik

Original scientific paper

Received: Dec 25, 2018
Accepted: Jan 08, 2019
DOI: 10.2478/rmzmag-2018-0021

Geotechnical Terrain Models and Types of Instabilities in the Durmitor Flysch Complex

Geotehnični Terenski Modeli in Vrste Nestabilnosti v Durmitorskem Flišnem Kompleksu

Aleksandar Golijanin[1,*], Vladimir Malbašić[2]

[1] Market Surveillance Agency of BiH, Karađorđeva 8, Sarajevo, Bosnia and Herzegovina

[2] Faculty of Mining, Prijedor, University of Banja Luka, Street of Savo Kovačević, Bosnia and Herzegovina

* aleksandar.golijanin@annt.gov.ba

Abstract

The Durmitor flysch complex represents a specific formation both in lithological and engineering geological sense. In the engineering geological sense this lithological formation is characterized by anisotropic and heterogeneous geotechnical properties, which depend on the dominant members within each individual package, as well as their spatial position.The Durmitor flysch complex consists of five superposition bed packages, which are mutually substantially different in their lithological, hydrogeological and geotechnical properties. For the first time in geological literature, this paper distinguishes five types of terrain construction within the Durmitor flysch complex. Contemporary geodynamic processes and their character within the flysch formation are defined. Particular emphasis is put on landslides, which represent a contemporary geodynamic phenomenon with certain specificities.

Key words: durmitor flysch complex, geotechnical models

Povzetek

Durmitorski flišni kompleks predstavlja posebno formacijo v litološkem in tudi inženirsko-geološkem smislu. V inženirsko-geološkem smislu so značilne zanjo anizotropne in heterogene geotehnične lastnosti, ki so odvisne od prevladujočih členov v vsakem posameznem paketu in prav tako od njihove prostorske lege. Durmitorski flišni kompleks sestoji iz petih drug na drugega naloženih paketov plasti, ki se medsebojno bistveno razlikujejo v litoloških, hidrogeoloških in geotehnični lastnostih. Prvič v geološki literaturi ta članek obravnava pet tipov terenske gradnje v durmitorskem flišnem kompleksu. Opredeljuje sodobne geodinamične procese v flišni formaciji in njihove posebnosti. Posebno pozornost posveča plazovom, ki predstavljajo sodobni geodinamski pojav z nekaterimi posebnimi lastnostmi.

Ključne besede: durmitorski flišni kompleks, geotehnični modeli

Introduction

This paper presents the categorization of terrain construction in the geotechnical sense with the aim of easier defining the conditions for safe and efficient exploitation of road infrastructure. In the paper is not performed only the characterization of the rock complex at a given time was carried out, as is the case in the previous practice in the world [1–3]. The categorization of the construction of the terrain was carried out on a specific case and a location within the very specific materials of the Durmitor flysch, whereby field geotechnical research and analysis of the existing literature data, provided sufficient material for this approach and categorization of the terrain construction.

The term "Durmitor flysch" was first introduced in geological literature in 1948 by Zarija Bešić [4]. This term implies a powerful geological formation, formed at the turn of the Upper Cretaceous to Palaeogene. It spreads from the North Albanian Plateau and the so-called Cukali zone in the south, across the central part of Montenegro and the northeast Herzegovina all the way to the central Bosnia and Mount Vlašić (Figure 1). It was named after the prominent and spacious development of the southwest slopes of Mount Durmitor, while the best gradation of this formation, as well as all the contemporary geodynamic processes, can be most clearly traced in the area of Čemerno mountain pass in the northeast Herzegovina. The subject of this paper will be precisely the specificities of that part of the Durmitor flysch complex.

Flysch sediments are characterized by complex lithological composition, i.e. they consist of: basal limestone breccias and conglomerates, limestones, siltstones, marly limestones, claystones and marlstones of different thickness and spatial position, which are classified into five superposition packages in this area.

These rock masses are characterized by specific engineering geological properties, which are determined by the specific lithological composition. Therefore, this formation is characterized by heterogeneous and anisotropic geotechnical properties, which depend on predominant lithologic members in the complex, as well as spatial position of the bed packages.

The formation of these sediments is related to the Upper Cretaceous, i.e. the Senonian stage (), and is presented as such on the Basic geological map of SFRY, sheet Gacko [5], while the formation in the region of Montenegro is identified as the Upper Cretaceous-Paleogene (K_2,Pg). These lithologic members were deposited in special sedimentary conditions and are therefore found in form of the beds of various thicknesses. The beds of different lithological composition are "packed" in five superposition packages, in which the lithologic members rhythmically and intermittently alternate. The rhythms have different composition as well as spatial spreading, which is a consequence of geological composition of the watershed, climatic conditions that prevailed during the cycle of sedimentation, as well as post-genetic, primarily tectonic conditions that these terrains were exposed to.

The post-genetic tectonic activity caused folding and faulting of these sediments and intensified the process of thrusting of Triassic limestones over the flysch formation, which additionally complicates defining physical-mechanical parameters of these environments and defining engineering geological conditions for construction of both road infrastructure facilities and other construction objects. In this context, the issue of defining stability of the terrain, i.e. the occurrence and type of instabilities is very complex.

Specific climatic conditions that prevailed during the Pleistocene and the Quaternary in the observed area caused formation of numerous glaciers, the melting of which during interglacial periods resulted in extremely intense erosion. Typical glacial forms of relief were formed: cirques, waves, moraines. The activity of the erosional process continued afterwards, so that numerous river valleys were formed: Piva, Tara, Drina, Morača, Neretva, Sutjeska and others, with several levels of fluvioglacial terraces and the accompanying erosional forms of the relief. Sedimentary conditions, tectonic and erosional activities in this region caused, inter alia, formation of various terrain constructions [6]. Terrain construction represents a particular arrangement of natural environments which can be distinguished by various mechanical properties, but in terms of statics act as a whole. The final result of these activities

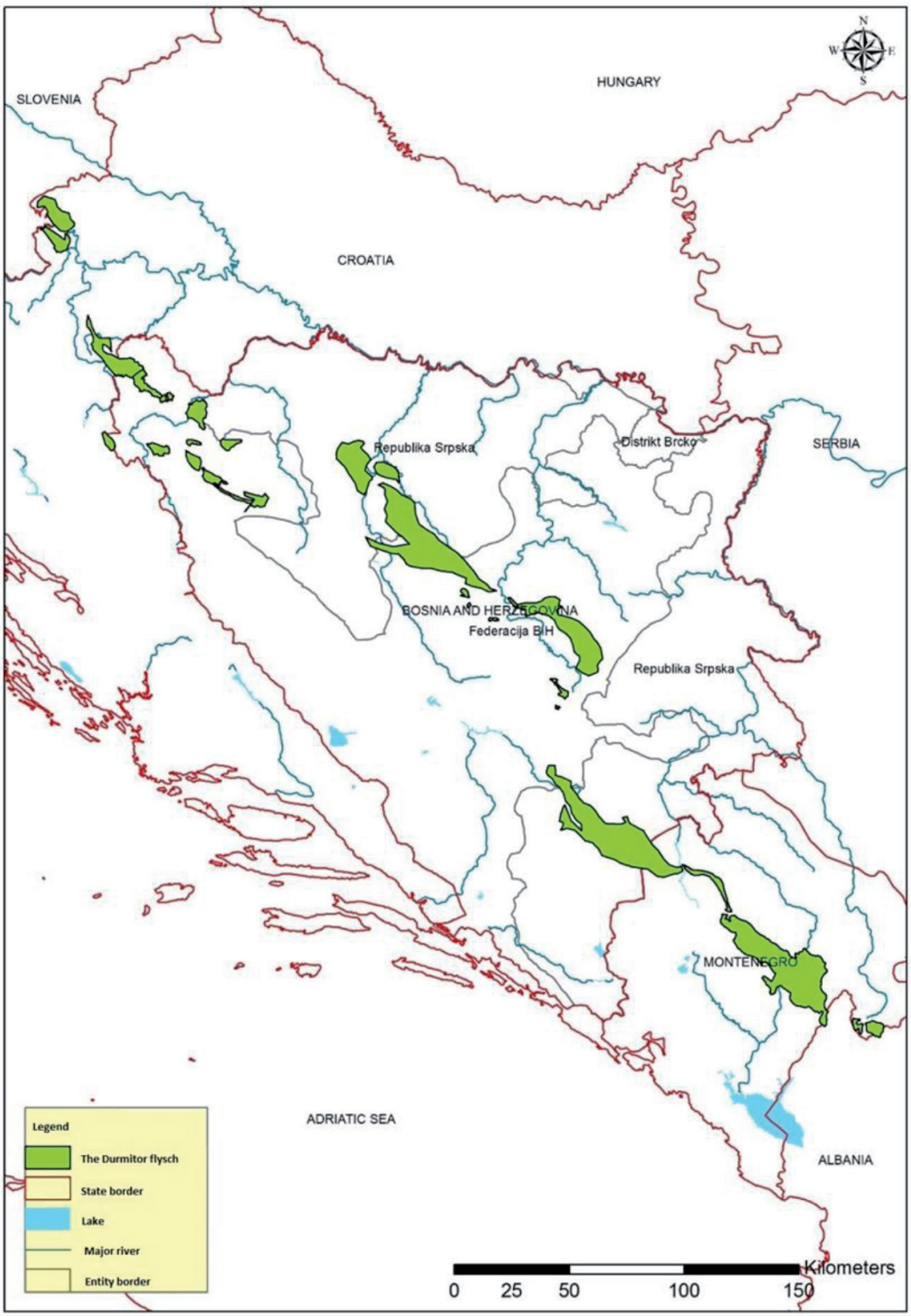

Figure 1: *The Durmitor flysch complex spreading.*

also caused the occurrence of various forms of instabilities [7]:

— In the surface areas of the terrain, landslides of the consequent type are predominantly present. The sliding surfaces are generally formed at the contact point of the surface decomposition crust and the bedrock.
— During the periods of intense precipitation (for example, the average annual precipitation in the area of Čemerno is 1650, and it often exceeds 2000 litre/m^2) mudslides are formed, as a specific form of instability in the deluvial slope zone.
— On the valley slopes, primarily depending on spatial position of the beds in the flysch packages, the conditions for formation of landslides are created, with the sliding surfaces predisposed by interlayer surfaces (consequent type of landslides according to Savarenski or lateral spread landslide according to Varnes).
— Instabilities in the form of rockfalls are usually the consequence of technogenic activities (construction of steep slopes during the construction of roads, but they also occur during the exploitation afterwards), while they are considerably less often the result of erosion (geological and natural processes).

In the report, special attention will be paid to the effect of the terrain construction types on the occurrence, types and basic characteristics of the terrain instabilities. This is very important, not only for engineering geological and geotechnical research for the purpose of remediation of instabilities, but also for the purpose of preventive action, i.e. the prevention of occurrence of instabilities during construction of various facilities.

Geological structure of the terrain

Lithological composition

The flysch complex was created in the conditions of interconnection of the land system and the presence of sedimentary basin. Namely, the surface streams and erosion of rock masses in the land zone transport the eroded material into the sedimentary basin. The amount and volume (granulometric composition) of the deposits are conditioned by the precipitation regime. This is one of the causes that contributed to the formation of lithologically heterogeneous rock masses and rhythmic alternation of breccias, conglomerates, limestone beds, siltstones, marly limestones, marlstones and claystones. Dimitrijević [8] considers that three facies can be distinguished in the Durmitor flysch complex: carbonate, siliciclastic and mixed facies. The siliciclastic facies is characteristic of the area covered by the sheet Gacko, BGM SFRY. When creating the Basic geological map of SFRY, sheet Gacko, Mirković, Kalezić, Pajović and Vujisić (1980) classified this lithological formation into five superposition packages (sub-stages) within the Upper Cretaceous Senonian Stage (K_2^3):

1. ***Basal limestone breccias and conglomerates*** ($^1K_2^3$) have the largest spread and thickness. Composition of breccias and conglomerates depends on the foundation over which they lie. Most often they are composed of pieces and pebbles of Lower Cretaceous limestone. Diameter of the pieces or fragments of limestone in breccias and conglomerates is up to 0.7 m. The binder is carbonate.
2. ***Layered breccias and limestones*** ($^2K_2^3$) are distinguished as the second package, mainly composed of carbonate sediments. Coarse-grained limestone conglomerates and breccias occur in the form of banks thick between 2 and 5 meters. The binder is marly and carbonate. In the geologic column, conglomerates turn into medium-grained, and these turn into fine-grained layered limestone breccias. Breccias are composed of pieces of limestone, chert and marlstone.
3. ***Breccias, limestones and marlstones*** ($^3K_2^3$) take up most of the space within this lithological formation. They occur in a wide belt in line with the Dinaric direction of spreading (northwest- southeast). Limestone breccias occur in the form of banks and beds. Their thickness varies from 0.5 to 10 meters. Sandy limestones with a thickness of layers varying from 0.25 to 0.5 meters lie over the breccias. In the geologic column, sandy limestones turn into sandy marlstones, and these turn into greyish-greento brown laminated marlstones.

4. ***Sandy-marly flysch series*** ($^4K_2^3$) is composed of microconglomerates, greywacke, siltstones and marlstones. This superposition package of the Durmitor flysch complex is characterized by very thin layers of individual components that intermittently and repeatedly alternate in the geologic column. They are characterized by prominent folds. The dimensions of the folds range in length from several centimetres (micro) to several hundreds of metres (macro). If the slope is composed of this package, landslides or mudslides are usually formed, i.e. the slopes should be treated as unstable or conditionally stable.
5. ***Breccias, limestones and marlstones*** ($^5K_2^3$) represent the fifth and the last package of the Durmitor flysch complex. It is mainly composed of carbonate sediments. Within this package, coarse-grained limestone conglomerates and breccias, limestone breccias, marly limestones and marlstones with chert nodules are present.

Types of instabilities, frequency of their occurrence, their dynamics and volume significantly depend on the slope structure (terrain construction) and these issues will be discussed in the chapter on the terrain constructions (Chapter 3).

Tectonic properties of the terrain

In the geological past, intense tectonic processes occurred in this area, which was primarily manifested through the process of thrusting of the Middle Triassic massive limestone (T_2^1) over the Durmitor flysch complex [5]. The angle of thrusting in the observed area is 30°–35°. The south-southwest side of the Durmitor flysch is erosionallydiscordant.

— Basal breccias and conglomerates ($^1K_2^3$ – package 1) are poorly stratified and have a general direction of decline towards the northeast.
— Breccias, limestones and marly limestones ($^2K_2^3$ – package 2) also have a general direction of decline towards the northeast. They are undisturbed, i.e. the folding process is not observed here, while the rupture forms occur as transverse and diagonal decametric faults.
— The package of layered stratified breccias, limestones and marlstones isfolded in numerous metric, decametric and hectometric, upright, inclined and overturned folds with a span from several metres to 500 meters. The folds are upright in one part, while they are inclined in the other part of the package. The axial surfaces are upright and inclined. The vergence is southwest and the vergence angle is up to 10°.
— Within the package of conglomerates, siltstones, marlstones and claystone ($^4K_2^3$) and the package oflayeredbreccias, limestones and marlstones ($^5K_2^3$), numerous metric and decametric, upright and inclined, overturned and recumbent folds developed. Their span ranges from 1 to about 10 metres. The terrain constructed from this package is mostly covered with vegetation and deluvial deposits so its development can be traced in the streambeds and the road cuts [9].

Hydrological and hydrogeological properties of the terrain

Hydrological properties

The area constructed from the Durmitor flysch complex in the observed part of the terrain abounds with a very high precipitation, as well as large oscillations in atmospheric temperatureduring the year. The amount of precipitation and temperature oscillations are the most important exogenous agents when it comes to shaping of the relief. Also, these agents significantly affect the occurrence of the terrain instabilities. As an illustration of the previous assertion, Table 1 shows the average precipitation during the year, measured at the rainfall monitoring station Čemerno, expressed in millimetres of deposited water.

Temperature oscillations are enormous both during the year and within a day. The lowest recorded temperature is about -40°C, while the highest is about 35°C. Such temperature range increases the intensity of the surface decomposition, i.e. the mechanical disintegration of the solid rock masses, which is very important in terms of the terrain stability.

Table 1: *Average monthly precipitation at the rainfall monitoring station Čemerno (according to HMIBiH)*

month	I	II	III	IV	V	VI	VII	VIII	IX	X	XI	XII	total per year
mm	125	130	160	170	130	100	70	70	125	180	220	170	1650

Hydrogeological properties

In hydrogeological terms, the Quaternary eluvial-deluvial deposits, degraded siltstones, claystones, sandstones and thin laminated marlstones in the periods of abundant precipitation constitute a water-saturated environment. In such conditions, physically bound water reduces the shear strength parameter, adds extra load to the slope and thus contributes to the activation of the sliding process, while the free groundwater in the fracture aggregates of the pores contributes to the physico-chemical decomposition and degradation of the basic rock mass by pressure and circulation [10].

Durmitor flysch sediments are mainly poorly permeable to impermeable rock masses. In the flysch sediments, the groundwater level is in the zone of surface decomposition (eluvial-deluvial part), while it is directly related to the water level in the watercourse in the Quaternary sediments lying over the flysch formation (alluvial planes and river terraces). By the type of porosity, hydrogeological function and the position within the terrain, i.e. by the hydrogeological conditions of formation of the aquifer, the following categories of rock masses can be distinguished in the terrain:

— Hydrogeological collectors with intergranular porosity consist of the Quaternary sediment (Q) including alluvial, proluvial and deluvial deposits.
— Relative hydrogeological collectors consist of basal limestone breccias and conglomerates ($^{1}K_{2}^{3}$), layered breccias and limestones ($^{2}K_{2}^{3}$) and, depending on the spatial position in the relief, they function as a relative hydrogeological collector with fracture porosity. There are no fractures of large dimensions with significant continuity of spreading in these sedimentary packages.
— The rocks with combined fracture-intergranular porosity partly consist of the sediments of the third and the fifth superposition packages ($^{3}K_{2}^{3}$, $^{5}K_{2}^{3}$) with breccias and limestones, while the marly component of this package is a classic hydrogeological isolator.
— Hydrogeological isolators, i.e. the impermeable rocks, consist of the fourth superposition package ($^{4}K_{2}^{3}$), within which the marly component is predominant. In contact with water, this component becomes drenched and, depending on its position in the structure, downslope mass movement may occur along the component.

Terrain construction types

It is known that rock masses, as real bodies in mechanical terms, exhibit very complex behaviour. This is due not only to their specific structure, but also to different states of stress to which they were exposed through the geological history. Therefore, all rock masses, even the youngest, are fragmented into a system of fractures (primary and secondary), which are the result of various stress effects and the dimensions of which exceed the rock masses strength. The terrain constructed from the Durmitor flysch formation has a highly heterogeneous lithological composition, where the lithological components of various physical-mechanical properties, i.e. environments intermittently and rhythmically alternate. Therefore, these are extremely complex terrain constructions, constructed from the following environments [6]:

1. Plastic environments - deluvial clayish debris;
2. Plastic to quasiplastic environments - eluvialdebris andmarly sediments;
3. Quasiplastic environments – sandy-marly flysch series, basal sediment;
4. Brittle environments - limestones, sandstones, greywacke.

Natural terrain constructions in the observed area are shown schematically in Figure 2.

On the basis of the presented terrain construction types in the Durmitor flysch formation, as

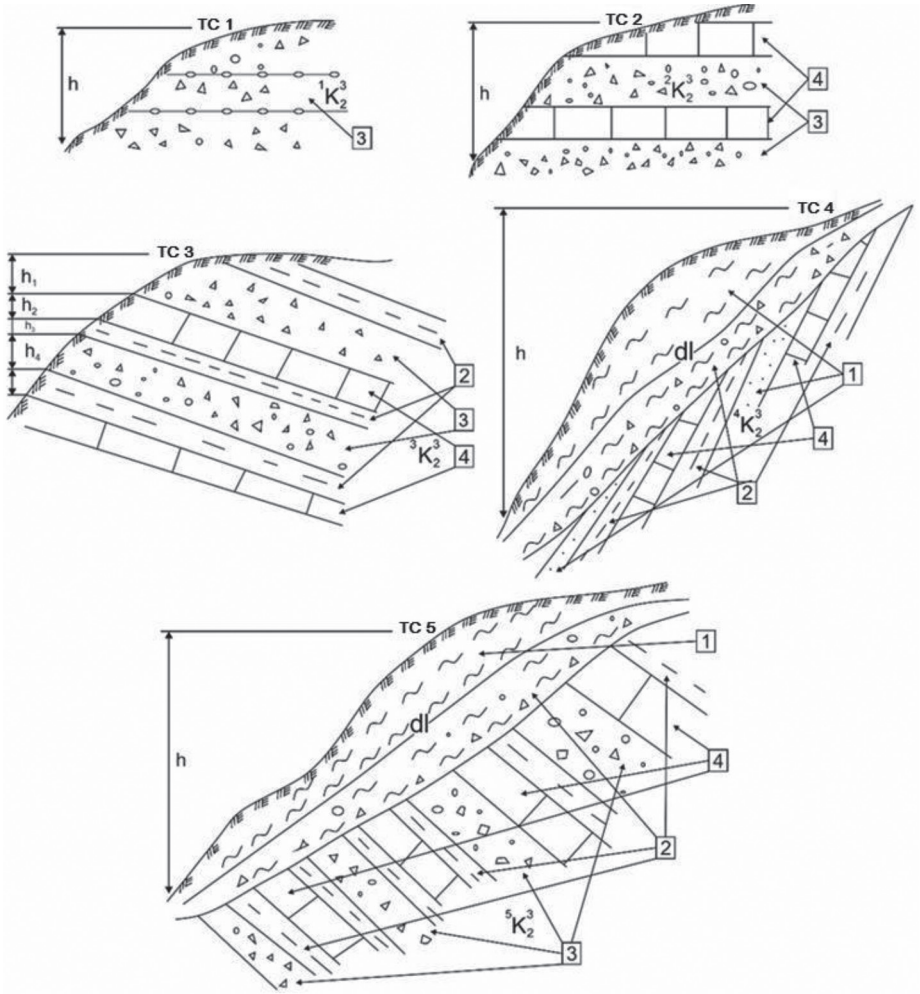

Figure 2: *Terrain construction types in the Durmitor flysch complex: 1 - plastic environment; 2 - plastic to quasiplastic environment; 3 -quasiplastic environment; 4- brittle environment; h - construction height; h_1-h_4 - environment height; TC 1-TC 5 - terrain construction designation.*

well as the tectonic relations in the slope, it can be concluded that the forms of deformation are extremely complex. Namely, depending on the spatial position of the geotechnical environments (lithologic members), which intermittently alternate in these packages and have significantly distinct physical-mechanical properties, they behave differently under the influence of particular stresses in the nature.

Contemporary geodynamic processes in the durmitor flysch belt

General classification of instabilities in our country has been used since 1962 [11]. According to this classification, contemporary slope processes are classified into the following:

- rockfalls;
- landslides;
- creeps;
- mudslides.

When it comes to contemporary geodynamic processes in the Durmitor flysch complex, we can say that landslides of various dimensions often occur, commonly in the areas where the fourth and fifth superposition packages ($^4K_2^3$ and $^5K_2^3$) are predominant. Rockfalls occur in riverbeds and in the notches and road cuts. Their dimensions are not significant. As for mudslides, geodynamic phenomena in which the mass movement over a sliding surface takes

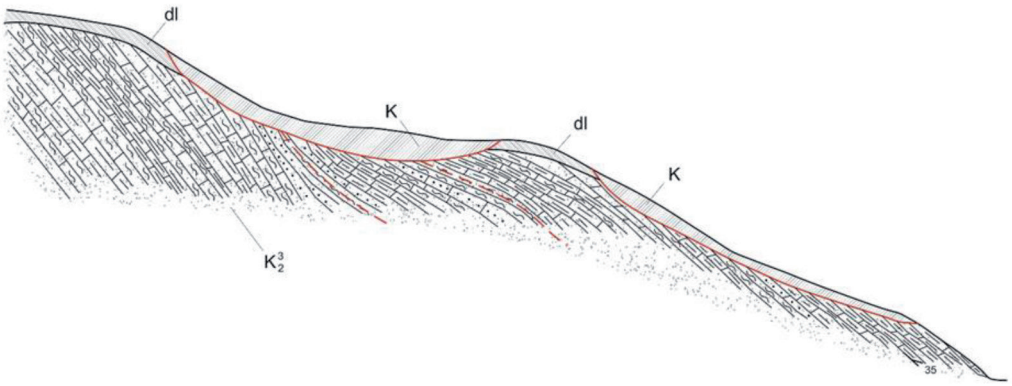

Figure 3: *The landslide "Ždralovpotok" is a typical example of a landslide on the Čemerno mountain pass (at the Čemerno tunnel exit portal, main road M 20, section Gacko - Foča, [7]).*

place at a very high speed, we can say that they occured on two occasions in the past.

Rockfalls in the area of the Durmitor flysch complex do not have significant spread and large volumes, and are mainly related to steep road cuts, as well as steep valley slopes whose toes are being undercut by the river flows. They occasionally happen due to large temperature differences (the effects of frost), as well as the influence of large amounts of precipitation. The rockfalls with occurrence of massive stone blocks are rare. In general, fragments of centimetric and decimetric dimensions occur, rarely metric. They often happen as a consequence of powerful earthquakes [12].

Screes in the flysch complex area have no significant spread and are mostly located in the area of the overthrustfront, where the massive limestones from the Anisian stage (T_2^1) are thrust over the flysch sediments.

Landslides as contemporary geodynamic processes represent mass movement on the slopes, without detachment from the base, over a clear shear surface (sliding surface). In the area constructed from the Durmitor flysch, especially the northeast side of the Čemerno mountain pass, landslides dominate (Figure 3). Some of them are active, while a number of them are dormant and relict landslides.

Shearing process in active landslides takes place at the contact points of the Cretaceous sediments and the Quaternary formations. In special conditions, in conditions of the complete watersaturation of the terrain and "favourable" position of the bedding surface, the landslide body can also cover the basic rock mass. Sliding takes place over the drenched layers of marlstone and claystone. The most typical example of such landslide is the landslide "ČemernskoOsoje" (Figure 4).

The causes of sliding are multiple and they usually complement each other. In this case, the main cause is the adverse impact of the stream that reduces the erosional base by its erosion activity, thereby removing, i.e. undermining the toes of the slope. In addition to this cause, the slope inclination and water saturation of the rock mass (deluvial deposits, as well as the basic rock mass) have crucial roles in the formation of the landslide. The position of the rock mass structure (the bedding position that is parallel to the slope or lower than the slope inclination) also has an important role. At the time of strong earthquakes, landslides are reactivated and numerous rockfalls occur [12].

Landslides in the observed area predominantly fall into the group of consequent landslides (Zolotarjev, 1983), i.e. the landslides of block structure with the predisposed sliding surfaces. Sliding surfaces are mainly located at the contact point of the eluvial-deluvialdebris and the bedrock, and at the interlayer surfaces that generally decline down the slope. In formation of these landslides, apart from the above-mentioned exogenous agents (water and temperature oscillations), the relief form and the position of the basic rock mass structure also have major roles. Sliding surfaces are usually formed over the layers of claystone and marly claystone.

Figure 4: *The landslide "ČemernskoOsoje".*

Mudslides as geodynamic phenomena represent a distinct group of terrain instabilities, which occur under conditions of the complete watersaturation of the deposit (eluvial-deluvial debris). The speed of the mass movement is quite high and it resembles a torrent. As far as is known, the first such occurrence happened in the fall of 1914 on the northeast slope of Čemerno. On that occasion, a huge amount of rock mass collapsed into the Sutjeska riverbed, dammed the river and temporarily created a lake. The same happened in November 2005 near Mojkovac in Montenegro, when a huge amount of rock mass tumbled into the Tara riverbed.

Discussion

The Durmitor flysch complex represents a specific lithological formation, formed during the Upper Cretaceous Senonian Stage (K_2^3). This lithological formation consists of five superposition bed packages, which are mutually substantially different in their lithological, hydrogeological and geotechnical properties [13].
Dimitrijević considers that three facies can be distinguished in the Durmitor flysch complex: carbonate, siliciclastic and mixed facies. This paper clearly distinguishes five packages within the Durmitor flysch.
For the first time in geological literature, this paper distinguishes five types of terrain construction. Terrain construction represents a particular arrangement of natural environments which can be distinguished by various mechanical properties, but in terms of statics act as a whole.
Contemporary geodynamic processes, as defined bygeneral classification [8] are present in this formation in all their forms, to a greater or lesser extent.
Particular emphasis is put on landslides, where in conditions of "favorable" position of the bedding surfaces a sliding plane is formed over them (the marly component). The landslides mostly have a block structure, they are formedover the predisposed surfaces and fall into the group of consequent landslides.

Conclusion

The Durmitor flysch complex represents a complex lithological formation, mainly formed during the Upper Cretaceous Senonian Stage (K_2^3), while the authors ofthe Basic geological map of SFRY classified this lithological formation in the region of Montenegro as the formation from the transitional period between the Upper Cretaceous and the Paleogene (K,Pg).
On the territory of Bosnia and Herzegovina, this lithological formation is represented with five superposition packages, which differ both in lithological composition and in thickness of the layers, as well as their rhythmicity.
The Durmitor flysch complex consists of the layers of basal limestone breccias and conglomerates, limestone and siltstone, marly limestone, marlstone and sporadic claystone. These rock masses are characterized by specific engineering geological properties, which are

conditioned by the heterogeneous lithological composition. Therefore, this complex is characterized by heterogeneous and anisotropic geotechnical properties, which depend on the predominant lithologic members in the complex, as well as spatial position of the superposition bed packages.

Lithological heterogeneity also influenced the heterogeneity of physical-mechanical properties and the behaviour of such environments under the influence of static and dynamic loads, i.e. in case of disturbance of primary geostatic conditions in the terrain.

The lithologic members were deposited in special sedimentary conditions and are therefore found in form of the beds of various thicknesses. They compose characteristic bed packages, which intermittently and rhythmically alternate.

Post-genetic tectonic activity caused folding and faulting of these sediments, which additionally complicates defining of physical-mechanical parameters of these environments and defining of geotechnical conditions for construction of various types of objects in this terrain.

Specific climatic conditions characterized by high precipitation, as well as large temperature oscillations, both within a day and during the year, caused the formation ofnumerous river valleys and other erosional valleys.As a result of these activities, inter alia, various terrain constructionswere formed and various types of instabilities occurred.

In the surface areas of the terrain, landslides of the consequent type are predominantly present. The sliding surfaces are generally formed at the contact point of the surface decomposition crust and the bedrock. Due to the fact that these landslides are practically moving and their activity is particularly manifested after intense precipitation and sudden snowmelt, problems with exploitation of the roads and other construction objects built on these terrains are evident.

On the valley slopes, primarily depending on spatial position of the beds in the flysch packages, the conditions for formation of landslides are created, with the sliding surfaces predisposed by interlayer surfaces.

The occurrence of instabilities of the rockfall type is less frequent.

Mudslides,as contemporary geodynamic phenomena with huge amounts of material tumbling into the riverbeds or erosional bases at a high speed, have been recorded on two occasions over the past 100 years.

References

[1] Jia-wen, Z., Chong, S., Fu-gang, X. (2013): *Geotechnical Characteristics and Stability Analysis of Rock-Soil Aggregate Slope at the Gushui Hydropower Station, Southwest China*. *The Scientific World Journal*, 540636, 16 p.

[2] Safaei, M., Omar, H., Yousof, Z.B.M., Motevalli, A. (2013): Application of a Physically based Model for Terrain Stability Mapping in North of Iran. *Global Journals Inc.* (USA), 13(2).

[3] Tofani, V., Bicocchi, G., Rossi, G., Segoni, S., D'Ambrosio, M., Casagli, N., Catani, F. (2017): Soil characterization for shallow landslides modeling: a case study in the Northern Apennines (Central Italy). *Landslides*, 14(2), pp. 755–770.

[4] Bešić, Z. (1948): *Geotectonic structure of northern Montenegro*, Bulletin of the Natural Science Museum of Serbian Land, ser. A-1, Belgrade.

[5] Mirković, M., Kalezić, M., Pajović, M., Vujisić, P. (1980): *BGM SFRY, Explanatory booklet for the sheet Gacko*, Federal Geological Institute of SFRY, Belgrade.

[6] Perić J., Šutić J., Božinović D. (1967): *Terrain constructions as the basis for research on the terrain stability, Advice on the issues of landslides in the road construction*, JDP, Belgrade.

[7] Lokin, P., Lapčević, R. (2000): *Project implementation plan, Book 1, Geotechnical investigations and geotechnical conditions, Main road M 20 Gacko – Foča, section Vrba – Trnovaluka*, Makspro Ltd., Belgrade.

[8] Dimitrijević, M. (1995): *Geology of Yugoslavia*, Geological Institute: Belgrade.

[9] Golijanin, A.: *The impact of engineering geological properties of the Durmitor flysch on geotechnical conditions for construction*, doctoral dissertation (in the making).

[10] Sunarić, D. (2017): *Engineering geodynamics, Theory and practice*, Academy of Engineering Sciences of Serbia and the Water Management Institute, "Jaroslav Černi", Belgrade.

[11] Janjić, M. (1962): *Engineering geological characteristics of the terrain of PR Serbia*, Belgrade.

[12] Sunarić, D., Stojinić, N., Nedeljković, S. (2008): *Seismicity of the terrain and exogenous geodynamic phenomena (landslides and rockfalls) in western Serbia*. The Water Management Institute, "Jaroslav Černi", Belgrade.

[13] Jevremović, D. (2015): *Methods of engineering geological research*. University of Belgrade - Faculty of Mining and Geology: Belgrade.

Original scientific paper

Received: Oct 18, 2018
Accepted: Dec 10, 2018
DOI: 10.2478/rmzmag-2019-0006

New Method of Visibility Network and Statistical Pattern Network Recognition Usage in Terrain Surfaces

Matej Babič[1,*], Miłosz Andrzej Huber[2], Elzbieta Bielecka[3], Metin Soycan[4], Wojciech Przegon[5], Ljubomir Gigović[6], Siniša Drobnjak[7], Dragoljub Sekulović[7], Ivan Pogarčić[8], George Miliaresis[9], Matjaž Mikoš[10], Marko Komac[10]

[1,*] Jožef Stefan Institute, Slovenia
[2] Maria Curie –Sklodowska University, Lublin, Poland
[3] Military University of Technology, Faculty of Civil Engineering and Geodesy, Poland
[4] Yildiz Technical University, Faculty of Civil Engineering, Department of Geomatic Engineering Davutpasa Campus TR-34220 Esenler-Istanbul-Turkey
[5] University of Agriculture in Krakow, Poland
[6] University of Defence, Military Academy, Serbia
[7] Military Geographical Institute, Belgrade, Serbia
[8] Juraj Dobrila University of Pula, Croatia
[9] University of Patras, Greece
[10] Faculty of Civil and Geodetic Engineering, University of Ljubljana Slovenia

Abstract

Many problems in the analysis of natural terrain surface shapes and the construction of terrain maps to model them remain unsolved. Almost the whole process of thematic interpretation of aerospace information consists of a step-by-step grouping and further data conversion for the purpose of creating a completely definite, problematically oriented picture of the earth's surface. In this article, we present application of a new method of drawing 3D visibility networks for pattern recognition and its application on terrain surfaces. For the determination of complexity of 3D surface terrain, we use fractal geometry method. We use algorithm for constructing the visibility network to analyse the topological property of networks used in complex terrain surfaces. Terrain models give a fast overview of a landscape and are often fascinating and overwhelmingly beautiful works by artists who invest all their interest and an immense amount of work and know-how, combined with a developed sense of the portrayed landscape, in creating them. At the end, we present modelling of terrain surfaces with topological properties of the visibility network in 3D space.

Key words: Network theory, complex pattern recognition, terrain surface analysis, modelling

POVZETEK

Obstaja mnogo nerešenih problemov s področja analize oblik terenov naravnih površin in izdelavo njihovega modela. Skoraj celoten proces tematske interpretacije letalskih in vesoljskih informacij je sestavljen iz skupine po korakih in nadaljnje pretvorbe podatkov z namenom oblikovanja popolnoma določene, problematično usmerjene slike zemeljske površine. V tem članku predstavljamo uporabo nove metode konstruiranja 3D omrežij vidljivosti za prepoznavanje vzorcev in njeno uporabo na površinah terena. Za določanje kompleksnosti 3D površine terena uporabljamo metodo fraktalne geometrije. Uporabljamo algoritem omrežja vidljivosti za analizo topoloških lastnosti omrežij, ki se uporabljajo na kompleksnih terenih. Terenski modeli omogočajo hiter pregled pokrajine in so pogosto očarljiva in lepa dela umetnikov, ki vlagajo vse svoje zanimanje in ogromno dela in znanja, skupaj z razvitim občutkom za predstavljene pokrajine pri njihovi ustvarjanju. Na koncu predstavljamo modeli površine terena s topološkimi lastnostmi 3D omrežij vidljivosti.

KLJUČNE BESEDE: Teorija omrežij, razpoznavanje kompleksnih vzorcev, analiza površine terena, modeliranje

Introduction

Network theory and graph theory are very useful in Geography. Landscape network models can be a useful tool (procedure) in landscape aesthetic value management and spatial planning processes [1]. Visibility calculations [2] are central to any computer graphics and geoinformation system (GIS) application. Visibility graph analysis [3] is a spatial analysis technique that can also be applied to terrain surface analysis. Existing or newly designed houses, structures, quarters, etc. are considered as peaks, and the connecting roads, engineering networks, transmission lines, etc., are like ribs. The process of creating terrain and landscape models [4] is important in various computer graphics and many visualisation applications. Figure 1 presents a terrain surface. Terrain surfaces [5] represent phenomena that have definite values at each point along the entire range of their extent. The values of an infinite set of points on the entire surface are extracted from a limited set of initial values. They can be based on direct measurements, for example, elevation height values or temperature values for temperature surfaces. The values for the surface between the measurement points are assigned by interpolation. Surfaces can also be mathematically calculated based on other data, for example, surface slopes or exposures, derived from terrain surface data, the surface of distances from bus stops in a city or a surface, showing the concentration of criminal activity or the possibility of strikes.

In problems of transforming the terrain into a project surface, mathematical methods are often used. In modern conditions of designing in real time or object-oriented design, the solution of some problems is eliminated with a geometric approach. This approach is called geometric modelling. More and more popular are the methods of geometric modelling in engineering design through computer modelling, since the solution to the problem acquires a spatial, visual appearance. In the design of the project surface relative to the terrain, a mathematical method is applied to the input data *x*, *y*, and *z* coordinates of discrete points of the relief. Transformation of the relief into the project surface requires a high-level engineer of the designer of mathematical skills that complicate the design process. Determination and selection of the optimal design surface along the structural relief lines [6] are becoming more and more in demand in the practice of engineering design, as the design takes place in real time and acquires a creative character. In modern systems of engineering design such as Compass, AutoCAD having input data on the topographic surface, it is possible to construct structural relief lines-profile and cross sections, isolines, slope lines, watersheds, and thalwegs [7]. All this is visualised in real time and gives the widest possibilities for analysis to a design engineer even of the middle class.

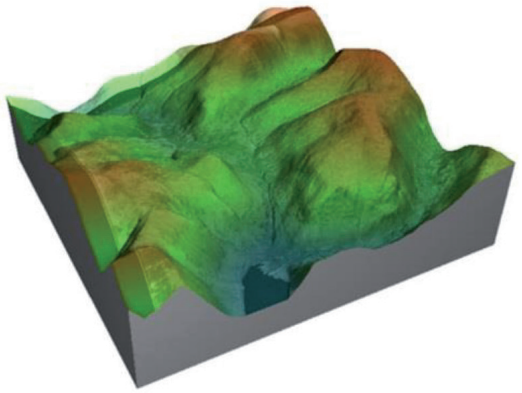

Figure 1: *Terrain surface.*

Consider an inclined line of an arbitrary flat curve, which is the profile or cross section of the relief. Having a number of such profile or cross sections interspersed at a certain distance (Dx, Dy), we can represent the framework model of the relief. The main task of the analysis of the relief is to determine the general slope of the terrain, and on the basis of it the design surface is selected. At the word "geometry", we have cylinders, triangles, hypotenuses, bisectors of corners, "find the area of a figure", slate boards, and breaking chalk from the depths of memory. The problem is that everything that comes to the mind is a language for describing an extremely narrow set of phenomena of the surrounding world. At home, sometimes, they are close to a parallelepiped, but trees – not the cylinders, the mountains are not cones, but the shape of the cloud is incomprehensible with what to compare. If we look closely, in the world around us this school geometry (we will

call it Euclidean) describes not so much. The scientists asked this question for a long time, but since they did not find a convincing answer, they wrote down these forms as "disordered", "monstrous", and "unexplored". A global breakthrough occurred only in the 1960–1970s, when the French mathematician Benois Mandelbrot invented and developed his theory of fractals [8]. It was a new, fractal geometry, which took for the object of research all that uneven, broken, and rough that surrounds us (that is, almost all). Mandelbrot found his wonderful order in complex forms of nature. Machine learning [9] is a highly specialised field of knowledge that is part of the main sources of technologies and methods used in the fields of large data and the Internet of things that studies and develops algorithms for automated extraction of knowledge from a raw data set, learning software systems based on the data received, generation of predictive and/or prescriptive recommendations, pattern recognition, etc. Statistics [10] is a science that uses many effective methods (including the method of mass observations, the method of groupings, and the method of generalising indicators) for the achievement of accurate results for the study of an object (subject, phenomenon, and process) and structuring them in a form convenient for the subject text, table, graph, and diagram with the subsequent analysis of the received data; the extracted information forms a statistical vision of the situation, the element of which is the object under study. Statistics is a general theoretical science (a complex of scientific disciplines) that studies the quantitative side of qualitatively defined mass socioeconomic phenomena and processes, their composition, distribution, spatial placement, and movement in time, revealing the current interdependencies and patterns in specific conditions of place and time. So, statistics is a branch of practical activity ("statistical accounting") for the collection, processing, analysis, and publication of mass digital data on various phenomena and processes of public life. Modern information systems and technologies include a large number of procedures that model or support data mining process. To the simplest procedures any type of classification quantitative data on given to users criteria, more complex provide analysis scenes, processes, phenomena for the purpose of selecting objects with given characteristics or properties. Procedures of this type are present not only in analysis problems in aerospace images but also when processing signals in technical systems, in medical diagnostics, biology, sociology, banking business, and other areas of human activity. As you expand sphere of application of geoinformation technologies and complicating procedures, geoinformation modelling procedures for analysis and classification aggregates of data, objects, and structures are very important in the new generation of GISs. For designing any system of thematic analysis classification of information objects and structures, its application requires a specialist knowledge. Research and development methods, algorithms, and systems for solving such tasks on a computer are engaged in a discipline called pattern recognition [11]. Our purpose in the present paper is to investigate different topological properties of visibility graphs in 3D space, which are being viewed as attractive alternatives in terrain surface analysis. The aim of the study is to use a visibility network algorithm for statistical pattern recognition of 3D classification for the prediction of complex terrain surfaces.

Materials and methods

A new algorithm for the construction of visibility networks in 3D space was presented in the study by Stempien [12]. This algorithm was used to analyse the topological properties of a complex surface (Figure1). In the visibility graph in 3D space, we calculated topological properties of the graph with the programme Pajek [13]. To analyse the topographical property of the terrain surface, we use the construction of the visibility graph in 3D space. Also, the problem in visibility points that we can connect together. In Figure 2, the problem of visibility network in 3D space is presented. Figure 3 presents the 3D surface and Figure 4 solution for constructing visibility graphs in 3D space for Figure 3.

We analysed a set of 22 randomly created terrain surfaces (Appendix 1). For each terrain surface, we constructed visibility graphs in 3D. After that, we calculated topological properties

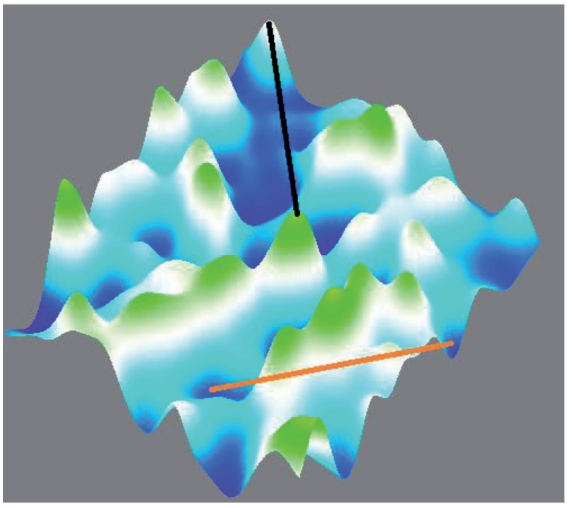

Figure 2: *Visibility points (black line) and unrelated points (orange line).*

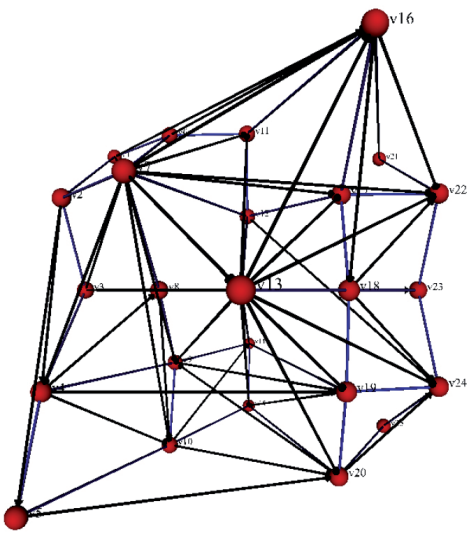

Figure 4: *Visibility network in 3D space for Figure 3.*

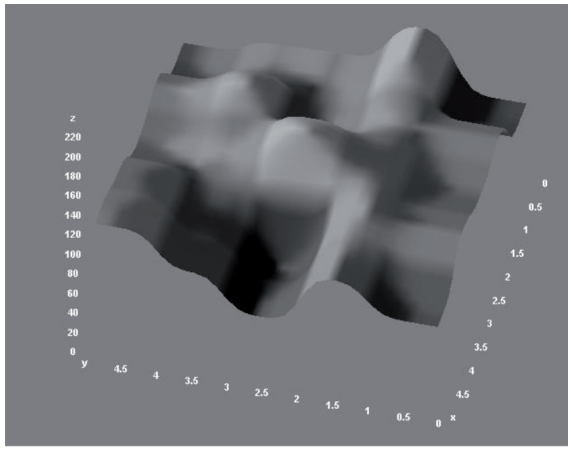

Figure 3: *3D surface.*

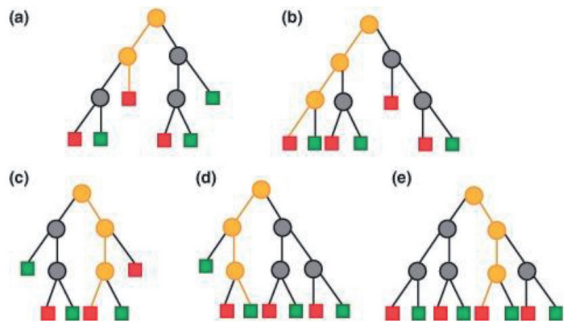

Figure 5: *Five illustrative decision trees forming a (very small) random forest for classification.*

of visibility graph in 3D for each terrain surface. Topological properties can apply to the network as a whole or to individual nodes and edges. Some of the most used topological properties and concepts are # extremes, # edges, and # k-core, All Degree Centralisation, Network Clustering Coefficient, Average Degree, and triadic census type 16–300 of visibility graphs in 3D for each terrain surface. We calculated statistical properties of topological properties of the 3D visibility network of all 22 terrain surfaces. For the determination of complexity of terrain surfaces, we use fractal geometry [14].

In fractal geometry, fractal dimension is the key, which determines the complexity of an object. Random forest (RF) [15] is one of the most stunning machine learning algorithms invented by Leo Bryman and Adele Cutler in the last century. He came to us in an "original form" (no heuristics could not substantially improve it) and is one of the few universal algorithms. The universality consists, first, that it is good in many tasks, second, that there are RFs for solving problem classification, regression, clustering, search of anomalies, selection of signs, etc. RF is a lot of decisive trees. In the task of regression, their answers are averaged, in the task of classification the decision is made by voting for the majority. Figure 5 presents five illustrative decision trees forming a (very small) RF for classification. We use parameters 30 fixed seed for random generator and growth control, not split subsets smaller than 5.

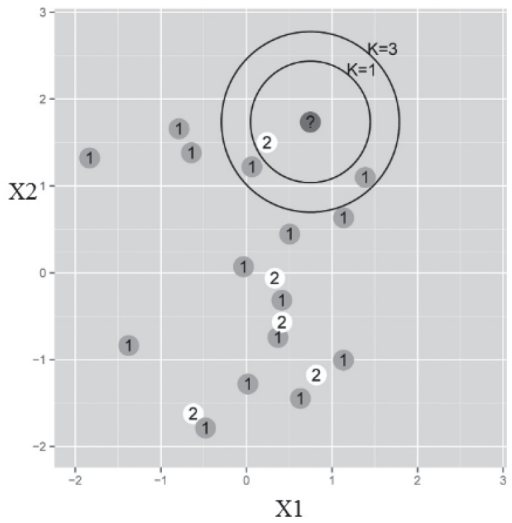

Figure 6: *K-nearest neighbours.*

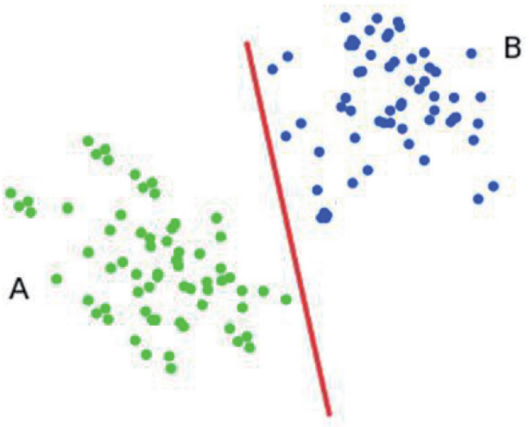

Figure 7: *Support vector method.*

The K-nearest neighbours model [16] is a method of machine learning, which saves itself as the knowledge of learning. For a given new example, the algorithm finds a given set of learning examples to the nearest, most similar cases and estimates the probability distribution from the relative distribution of these to examples by grade. In the simplest variant of this method, the algorithm is compiled by the new case as the class to which most of the closest neighbours belong. The advanced method takes into account the weighting of the impact of learning examples on the classification of a new case by distance. Figure 6 presents the k-nearest neighbours method. We use parameters 2 neighbours, Chebyshev metric and uniform weight.

The solution of the problem of binary classification using the support vector method [17] consists of finding a linear function that correctly divides the data set into two classes. The problem can be formulated as the search for a function f(x) that takes values less than zero for vectors of one class and greater than zero for vectors of another class. As initial data for the solution of the task, that is, search for the classifying function f(x), given a training set of space vectors for which they are known to belong to one of the classes. The family of classifying functions can be described in terms of the function f(x). The hyperplane is defined by the vector a and the value b, i.e. $f(x) = a.x + b$. As a result of solving the problem, i.e. constructing an SVM model, a function is found that takes values less than zero for vectors of one class and greater than zero for vectors of another class. For each new object, a negative or positive value determines whether the object belongs to one of the classes. Figure 7 presents the support vector method. We use v-SVM type with regression cost (C) 1.05. Optimisation parameters, we use 100 iteration limit and numerical tolerance 0.002. We use Kernel $(g \times x \times y + 0.15)^3$ and g was auto.

Results and discussion

In Table 1, the topological properties of 3D visibility network are presented. Topological properties present input of predictive models of complexity of terrain surfaces. We mark terrain surfaces from T1 to T22. Column one presents topological property # extremes, column two presents topological property # edges, column three presents topological property # k-core, column four presents topological property All Degree Centralisation, column five presents topological property Network Clustering Coefficient, column six presents topological property Average Degree, and the last column presents topological property triadic census type 16–300. The last column presents complexity of terrain surfaces. Terrain surface T22 has the best topological properties of the 3D visibility network, because T22 has maximal number of edges, Network Clustering Coefficient, and triadic census type 16–300. Terrain surface

Table 1: *Topological properties of the 3D visibility network and fractal dimension.*

SP	# extremes	# edges	# k-core	All Degree Centralisation	Network clustering coefficient	Average degree	Triadic census type 16–300	Fractal dimension
T1	120823	3500351	16	0.00020627	0.364	6.675	4865624	2.7365
T2	125787	3308776	12	0.00019998	0.364	6.311	4191425	2.668
T3	123943	3335861	13	0.00017608	0.371	6.363	4267175	2.6871
T4	124833	3355735	13	0.00017319	0.379	6.401	4353872	2.7458
T5	124626	3314397	12	0.00016182	0.378	6.322	4212248	2.8065
T6	131540	3190001	12	0.00013725	0.364	6.084	3796016	2.4956
T7	126962	3311163	12	0.00017518	0.373	6.316	4196282	2.1664
T8	130799	3173601	12	0.00018496	0.36	6.053	3741603	2.4784
T9	123393	3355056	11	0.00016842	0.385	6.399	4256560	2.622
T10	126395	3386391	13	0.00015883	0.378	6.459	4483986	2.7426
T11	124296	3315948	11	0.00026577	0.367	6.325	4207031	2.6142
T12	123829	3355735	13	0.00017319	0.379	6.401	4353872	2.6982
T13	128143	3451450	16	0.00018446	0.352	6.583	4862060	2.6743
T14	122500	3685175	20	0.00027177	0.372	7.029	5877473	2.3634
T15	120818	3338595	11	0.00012649	0.386	6.368	4199754	2.5155
T16	116812	3733624	18	0.00020016	0.364	7.121	5848517	2.5342
T17	133031	3178192	12	0.00013822	0.36	6.062	3774789	2.6528
T18	130974	3182544	15	0.00014298	0.357	6.070	3819193	2.2996
T19	131043	3170121	13	0.00014205	0.359	6.047	3746658	2.6427
T20	95090	4151533	16	0.00010784	0.387	7.918	7284078	2.1693
T21	106916	5653616	33	0.00021764	0.363	10.783	1764141	2.1042
T22	86871	5735036	19	0.00015646	0.394	10.939	1466536	2.1332

T17 has a maximal number of extremes of the 3D visibility network. Terrain surface T14 has maximal number of k-core and triadic census type 16–300 of the 3D visibility network. Terrain surface T11 has a maximal number of All Degree Centralisation of 3D visibility network. Table 2 presents statistical properties of topological properties of the 3D visibility network of terrain surfaces. We calculated statistical properties such as mean, standard deviation, standard error, median, geometric mean, harmonic mean, variance, skewness, Kurtosis, Fisher's g1, Fisher's g2, coefficient of variation, coefficient of dispersion, communality, area under curve, mean direction (Theta), mean resultant length, circular variance (V), circular standard deviation (v), circular dispersion (Delta), von Mises concentration (Kappa), Phi Pearson's Contingency, Coefficient Tschuprow's T, lambda B, symmetric lambda, Kendall's tau-B, Kendall's tau-C, and gamma of topological properties of the 3D visibility network of terrain surfaces. Terrain surface T21 has maximal # k-core.

Mostly, we have positive amount in Table 2 unless Skewness and Fisher's g1 for # extremes, average degree and triadic census type 16–300, kurtosis for average degree and triadic census type 16–300, Kendall's tau-B, Kendall's tau-C and Gamma for # extremes, All Degree Centralisation, average degree, and triadic census type 16–300. Terrain surface T5 has most complexity. Terrain surface T21 has minimal complexity. This statistic measures the heaviness of the tails of a distribution. The usual reference point

Table 2: *Statistical properties of topological properties of the 3D visibility network.*

SP	# extremes	# edge	# k-core	All Degree Centralisation	Network clustering coefficient	Average degree	Triadic census type 16–300
Mean	121792	3599223	14.68	17586.41	3.71E+07	5.98E+08	4253132
Standard deviation	11531.35	714391.3	4.86	4048.007	1119925	1.64E+08	1201353
Standard error	2458.49	152308.8	1.04	863.038	238768.9	3.50E+07	256129.4
Median	124461	3346826	13.00	17319	3.69E+07	6.34E+08	4209640
Geometric mean	121194	3546497	14.14	17168.05	3.71E+07	5.49E+08	4055020
Harmonic mean	120509	3505535	13.75	1.68E+04	3.70E+07	4.45E+08	3790200
Variance	1.3E+08	5.10E+11	23.66	1.64E+07	1.25E+12	2.69E+16	1.44E+12
Skewness	-1.89	2.409759	2.60	0.8111144	0.3436712	-2.462485	-0.026658
Kurtosis	5.90	7.454659	10.23	3.508959	2.195798	8.01742	4.719475
Fisher's g1	-2.04	2.58979	2.79	0.8717122	0.3693466	-2.646456	-0.028649
Fisher's g2	4.03	5.993685	9.52	0.9784921	-0.6906038	6.708983	2.517122
Coefficient of variation	0.094	0.1984849	0.33	0.2301782	0.03020786	0.2743574	0.2824632
Coefficient of dispersion	0.05	0.1024648	0.21	0.1684723	0.02531182	0.114327	0.1701942
Communality	1.007201	1.000102	0.55	0.062183	0.474759	0.964151	0.570508
Area under curve	2575577	7.46E+07	305.50	368764.5	7.78E+08	1.28E+10	9.04E+07
Mean direction (Theta)	103.14	178.3926	14.67	120.4838	157.2197	148.077	188.3852
Mean resultant length	0.11	0.1746	1.00	0.0943	0.2903	0.3947	0.1533
Circular variance (V)	0.88	0.8254	0.00	0.9057	0.7097	0.6053	0.8467
Circular standard deviation (v)	118.11	107.0477	4.74	124.5001	90.1178	78.124	110.9654
Circular dispersion (Delta)	32.66	12.9282	0.01	48.9952	5.2048	2.7628	18.7855
von Mises concentration (Kappa)	0.24	0.3546	146.45	0.1895	0.6069	0.8603	0.3103
Phi	4.58	4.4721	2.83	4.4721	4.4721	4.4721	4.4721
Pearson's contingency coefficient	0.97	0.9759	0.94	0.9759	0.9759	0.9759	0.9759
Tschuprow's T	1	0.9879	0.79	0.9879	0.9879	0.9879	0.9879
Lambda B	1	0.9524	0.38	0.9524	0.9524	0.9524	0.9524
Symmetric lambda	1	0.9756	0.65	0.9756	0.9756	0.9756	0.9756
Kendall's tau-B	-0.19	0.2338	0.28	-0.2165	0.026	-0.1126	-0.1558
Kendall's tau-C	-0.19	0.2338	0.28	-0.2165	0.026	-0.1126	-0.1558
Gamma	-0.19	0.2348	0.32	-0.2174	0.0261	-0.113	-0.1565

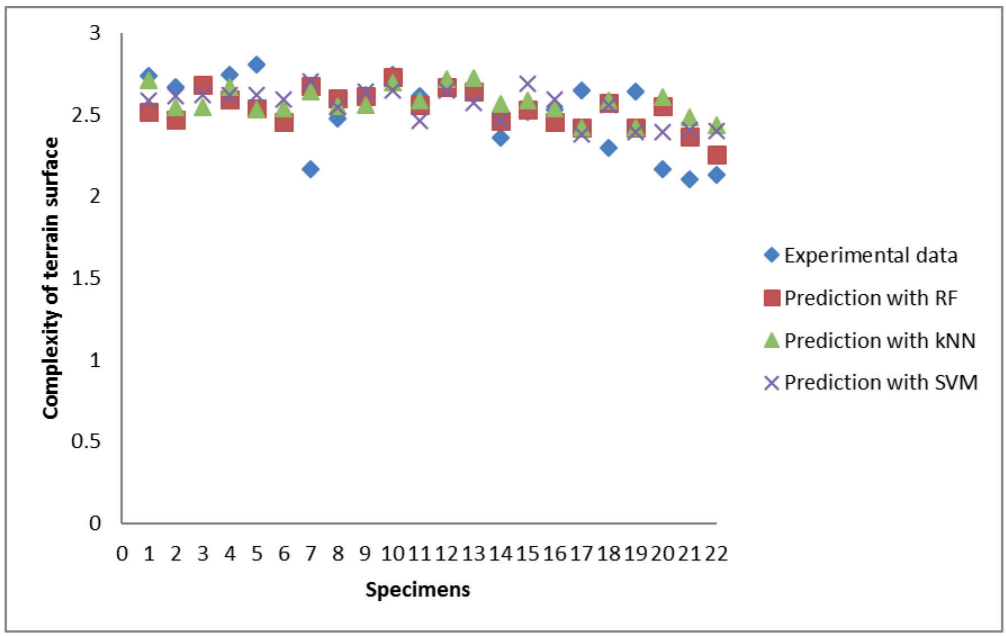

Figure 8: *The calculated and predicted surface terrain complexity.*

in kurtosis is the normal distribution. If this kurtosis statistic equals three and the skewness is zero, the distribution is normal. Also, we found positive significance between Kurtosis and topological properties of visibility graphs in 3D space of terrain surface. Pearson's contingency coefficient is a measure of association independent of sample size. It ranges between 0 (no relationship) and 1 (perfect relationship). For any particular table, the maximum possible depends on the size of the table (a 2 × 2 table has a maximum of 0.707), and so it should only be used to compare tables with the same dimensions. Also, in our result mostly topological properties have Pearson's contingency coefficient 0.97. Tschuprow's T is a measure of association independent of sample size. This statistic is a modification of the Phi statistic so that it is appropriate for larger than 2 × 2 tables. T ranges between 0 (no relationship) and 1 (perfect relationship), but 1 is only attainable for square tables. In our result, mostly topological properties have Tschuprow's T = 0.98.

Calculated and predicted data are presented in Table 3. The RF model presents a 6.28% deviation from the measured data. The k-nearest neighbours model presents a 6.88% deviation from the measured data. The support vector machine model presents a 6.82% deviation from the measured data. The calculated and

Table 3: *Calculated and predicted data.*

S	ED	P RF	kNN	P SVM
T1	2.7365	2.522	2.710	2.589
T2	2.668	2.470	2.545	2.617
T3	2.6871	2.683	2.545	2.625
T4	2.7458	2.592	2.673	2.621
T5	2.8065	2.538	2.530	2.619
T6	2.4956	2.460	2.537	2.596
T7	2.1664	2.678	2.645	2.705
T8	2.4784	2.601	2.552	2.546
T9	2.6220	2.612	2.558	2.646
T10	2.7426	2.730	2.697	2.650
T11	2.6142	2.563	2.590	2.462
T12	2.6982	2.668	2.721	2.649
T13	2.6743	2.644	2.722	2.573
T14	2.3634	2.463	2.564	2.462
T15	2.5155	2.535	2.590	2.694
T16	2.5342	2.460	2.537	2.596
T17	2.6528	2.425	2.422	2.384
T18	2.2996	2.572	2.587	2.563
T19	2.6427	2.425	2.422	2.396
T20	2.1693	2.554	2.610	2.396
T21	2.1042	2.366	2.481	2.407
T22	2.1332	2.258	2.439	2.400

predicted surface terrain complexity is shown in the graph in Figure 8.

Conclusions

The visibility graph problem itself has long been studied in computational geometry and has been applied to various areas. Finally, in this work the visibility network in 3D space, which contains more information than the visibility graph, has been used to analyse the terrain surfaces. Furthermore, we used the new method of construction of the visibility graphs in 3D space to describe the different terrain surfaces for possible further applications in studies of temporal and spatial landscape and/or terrain changes and evolution [18]. The main findings can be summarised as follows:

— We describe the different terrain surfaces by using the topological properties of the visibility graphs in 3D space.
— We present statistical properties of topological properties of the 3D visibility network.
— We use method of machine learning to predict complexity of terrain surfaces.
— With topological properties of 3D visibility network of terrain surface, we model complexity of terrain surface.
— With statistical statistical properties of topological properties of 3D visibility network of terrain surface, we can better analyse and understand complexity of terrain surfaces.
— With statistical properties of 3D visibility network of terrain surface, we can better understand structure of terrain surfaces.
— Terrain surface with minimum complexity has maximal #k-core.

Possible further testing of the proposed method in the field of landscape/terrain morphology would be:

— Description of temporal changes resp. development of a landscape/terrain using temporal changes in visibility graphs produced on multitemporal LiDAR data [19].
— Application in LiDAR derived high-resolution topography for landform recognition and analysis [20].
— Comparison of visibility graphs with other techniques for analysing terrain texture [21] or landform recognition, such as for landslides [22].

References

[1] Kowalczyk, A.M. (2015): The use of scale-free networks theory in modeling landscape aesthetic value networks in urban areas. *Geodetski vestnik*, 59(1), pp. 135–152.

[2] Ben-Moshe, B., Hall-Holt, O., Katz, M.J., Mitchell, J.S.B. (2004): Computing the visibility graph of points within a polygon. SCG'04 Proc. of the 20th Annual Symposium on Computational Geometry: Brooklyn, New York, USA; pp. 27–35.

[3] Overmars, M.H., Welzl, E. (1998): New methods for constructing visibility graphs. In: Proc. 4th Annu. ACM Symp. Computational Geometry. Urbana: Illinois; pp. 164–171.

[4] Stempien, D.C. (2002): Terrain models as battlefield visualization training tools. In: Military Intelligence Professional Bulletin. 28(4). Huachuca City. Arizona; pp. 33–35.

[5] Wilson, J.P., Gallant, J.C. (2000): Digital Terrain Analysis. In: Wilson. J.P., Gallant, J.C. (ed.). Terrain Analysis: Principles and Applications, Chapter 1. New York: Wiley; pp. 1–27.

[6] Haitov, B.U. (2014a): Geometric modeling of the relief for the problems of choosing the optimal design surface and water disposal//Young scientist: Monthly scientific journal. – Kazan, 4(63), pp. 292–194.

[7] Haitov, B.U. (2014b): On the construction of structural relief lines. Young scientist: Monthly scientific journal. – Kazan, 4(63), pp. 289–291.

[8] Boeing, G. (2016): Visual Analysis of Nonlinear Dynamical Systems: Chaos, Fractals, Self-Similarity and the Limits of Prediction. *Systems*, 4(4), pp. 37–54.

[9] Bridge, J.P., Holden, S.B., Paulson, L.C. (2014): Machine learning for first-order theorem proving. *Journal of automated reasoning*, 53(2), pp. 141–172.

[10] Marjetič, A., Kregar, K. (2016): Definition of appropriate geodetic datum using robust statistical. *Geodetski vestnik*, 60(2), pp. 212–226.

[11] Bishop, C.M. (2006): *Pattern Recognition and Machine Learning*. New York: Springer-Verlag, 738 p.

[12] Babič, M. (2014): *Analiza kaljenih materialov s pomočjo fraktalne geometrije*. Ph. D. Thesis. Maribor: University of Maribor 2014; 167 p.

[13] De Wouter, N., Mrvar, A., Batagelj, V. (2005): *Exploratory Social Network Analysis with Pajek*. New York: Cambridge University Press; 334 p.

[14] Babič, M., Kokol, P., Guid, N., Panjan, P. (2014): A new method for estimating the Hurst exponent H for 3D objects = Nova metoda za ocenjevanje Hurstovega eksponenta H za 3D-objekte. *Materiali in tehnologije*, 48(2), pp. 203–208.

[15] Lewoniewski, W., Węcel, K., Abramowicz, W. (2016): Quality and Importance of Wikipedia Articles in Different Languages. Information and Software Technologies. ICIST 2016. *Communications in Computer and Information Science*, 639, pp. 613–624.

[16] Malkov, Y., Ponomarenko, A., Krylov, V., Logvinov, A. (2014): Approximate nearest neighbor algorithm based on navigable small world graphs. *Information Systems*, 45, pp. 61–68.

[17] Wenzel, F., Galy-Fajou, T., Deutsch, M., Kloft, M. (2017): Bayesian Nonlinear Support Vector Machines for Big Data (PDF). Machine Learning and Knowledge Discovery in Databases (ECML PKDD). Archived (PDF) from the original on 2017-08-30.

[18] Roering, J.J., Mackey, B.H., Marshall, J.A., Sweeney, K.E., Deligne, N.I., Booth, A.M., Handwerger, A.L., Cerovski-Darriau, C. (2013): "You are HERE": Connecting the dots with airborne lidar for geomorphic fieldwork. *Geomorphology*, 200, pp. 172–183.

[19] Eitel, J.U.H., Höfle, B., Vierling, L.A. Abellán, A., Asner, G.P., Deems, J.S., Glennie, C.L., Joerg, P.C., LeWinter A.L., Magney, T.S., Mandlburger, G., Morton, D.C., Müller, J., Vierling, K.T. (2016): Beyond 3-D: The new spectrum of lidar applications for earth and ecological sciences. *Remote Sensing of Environment*, 186, pp. 372–392.

[20] Lo Ren, G., Fuller, I.C., Sofia, G., Tarolli, P. (2018): High-resolution mapping of Manawatu palaeochannels. *New Zealand Geographer,* 74(2), pp.77–91.

[21] Tasse, F.P., Gain, J., Marais, P. (2012): Enhanced Texture-Based Terrain Synthesis on Graphics Hardware. *Computer Graphics Forum*, 31(6), pp. 1959–1972.

[22] Booth, A.M., Roewring, J.J., Perron, J.T. (2009): Automated landslide mapping using spectral analysis and high-resolution topographic data: Puget Sound lowlands, Washington, and Portland Hills, Oregon. *Geomorphology*, 109, pp.132–147.

Appendix 1

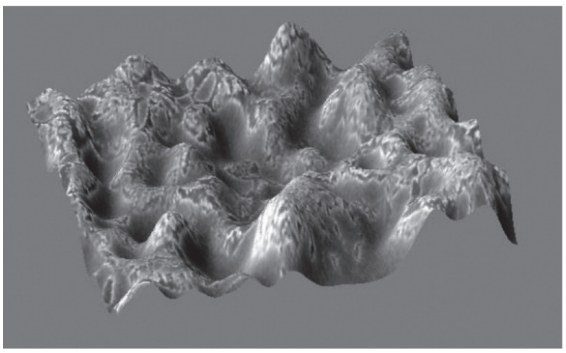

Terrain surface T1

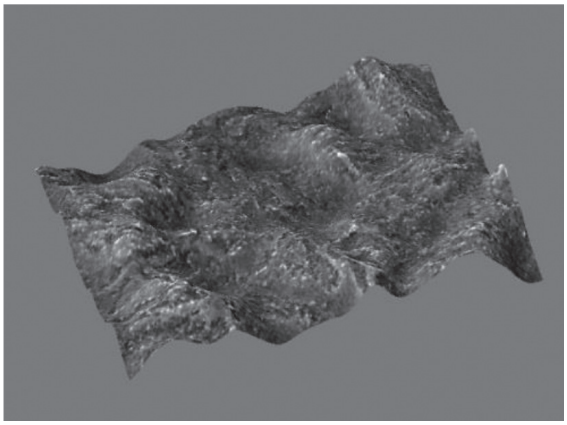

Terrain surface T2

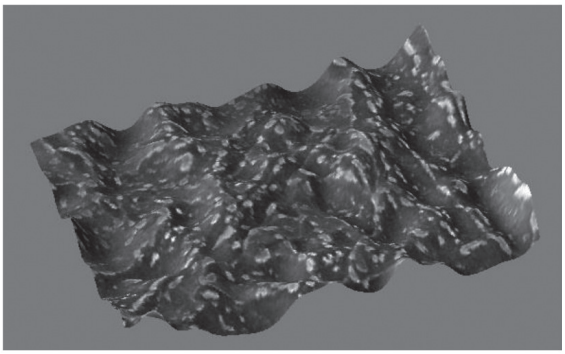

Terrain surface T3

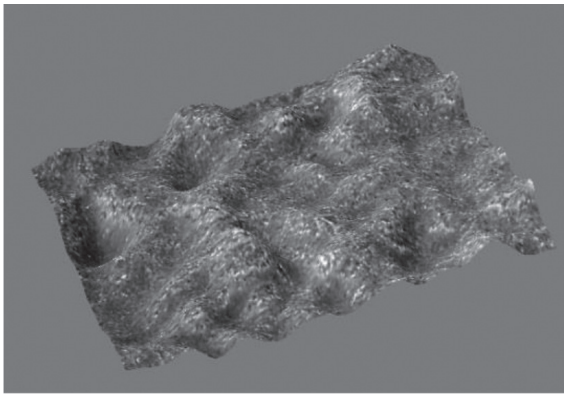

Terrain surface T4

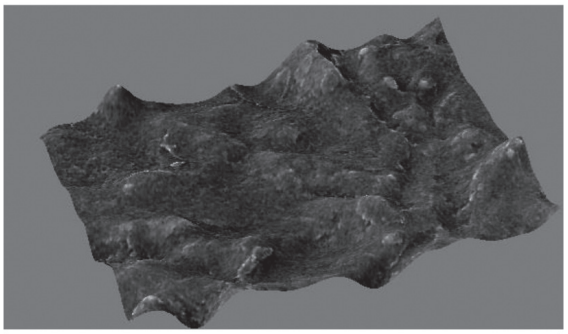

Terrain surface T5

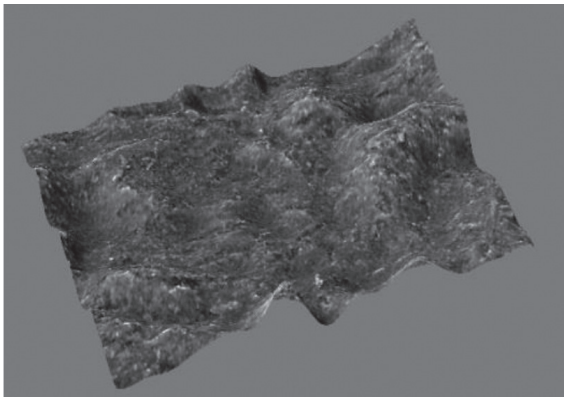

Terrain surface T6

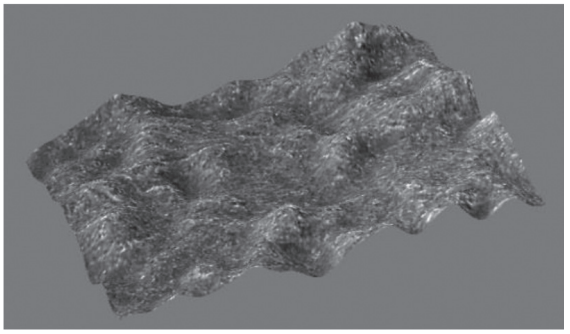

Terrain surface T7

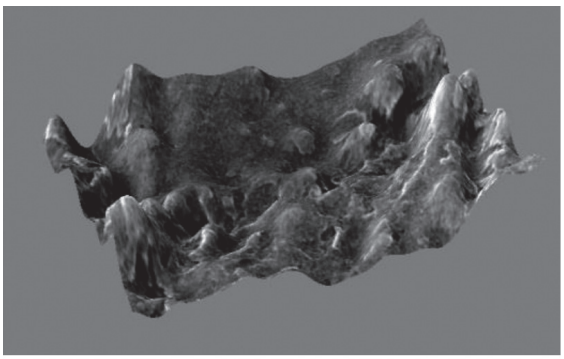

Terrain surface T8

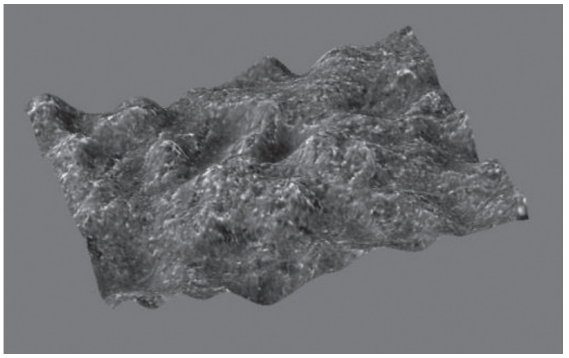

Terrain surface T12

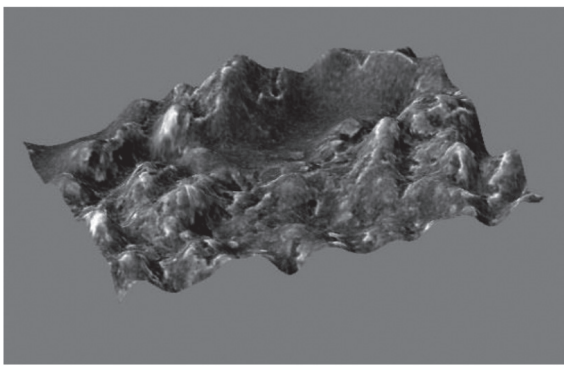

Terrain surface T9

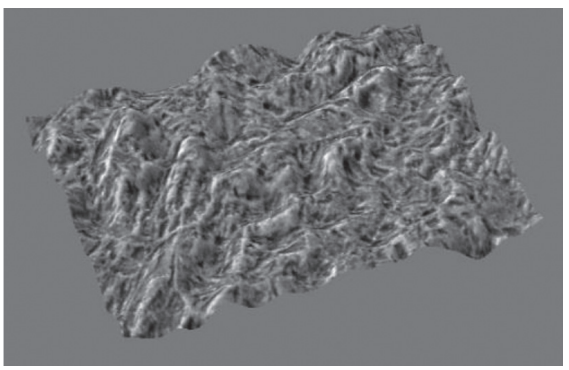

Terrain surface T13

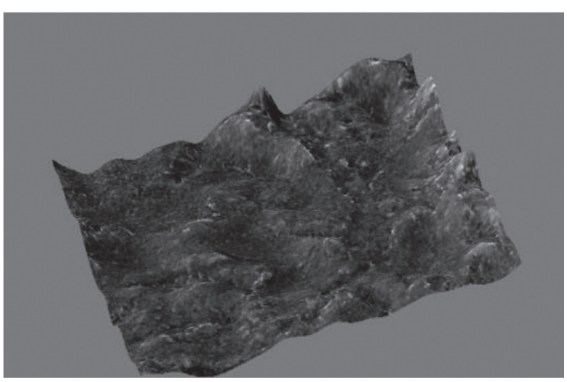

Terrain surface T10

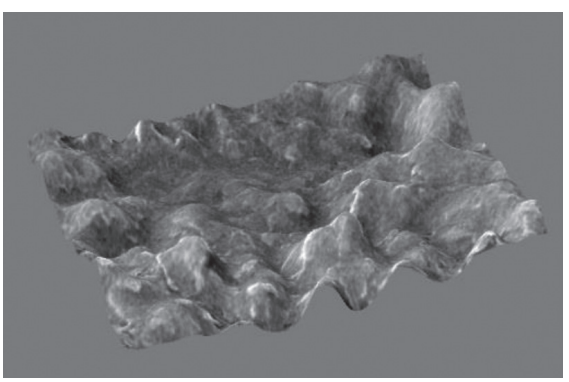

Terrain surface T14

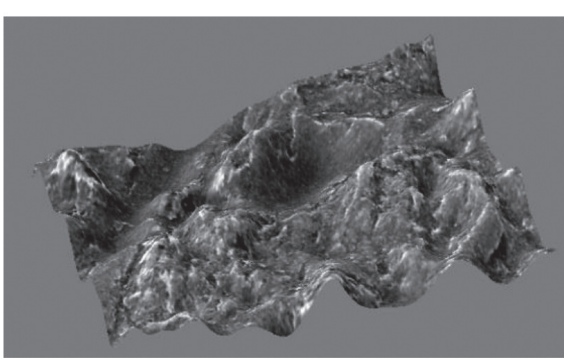

Terrain surface T11

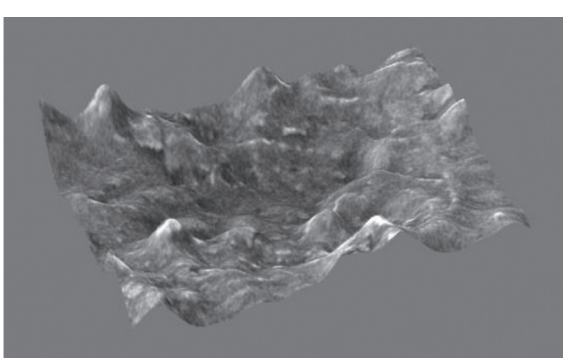

Terrain surface T15

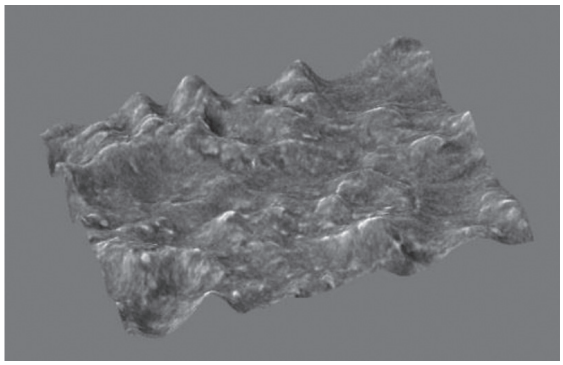

Terrain surface T16

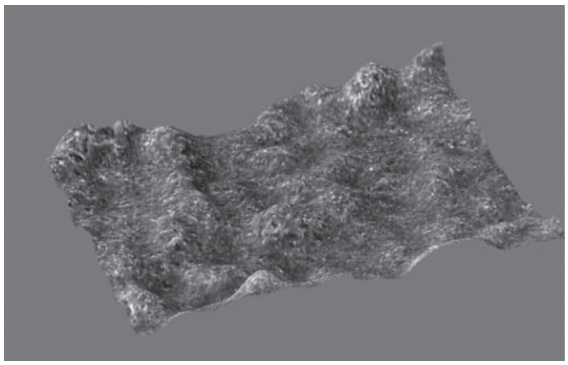

Terrain surface T20

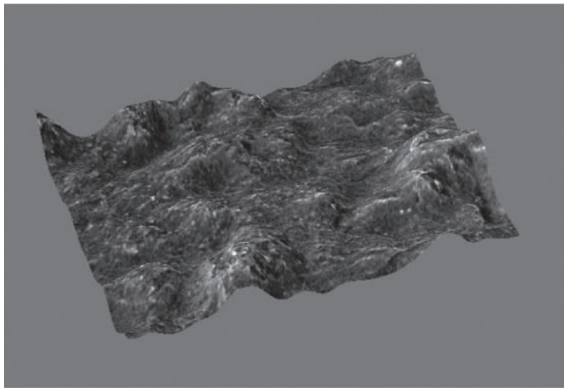

Terrain surface T17

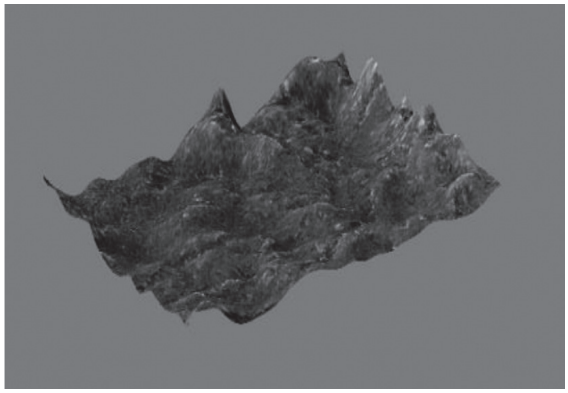

Terrain surface T21

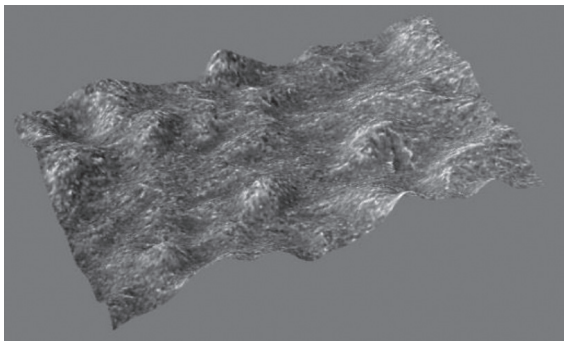

Terrain surface T18

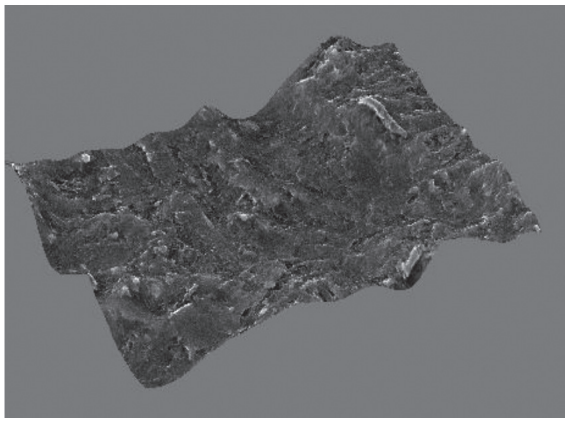

Terrain surface T22

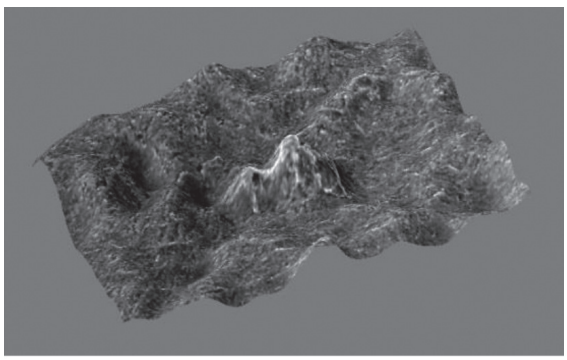

Terrain surface T19

Original scientific paper

Received: Oct 19, 2017
Accepted: Sep 10, 2018
DOI: 10.2478/rmzmag-2019-0007

Estimation of Magnetic Contact Location and Depth of Magnetic Sources in a Sedimentary Formation

Ocena lokacije magnetnega kontakta in globine magnetnih virov v sedimentni formaciji

Alabi A.A[1,*], Makinde V[1], Adewale A.O[2], Coker J.O[3], Aluko T.J[1]

[1] Department of Physics, College of Physical Sciences, Federal University of Agriculture, Abeokuta, Nigeria

[2] Department of Science Laboratory Technology, Moshood Abiola Polytechnic, Abeokuta, Nigeria

[3] Department of Physics, Faculty of Science, Olabisi Onabanjo Univesity, Ago Iwoye, Nigeria

* Corresponding author: Alabi AA; e-mail: derylab@yahoo.com

Abstract

The aeromagnetic data of Idogo, Southwestern Nigeria, have been used to study the lithology and to determine the magnetic source parameters within Idogo and its environs. Idogo lies between latitudes 6°30′N and 7°00′N and between longitudes 2°30′E and 3°00′E. The magnetic anomaly map, the regional geology, the analytic signal and the local wavenumber were used to identify the nature and depth of the magnetic sources in the region. Data enhancement was carried out to delineate the residual features relative to the strong regional gradients and intense anomalies due to the basin features. The estimated basement depth using the horizontal gradient method revealed depths ranging between 0.55 km and 2.49 km, while the analytic signal amplitude and local wavenumber methods estimated depth to the magnetic sources to range from 0.57 km to 4.22 km and 0.96 km to 2.43 km, respectively. Depth computations suggested the presence of both shallow and deep sources. The total magnetic intensity values ranged from 3.1 nT to 108.3 nT. The area shows magnetic closures of various sizes in different parts of the area trending West, with prominence at the centre and distributed East–West.

Key words: aeromagnetic, analytic signal amplitude, local wavenumber, total magnetic intensity, reduction to equator

Povzetek

Aeromagnetne podatke iz Idoga v jugozahodni Nigeriji smo uporabili za določitev litološke sestave in ugotovitev parametrov magnetnih virov na območju Idoga in okolice. Območje leži med širinama 6°30′N in 7°00′N in dolžinama 2°30′E in 3°00′E. Za identifikacijo narave in globine magnetnih virov smo uporabili karto magnetnih anomalij, karto regionalne geologije, analitične signale in lokalno valovno število. Ojačanje podatkov smo izvedli z namenom omejitve vpliva rezidualnih vzorcev glede na močne regionalne gradiente in intenzivne anomalije, ki so posledica oblikovanosti kadunje. Ocenjene globine podlage z metodo horizontalnih gradientov so bile med 0,55 in 2,49 km, medtem ko so bile z metodo amplitude analitičnega signala in lokalnega valovnega števila ocenjene globine do magnetnih virov od 0,57 do 4,22 km in od 0,96 do 2,43 km. Izračunane globine nakazujejo navzočnost tako plitvih kot tudi globokih virov. Vrednosti celotne magnetne intenzitete se gibljejo med 3,1 nT in 108,3 nT. Na ozemlju so vidne v različnih delih terena magnetne oblike raznih velikosti s štrlino v sredi in smerjo vzhod-zahod.

Ključne besede: aeromagnetika, amplituda analitskega signala, lokalno valovno število, celotna magnetna intenziteta, redukcija na ekvator

Introduction

An aeromagnetic geophysical survey presents the opportunity of carrying out comparative surveys of very large areas and unreached terrain within a short period of time, which makes it cost-effective. Aeromagnetic survey is a passive [1] geophysical method because it requires no energy source during data acquisition [2]. The investigations are based on the physical properties of the Earth, which can be used for the provision of solutions to various geological problems and for the structural mapping of an area. The Earth's physical properties and the formation of different rock types vary from one area to another due to the composition of the Earth [3]. The purpose of the magnetic survey is to identify the deviations in the geomagnetic field intensity from the local geology. Anomalies are mostly caused by magnetisation contrast of the sub-surface rocks [4], which occurs due to changes in the quantity of magnetite in rocks. In the realm of applied geophysics, anomalous magnetisations might be associated with local mineralisation, which is potentially of commercial interest, or could be due to the sub-surface structures that have a bearing on the location of oil deposits [5]. Regional aeromagnetic study of the anomaly map depicts the regional geological pattern and the structural features that provide the background for explicit interpretation [4]. Mathematical modelling can be used to deduce the shape, depth and characteristics of the rock bodies, which are accountable for the magnetic anomalies [6]. In sedimentary rocks, the magnetic properties are usually insignificant, due to low content of magnetic material, while igneous and metamorphic rocks usually display significant variations in the aforementioned properties, which are helpful in exploring the geological properties of the bedrock. The Earth's magnetic field is generated predominantly in the Earth's core, which is though complex in configuration but can be approached by a dipole field, such as that of a bar magnet. Some materials develop an induced magnetic field in the presence of an applied magnetic field and thus become magnetised, while others have remanent magnetisation or residual magnetism. The interaction of such fields with the Earth's primary field produces the magnetic field at the Earth's surface; thus, magnetic data collected over an area can be used to investigate the magnetic properties of rocks, which reveal the sub-surface structure of the area.

Asadi and Hale [7] applied the analytical signal of the total magnetic intensities to delineate intermediate-composition magmatic rocks in the Takab area of Iran. Chandler [8] used the second vertical derivative enhanced-aeromagnetic data, together with gravity data, to interpret the geology of the poorly exposed central part of the Duluth Complex. Experience from Finland showed high degree of correlations between the results from aeromagnetic data and geological structure [9]. Results from the magnetic survey of 1960 by Hunting Survey Limited across the Ashanti Belt – comprising the mineral and rock resources of Ghana – were quite satisfactory [10]. Geological interpretation based mostly on the magnetic maps was effective in segregating lithologies, faults and fracture zones. El-Awady et al. [11] carried out interpretation of the aeromagnetic survey over the Fayum area, Western Desert, Egypt, and obtained information about the crystalline basement structure and local structure in the sedimentary section. The analysis of the constructed magnetic map serves as foundation for studying the structural pattern of the basement complex and the surface structures. The aim of this study was to delineate the sub-surface structure of the area under consideration, hence deducing the lithology of the area and estimate the depth to the basement using horizontal gradient magnitude (HGM) method, local wavenumber (LWN) method and analytic signal amplitude (ASA) method.

Location and Geological Setting of the Study Area

The study area is located between latitudes 6°30′N and 7°00′N and longitudes 2°30′E and 3°00′E, measuring about 3,025 km^2 (Figure 1). It is located in the western part of Ogun State, Southwestern Nigeria.

The study area falls in the Oshosun Formation, which is one of the sedimentary formations of the Dahomey (Benin) Basin. The Dahomey Basin, which covers South-Eastern Ghana,

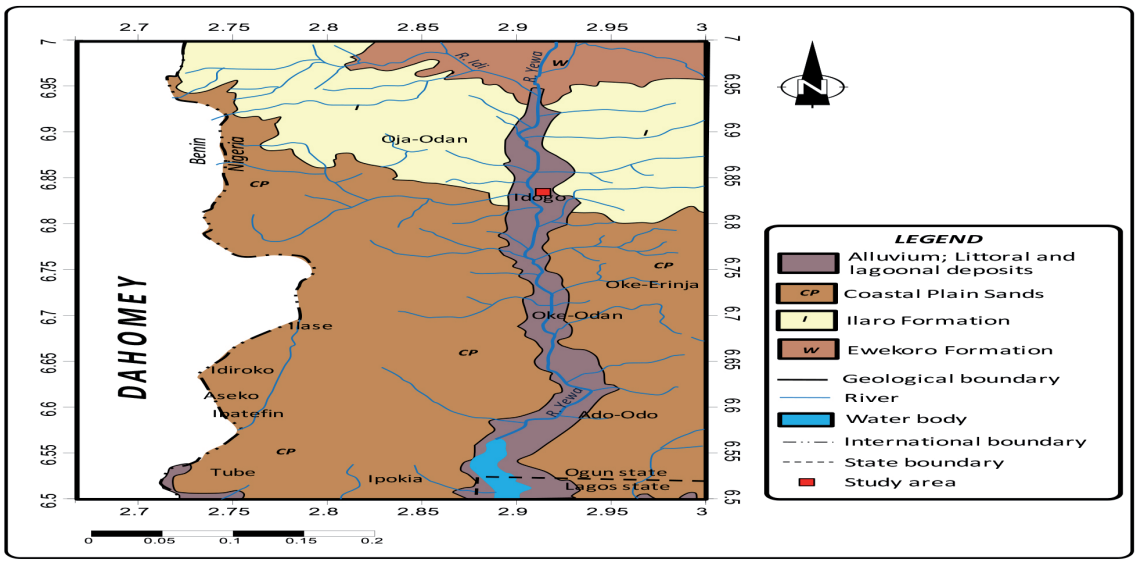

Figure 1: *Geological map of study area.*

Togo, Benin Republic and Western Nigeria, is an extensive sedimentary basin on the continental margin of the Gulf of Guinea [12,13]. The basin is a marginal pull-apart basin [14], which developed in the Mesozoic Era due to the separation of the African and South American lithospheric plates [15]. The basin encloses an extensive wedge of Cretaceous-to-recent sediments, which sets towards the offshore [16]. The sediments of Oshosun Formation in the western part of Dahomey Basin are underlain by lower Cretaceous-to-Palaeocene strata: Ise Formation, Afowo Formation and Araromi Formation, which belong to the old Abeokuta Group, and the Ewekoro Formation [17]. Overlying the Oshosun Formation are the old Ilaro Formation, coastal plain sands and alluvial deposits. All the sedimentary sequences lie on the crystalline Precambrian Basement Complex of Southwestern Nigeria.

Materials and Methods

Data Acquisition

The dataset used in this study includes the contoured aeromagnetic data obtained from the Nigerian Geological Survey Agency. The aeromagnetic data were obtained using a proton precession magnetometer with resolution 0.1 nT, at 80 m altitude, along the flight orientation of NE–SW, with a flight line spacing of 500 m and tie line spacing of 5,000 m. The azimuth of the flight line direction was 135°, while the azimuth of the tie line direction was 45°. The geomagnetic gradient was eliminated from the data using the International Geomagnetic Reference Field (IGRF) of Epoch 2009. The map of the study area was published on a scale of 1:10,000. The topography detail of the map was based on 1:10,000 topography series of the Federal Surveys of Nigeria. The average magnetic inclination, magnetic declination and magnetic field strength across the survey were –13.0364°, –2.3844° and 32,896.0 nT, respectively.

Data Processing and Gridding

The processing of aeromagnetic data for this research involved the application of the enhancement technique, the application of a gridding routine and removal of the Earth's background magnetic field. Some corrections, such as background correction (aircraft, radon and cosmic radiation), stripping, micro-levelling, as well as removal of the diurnal variation of the Earth's magnetic field, aircraft heading, instrument variation, lag error between the aircraft and the sensor, and the inconsistencies between flight lines and tie lines, were done by Fugro Airborne Surveys Ltd., USA. The main software packages

used for the processing and enhancement of the airborne geophysical data were the Geosoft® Oasis montaj 6.4, Surfer 13 and the US Geological Survey (USGS) Potential-Field software.

Gridding interpolates the aeromagnetic data from the measurement locations to the nodes of a regular mesh and thereafter creates a new and fundamentally different construct of the data [18]. The data were gridded to a 55 m interval using the minimum curvature technique described by Briggs [19]. Once a grid was produced, it was displayed as an image (Figure 2). The minimum curvature gridding technique was applied to the aeromagnetic data, which takes the randomly distributed survey data and interpolates it onto a regular grid. The images observed were spatially referenced to make it visible in a geographic information system (GIS) setting.

Enhancement of Aeromagnetic Data

Aeromagnetic data were enhanced by a collection of linear and non-linear filtering processes. Mathematical enhancement techniques [20] were applied to a range of imaging routines to visually enhance the properties of the selected magnetic sources represented by geological lithological features.

Significant concentrations of mineral deposits are correlated with high-frequency magnetic responses. High-pass and horizontal gradient filtering were applied to the aeromagnetic data to enhance the high frequencies and define geological body edges. All the enhancement techniques were performed with the Geosoft® (Oasis montaj 6.4) and Surfer13. The *MagMap* extension in Geosoft® was used on the magnetic anomaly grid for the processing and application of filters. The necessary filter was applied, and the magnetic anomaly was displayed as an image by means of the grid and the imaging device.

Reduction to Equator

Reduction to equator (RTE) is a useful and effective operation designed to transform a total magnetic intensity (TMI) anomaly caused by an arbitrary source into the anomaly that this same source would produce if it were located at the pole and magnetised by induction only [21]. Reduction to pole (RTP) converts the magnetic field from the magnetic latitude where the Earth's field is inclined to that field at a magnetic equator where the inducing field is vertical [22]. When the field of the Earth is inclined, magnetic anomalies caused by induction are related to their sources asymmetrically, but when the Earth`s inducing field is vertical, the associated anomalies would be directly over their sources [20]. Fourier transform is applied to transform the RTE from the space domain into the wavenumber domain. The RTE operation in wave number domain is expressed as presented in Eq. (1)

$$A_p(u,v) = \frac{A_c A_p}{(\sin I + i \cos I \cos(D - \Omega))} \qquad (1)$$

where $A_p(u, v)$ is the Fourier transform of these observed magnetic data; $A_c(u, v)$ is the Fourier transform of the vertical magnetic field; I and D are the inclination and declination of core field, respectively; (u, v) is the wavenumber corresponding to the (x, y) directions, respectively; and $\Omega = \arctan(u/v)$ [22]. The RTE for low geomagnetic latitudes was applied to the magnetic anomaly data. The method utilises an azimuthal filter in the frequency domain to minimise directional noise initiated by the low geomagnetic latitude [23]. The central coordinates of the area were used in calculating inclination and declination. The inclination, declination and average total field of the study area were –13.0364°, –2.3844° and 32,896.9 nT, respectively.

Direct Detection of Structural Trends

Interpretation of the aeromagnetic survey could be performed quantitatively or qualitatively. In this study, the detection of structural trends data aims to map the surface and the sub-surface regional structures such as faults and contact bodies; mineralisation was determined qualitatively. The qualitative interpretation of the shape and trend of magnetic anomalies was conducted by a visual examination of the structural trends and characteristic features. Some of these features [24] are the relative location and amplitudes of the positive and negative contour parts of the anomaly, the elongation and aerial extent of the contour and the sharpness of the anomaly as seen by the contour spacing.

Estimation of Depth

Since magnetisation is primarily a tool for sub-surface mapping, it follows that determination of the depths as well as other physical properties of bodies causing anomalies is important for its application in geological exploration. The depth to basement allows mapping of the sub-surface and indicates the thickness of the sediments. Areas underlain by sediments or other sedimentary deposits may be regarded as profitable depending on the depths.

The LWN Method

The LWN method, which is based on the extension of complex analytical signals, was used for estimation of the magnetic depths. The original LWN, also known as the source parameter imaging (SPI) method [25] works for two models: a 2-D sloping contact or a 2-D dipping thin sheet. For the magnetic field M, the LWN is given by Eq. (2) [25]:

$$K = \frac{\frac{\partial^2 M}{\partial x \partial z}\frac{\partial M}{\partial x} - \frac{\partial^2 M}{\partial x^2}\frac{\partial M}{\partial z}}{\left(\frac{\partial M}{\partial x}\right)^2 + \left(\frac{\partial M}{\partial z}\right)^2} \quad (2)$$

For the dipping contact, the maxima of K are located directly over the isolated contact edges and are independent of the magnetic inclination, declination, dip, strike and any remanent magnetisation. The depth is estimated at the source edge from the reciprocal of the LWN, as shown in Eq. (3).

$$Depth_{(x=0)} = \frac{1}{k_{max}} \quad (3)$$

where K_{max} is the peak value of the local wave number K over the step source. One more advantage of this method is that the interference of anomaly features is reducible, since the method uses the second-order derivatives. In practice, the method is used on gridded data by first estimating the direction of magnetic field at each grid point. The vertical gradient is computed in the frequency domain, and the horizontal derivatives are computed in the direction perpendicular to the strike using the least-squares method.

Analytic Signal Method

The absolute analytic signal magnitude is defined as the square root of the squared sum of the vertical and horizontal derivatives of the magnetic field, as presented in Eq. (4).

$$ASM(x,y) = \sqrt{\left(\frac{\partial M}{\partial x}\right)^2 + \left(\frac{\partial M}{\partial y}\right)^2 + \left(\frac{\partial M}{\partial z}\right)^2} \quad (4)$$

The advantage of this method of magnetic data enhancement is that its amplitude function is always positive and does not need any assumption of the direction of body magnetisation [26]. In a manner identical to that used in the HGM, peaks in the ASA are located. The maxima of the analytic signal are used to detect the structures responsible for the observed magnetic anomalies over the studied area.

Spectral Analysis

Spectral analysis provides an opportunity for calculating and interpreting the spectrum of geophysical data. The spectrum analysis, is a transformation of data from the time or space domain to the frequency or wavenumber domain, respectively. The spectral depth method is based on the principle that a magnetic field measured at the surface can be considered as the integral of the magnetic signature from all depths [27]. The power spectrum of a surface field can be used to identify the average depths of the source ensembles [28]. The spectral analysis method provides the average depth value to the top of the statistical ensemble of blocks of anomalies. The discrete Fourier transform, presented in Eq. (5), is a mathematical tool for spectral analysis and is applicable to aeromagnetic data [29].

$$f(x) = a_0 + \sum_{n=1}^{\infty}\left(a_n \cos\frac{n\pi x}{L} + b_n \sin\frac{n\pi x}{L}\right) \quad (5)$$

The aeromagnetic data were divided into grids, and the graph of the logarithm of spectrum energy against the frequency were obtained for each block. Previous studies [30–32] have proposed a two-step technique that can evaluate the bottom depth (Z_b) of the deepest magnetic sources with the aid of the spectral analysis designed by

Spector and Grant [28]. The first step of the 2-D analysis is the determination of the depth to the centre of the magnetic body (Z_o), while the second step is the calculation of the depth to the top (Z_t) of the magnetised body. These depth values of the magnetic sources are determined from the slope of the log power spectrum fit. The bottom depth, Z_b, is then obtained from these two depths by using Eq. (6) [32].

$$Z_b = 2Z_o - Z_t \quad (6)$$

Results and Discussion

TMI Map Interpretation

The TMI variation of the aeromagnetic map of Idogo and its environs ranges between 3.1 nT and 108.3 nT, with a group of long-wavelength anomalies in the NE–SW direction. The TMI field of the area under consideration is presented in Figure 2. The map reveals the existence of a thick sediment cover that tends towards the south-east. The TMI field variation reveals two distinct magnetic structural trends of high and low reliefs. The high side runs from the north-western part to the south-eastern part, while the low side runs from the south-western part to the south-eastern part, having distinct and different magnetic intensities. Presence of long-wavelength anomaly in the TMI map (Figure 2) reveals that the study area is a sedimentary basin, and a blanket of sedimentary rocks covers the region.

RTE Approach

The effect of the application of reduction–to-the-magnetic-equator filter is shown in Figure 3. The filtering process attempts to reduce the low-latitude effect of the horizontal elongated anomalies. It has been applied to produce the RTE map (Figure 3), which shows that the correction in the asymmetries of the observed anomalies had been minimised and the anomalies are centred directly over the causative elongated bodies. The reduced-to-equator magnetic intensity values range from 32.90 nT to 72.2 nT. The reduced-to-equator map is characterised by high frequency, small size, weak intensity, sharp boundary and nearly irregular-shaped anomalies, which are the effect of near-surface sources, such as shallow geologic units and cultural features within the area under consideration.

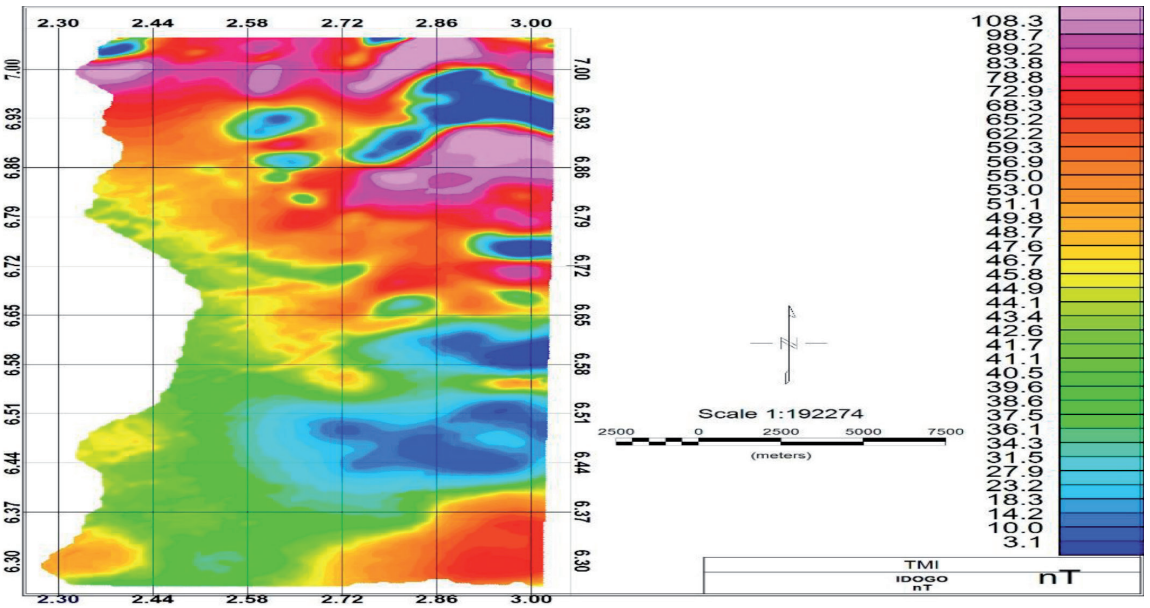

Figure 2: *TMI map of the study area.*

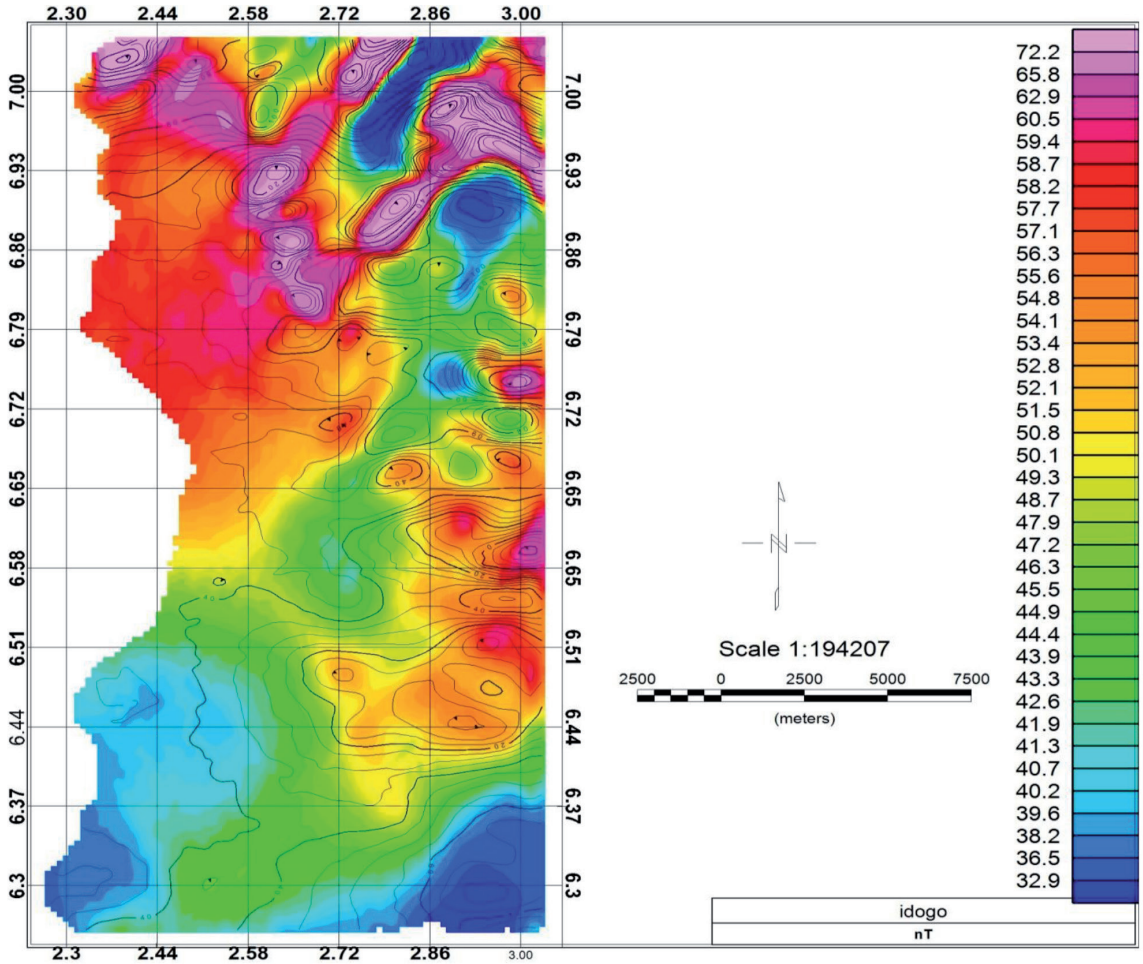

Figure 3: *RTE map of the study area.*

Magnetic Source Location and Depth Estimation

The magnetic sources location and magnetic contact depth solutions were computed by the HGM of the reduced-to-pole grid, the ASA of the TMI grid, and the LWN of the TMI grid, with a maximum standard error of 15%. Depths on Sheet No. 278 (Idogo) are shown in Figures 4, 5 and 6, respectively. The results obtained indicate that HGM records the highest number of contacts, with 113 solutions at comparatively deeper depths than do the other methods. The solutions from the HGM and ASA functions are comparable and better than the solutions from the LWN method because the LWN uses second derivatives, which makes it susceptible to noise in the data. In each diagram, the centre of each circle coincides with the location of the maximum for that function and the diameter of the circle is proportional to the depth estimate for the magnetic source point. A close examination of the maps obtained by HGM, ASA and LWN reveal the differences in the diagnostic attributes of the gradient functions.

The results obtained using HGM (Table 1) showed that the estimated depth ranges from 0.55 km to 2.49 km, which implied that the limit to shallow magnetic source depth is 0.72 km and the limit to deep magnetic source depth is 2.94 km (Figure 4).

The results obtained using analytic signal method (Table 2) showed that the estimated depth ranges from 0.57 km to 4.22 km, which implied that the limit to shallow magnetic source depth is 0.57 km and the limit to deep magnetic source depth is 4.22 km (Figure 5). The lines in the circles (Figures 4, 5 and 6) indicate the direction of strike, which suggest possible fault trend.

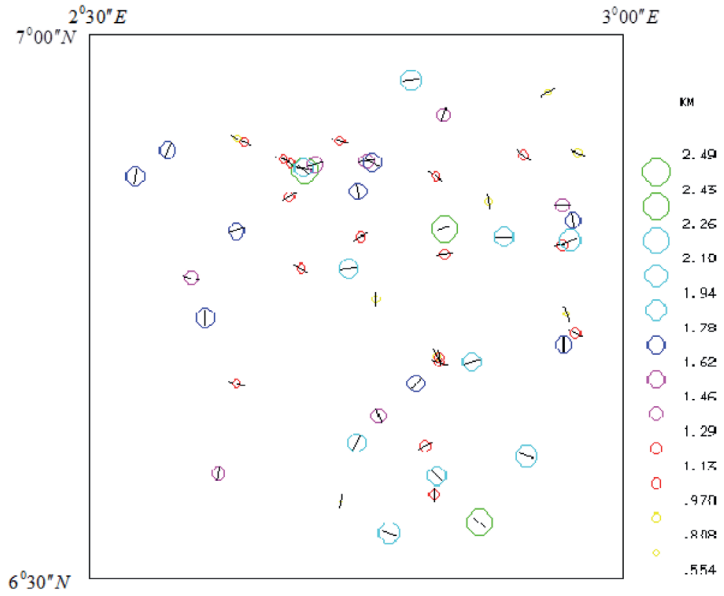

Figure 4: *Magnetic source depth estimated using the HGM (USGS Potential-Field software).*

Table 1: *Magnetic source depth parameters as Estimated by the HGM.*

Serial no.	Depth (km)	Percentage error in depth	Strike of contact
1	2.14	10.57	55.36
2	0.55	14.24	92.00
3	0.74	13.77	87.17
4	2.49	14.00	–83.30
5	1.20	9.96	88.90
6	1.32	8.57	83.20
7	1.70	3.29	101.78
8	1.23	6.66	93.88
9	1.22	12.09	87.40
10	1.00	9.91	91.32

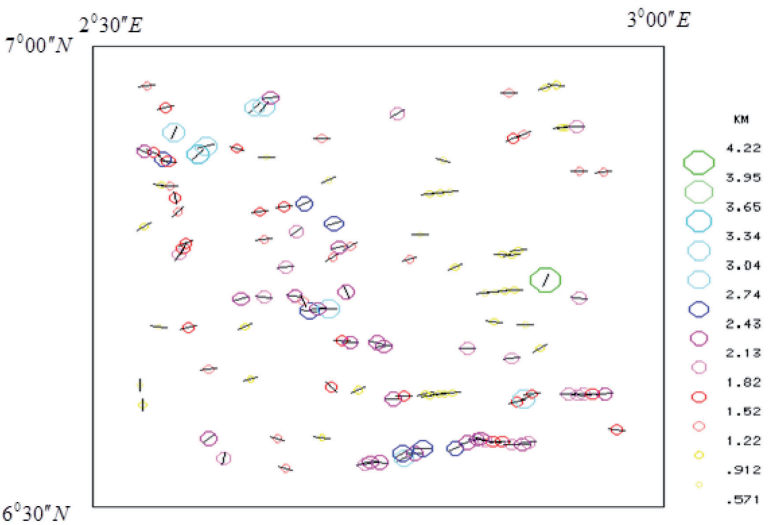

Figure 5: *Magnetic source depth estimated using the analytic signal method (USGS Potential-Field software).*

Table 2: *Magnetic source depth parameters as estimated by the analytic signal method.*

Serial no.	Depth (km)	Percentage error in depth	Strike of contact
1	3.49	10.19	–67.08
2	4.22	5.47	–60.25
3	2.17	8.22	80.96
4	1.76	4.55	99.52
5	1.17	6.82	114.50
6	0.57	14.65	95.98
7	4.04	8.72	–51.62
8	2.47	2.98	5.06
9	2.67	10.98	5.68
10	0.99	12.60	59.84

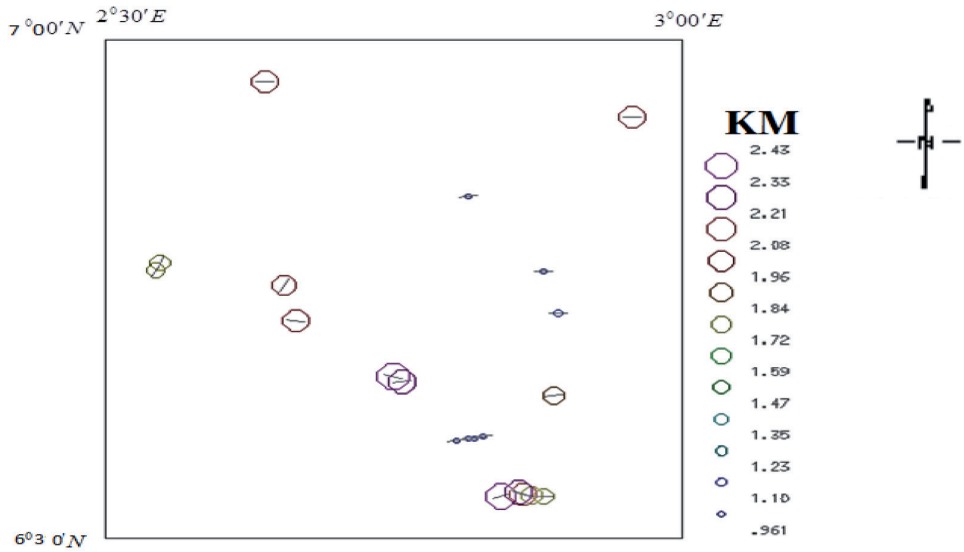

Figure 6: *Magnetic source depth estimated using the LWN method (USGS Potential–Field software).*

Table 3: *Magnetic source depth parameters as estimated by the LWN method .*

Serial no.	Depth (km)	% Error in depth	Strike of contact	Dip angle	Dip azimuth	Susceptibility contrasts
1	0.96	8.20	82.86	–7.14	485.25	0.00
2	1.91	13.23	79.04	–10.96	360.33	–0.003
3	0.99	13.66	81.43	–8.57	476.36	0
4	2.19	12.67	85.72	175.72	46.43	0
5	2.43	13.40	105.56	–164.44	160.93	0
6	2.14	13.99	100.67	–169.33	150.60	0
7	1.00	8.69	88.76	178.76	101.94	0
8	1.15	13.04	87.00	–3.00	394.13	0
9	2.26	5.16	83.83	173.83	158.71	0
10	1.15	13.04	87.00	–3.00	394.13	0

LWN was applied on the gridded data of the area under consideration. The results (Table 3) show that the estimated depth ranges from 0.96 km to 2.43 km, which implied that the limit to shallow source depth is 0.96 km and the limit to deep source depth is 2.43 km (Figure 6), and the susceptibility contrasts ranges from –0.001 to 0.001.

Conclusion

The study was carried out using the digitised aeromagnetic data of the entire Idogo area and its environs to map both the locations and the depths of the magnetic source edges as an aid to magnetic source interpretation. The data were analysed using advanced and suitable magnetic gradient interpretation techniques. These techniques were applied to gridded digitised data from aeromagnetic sheets that cover the study area in order to demonstrate their efficiency and accuracy in mapping the magnetic source edges.

These magnetic interpretation techniques include the RTP, ASA, HGM and LWN methods. The phase-shift effect in the total magnetic anomalies resulting from a non-vertical geomagnetic field vector was removed using RTP filtering, in which the intended effect is to move the anomaly peaks and gradients directly over their magnetic sources to aid in the interpretation.

The automated magnetic gradient interpretation methods were also used to estimate the locations and depths of magnetic sources. Since each automated method makes different assumptions about the magnetic sources, the use of several interpretational techniques was adopted to provide a reality check for the results. HGM, ASA and LWN methods were adopted for automatic estimation of the location and depth of magnetic sources. The estimated basement depth for Sheet No. 278 using HGM revealed a depth range of 0.55–2.49 km, while the ASA gave an estimated depth to the magnetic sources between the range of 0.57 km and 4.22 km. The LWN method revealed an estimated depth within the range of 0.96–2.47 km.

The location and depth to magnetic contacts were estimated from the maxima of the HGM, LWN and ASA functions of the total intensity magnetic data. The results of this study showed that the estimates of the depth limit to shallow magnetic contact obtained by the HGM and LWN methods are relatively close and comparable.

References

[1] Henry, L. (2010): Magnetic and Gravity Methods in Mineral Exploration: the Value of Well-Rounded Geophysical Skills. CSEG recorder, 27(2), pp. 31–35.

[2] Jose, R. (2009): Gravity and magnetic methods: Presented at "Short Course on Surface Exploration for Geothermal Resources", organized by UNU-GTP and LaGeo, in Ahuachapan and Santa Tecla, El Salvador, pp. 1–13.

[3] Roy, A. (1966): The method of continuation in mining geophysics. Geoexploration, 4, pp. 65–83.

[4] Mariita, N.O. (2007): The magnetic method. Presented at Short Course II on Surface Exploration for Geothermal Resources, organized by UNU-GTP and kenGen, at Lake Naivasha, Kenya, pp. 1–8.

[5] Lowrie W. (2004): Fundamentals of Geophysics. Swiss Federal institute of technology.

[6] Koulomzine, T., Lamontagne, Y., Nadeau, A. (1970): New methods for the direct interpretation of magnetic anomalies caused by inclined dykes of infinite length. Geophysics, 35, pp. 812–830.

[7] Asadi, H., Hale, M. (1999): Integrated analysis of aeromagnetic, Landsat TM and mineral occurrence data for epithermal gold exploration in northwest Iran.13th International Conference on Applied Geologic Remote Sensing, Vancouver. British Columbia.

[8] Chandler, V. (1990): Geological interpretation of gravity and magnetic data over the central part of the Duluth Complex northeastern Minnesota. Economic Geology, 85, pp. 861–829.

[9] Airo, M., Loukola-Ruskeeniemi, K. (2003): Characterization of sulfide deposits by airborne magnetic and gamma-ray responses in eastern Finland. Ore Geology Reviews, 24, pp.67–84.

[10] Kesse, G. (1985): The mineral and rock resources of Ghana. United States: A.A. Balkema Publishers, 610 p.

[11] El-Awady, M., El-etr, H., Bakrah, A. (1984): Aeromagnetic geophysical investigation in El-Faiyum district, western desert, Egypt. Qatar University Science Journal, 5, pp. 335–357.

[12] Slansky, M. (1962): Contribution a prelude geologique du basin sedimentaire cotier au Dahomey at du Togo.

Bulletin de la Société Géologique de France, 12, pp.18–31.

[13] Antolini, P. (1968): Eocene phosphate in the Dahomey Basin. Journal of Mining Geology, 17, pp. 17–23.

[14] Klemme, H.D. (1975): Geothermal Gradient Heat flow and hydrocarbon Recovery In: Fischer, A.G., Judson, S. (Eds.). Petroleum and Global Tectonics. Princeton University Press, pp. 251–304

[15] Burke, K.G, Dessauvagie, T.F.J, Whiteman, A.J. (1972): Geological history of the Benue Valley and adjacent areas. In: Burke, K.G., Whiteman, A.J. (Eds.). African Geology. Geology Dept., Univ. of Ibadan, Nigeria, pp. 188–205.

[16] Whiteman, A. (1982): Nigeria: Its Petroleum Geology, Resources and Potentials. 1 and 2, Graham and Trotham Limited: London, UK.

[17] Omatsola, M.E., Adegoke, O.S. (1981): Tectonic Evolution and Cretaceous Stratigraphy of Dahomey Basin. Journal of Mining and Geology, 18, pp. 130–137.

[18] Foss, C. (2011): Magnetic data Enhancement and Depth Estimation. Encyclopedia of Earth Sciences Series, pp. 736–746.

[19] Briggs, I. (1974): Machine contouring using minimum curvature. Geophysics, 39(1), pp. 39–48.

[20] Gunn, P., Maidment, D., Milligan, P. (1997): Interpreting aeromagnetic data in areas of limited outcrop. AGSO Journal of Australian Geology and Geophysics, 17(2), pp. 175–185.

[21] Li, X. (2008): Magnetic reduction-to-the-pole at low latitudes. Fugro Gravity and Magnetic Services. Houston, USA. Fugro.

[22] Luo, Y., Xue, D.J., Wang, M. (2010): Reduction to the Pole at the Geomagnetic Equator. Chinese Journal of Geophysics, 53(6), pp. 1082–1089.

[23] Philips, J. (1997): Potential-Field Geophysical Software for the PC, U.S.G.S. Open File Report, pp. 97–725.

[24] Sharma, P.V. (1976): Geophysical Methods in Geology, Elsevier Scientific Publishing Company, Amsterdam-Oxford-New York, 428 p.

[25] Thurston, J.B., Smith, R.S. (1997): Automatic conversion of magnetic data to depth, dip, and susceptibility contrast using the SPIÔ method. Geophysics, 62 (3), pp. 807–813.

[26] Jeng, Y., Lee, Y.L., Chen, C.Y., Lin, M.J. (2003): Integrated signal enhancements in magnetic investigation in archaeology. Journal of Applied Geophysics, 53, pp. 31–48.

[27] Taha R. (2009): Prospecting for the ferromagnetic mineral accumulations using the magnetic method at eastern desert. Egypt Geophysics Engineering, 6, pp. 401–411.

[28] Spector, A., Grant F.S. (1970): Statistical model for interpreting aeromagnetic data. Geophysics, 35, pp. 364–383.

[29] Onwuemesi, A. (1997): One-dimensional spectral analysis of aeromagnetic anomalies and Curie depth isotherm in the Anambra Basin of Nigeria. Journal of Geodynamics, 23(2), pp. 95–107.

[30] Bhattacharyya, B.K., Leu L.K. (1975): Spectral analysis of gravity and magnetic anomalies due to two dimensional structures. Geophysics, 40, pp. 993–1013.

[31] Bhattacharya, B.K., Leu, L.K. (1977): Spectral analysis of gravity and magnetic anomalies due to rectangular prismatic bodies, Geophysics, 42, pp. 41–50.

[32] Tanaka, A., Okubo, Y., Matsubayashi, O. (1999): Curie point depth based on spectrum analysis of the magnetic anomaly data in East and Southeast Asia. Tectonophysics, 306, pp. 461–470.

Original scientific paper

Received: May 17, 2018
Accepted: Nov 30, 2018
DOI 10.2478/rmzmag-2019-0009

Investigation of Land Use Types on Physical and Chemical Properties of Soil in a Basement Terrain

Raziskava vpliva uporabe zemljišča na fizikalne in kemijske lastnosti tal

Aderemi, A. Alabi[1], Johnson, O. Aina[1]*, Adebambo, O. Adewale[2] and Abass, A. Ajanaku[1]

[1] Department of Physics, Federal University of Agriculture, Abeokuta, Nigeria

[2] Department of Science Laboratory Technology, Moshood Abiola Polytechnic, Abeokuta, Nigeria

* Correspondence: Department of Physics, Federal University of Agriculture, Abeokuta, Nigeria;
e-mail: johntemini20@gmail.com

Abstract

We assessed the effect of different land use types on the physical and chemical properties of soil. We analysed three cases. Nine soil samples were taken at different depths (0–10, 10–20 and 20–30 cm) from three locations, namely, sawmill, dumpsite and market. Analyses were carried out to determine the influences on the physical and chemical properties of the soil. All the land types had considerably high sand contents, with minor silt and clay. Available phosphorus and the exchangeable bases were significantly ($p \leq 0.05$) affected by land use and soil depth. Moisture content ($p \leq 0.05$) was significantly affected by land use, while bulk density ($p \leq 0.01$) was significantly affected by soil depth. Soil organic matter and carbon were also generally low in all three locations. Consequently, ameliorative land management practices have to be adopted to prevent nutrient loss and land degradation.

Key words: land use, chemical properties, land degradation, bulk density, soil nutrient depletion.

Povzetek

Raziskali smo vpliv raznih tipov uporabe zemljišča na fizikalne in kemijske lastnosti tal. Analizirali smo tri primere. Devet vzorcev tal smo vzorčili v različnih globinah, 0–10, 10–20 in 20–30 cm na treh lokacijah, z območja žage, odlagališča odpadkov in tržnice. Namen analize je bil opredeliti vplive na fizikalne in kemijske lastnosti tal. Vsi trije tipi vsebujejo znatno količino peska in malo meljevca in gline. Uporaba zemljišča in globina statistično značilno ($p \leq 0.05$) vplivata na dostopni fosfor in izmenjevalne baze. Na vlago statistično značilno ($p \leq 0.05$) vpliva tip uporabe zemljišča, medtem ko ima statistično značilen ($p \leq 0.01$) vpliv na celotno gostoto tal globina vzorca. Organska snov in ogljik sta v vseh lokacijah splošno nizka. Sledi, da je potrebno s postopki melioracije omejiti izgubo hranil in degradacijo tal.

Ključne besede: uporaba zemljišča, kemijske lastnosti, degradacija zemljišča, celotna gostota, osiromašenje s hranili

Introduction

Nigeria, the most populous country in Africa, is faced with the evident problem of land degradation and soil infertility. Over the years, increase in population is leading to a noticeable modification in land use patterns. Enhanced land degradation processes have been attributed not only to rapid human population growth but also to associated escalation of land use [1]. Population increase poses different number of threats, including adequate food production, management of soil resources, meeting the challenges of intensive agriculture and adoption of appropriate technologies for sustainable agriculture production [2]. For successful soil management, it is imperative to understand the two determinant mechanisms, namely, the chemical properties (soil fertility) and physical properties of the soil. These properties are particularly important for both crop growth and soil quality maintenance [3]. Soil fertility is influenced by both land use and soil management practices, and it varies spatially from the field to larger scale of regions. High-quality soils not only produce better food and fibre but also help to maintain natural ecosystems, air quality and water quality [4].

A major indicator of the physical quality in agricultural soils is the soil water retention capacity; this includes soil parameters such as organic carbon content, dry bulk density, soil macroporosity, soil matrix porosity, air capacity, plant available water capacity and saturated hydraulic conductivity (K_{sat}) [5].

Various studies have been conducted to assess the effect of land use changes on physical and chemical properties of soil in Nigeria [1, 6, 7]. The research is directed towards providing adequate information on the effect of different land use patterns on the physical and chemical properties of soil in the study area.

Materials and methods

Description of the study area

The study was conducted in some selected parts of Abeokuta; the capital of Ogun State. Abeokuta lies between latitudes 7°00′ N to 7°30′ N and longitudes 3°00′ E to 3°30′ E [8]. The climatic condition of Abeokuta consists of high annual temperature, lack of cold season, high precipitation and low pressures.

Site selection, soil sampling and preparation

Planning, surveying and appropriate sampling must be considered when measuring changes in soil's chemical and physical spatial variation [4]. Soil samples were collected at different soil depths (0–10, 10–20 and 20–30 cm) from three different land areas (sawmill, market and dumpsite) located at Lafenwa, Osiele and Saje areas of Abeokuta (Figure 1). The samples were placed in black, leak-proof sealed columns to prevent evaporation and labelled accordingly. After 72 hours of air-drying, the dried samples were crushed and sieved using a 2 mm sieve.

Laboratory analysis

Laboratory analyses were carried out to determine the physical and chemical properties of the soil. These properties include soil pH, soil texture, bulk density, moisture content, hydraulic conductivity, total nitrogen, organic carbon and matter, available phosphorus (AvP), exchangeable bases (Ca, Mg, Na and K), exchangeable acidity and cation exchange capacity.

The soil pH was measured in 1:1 soil–water suspension using glass electrode pH meter. Soil texture was determined by the hydrometer method [9] after destroying organic matter and dispersing the soil using sodium hexametaphosphate, as described earlier [10]. The core method was used in determining the bulk density of the undisturbed soil sample after drying a defined volume of soil in an oven at 105°C to a constant weight. The bulk density was calculated as the ratio of the weight of oven-dried soil to the volume of the sampling core. The moisture content was calculated as the ratio of the weight of wet soil to that of oven-dried soil multiplied by the bulk density. Soil organic carbon was estimated using the wet oxidation method [11] and converted to organic matter by multiplying the percentage of organic carbon content by a factor of 1.724, assuming that organic matter is composed of 58% carbon [11].

The exchangeable basic cations (K^+, Ca^{2+}, Mg^{2+} and Na^+) were extracted with 1 M ammonium acetate at pH equal to 7.0. The cation exchange capacity (CEC) was calculated from the sum of

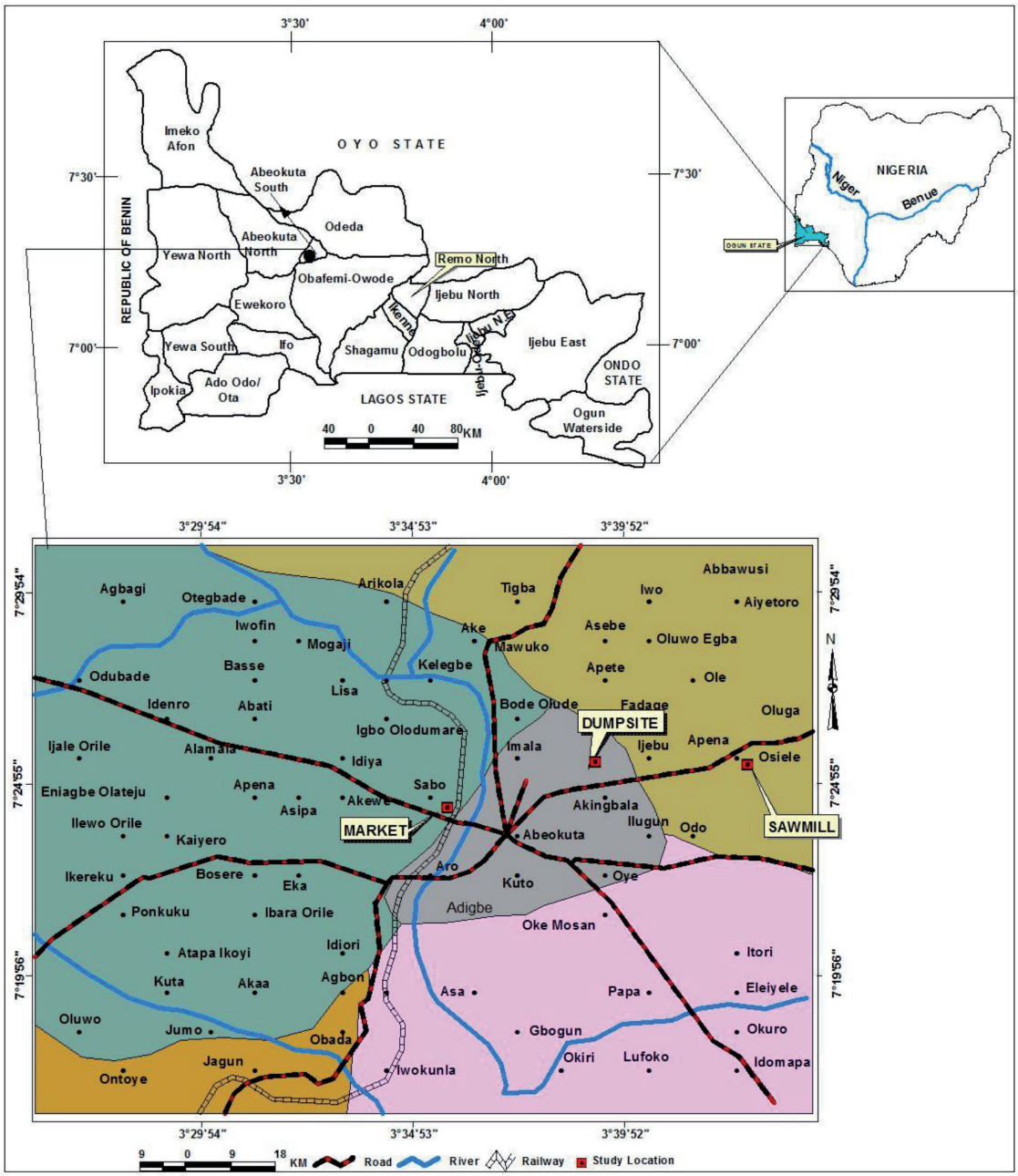

Figure 1: *Map of the study area showing sample locations.*

all exchangeable cations, which was expressed in centimoles (cmol) of charge per kilogram of air-dried soil. The Bray method [12] was used to determine the AvP. The soil samples were digested in a Kjeldahl apparatus, and the amount of ammonia trapped was determined to calculate the total nitrogen in the soils [13].

Data analysis

The univariate analysis of variance (ANOVA) procedure of IBM SPSS Statistics 20.0 software was used for assessing the significance of differences in the soil parameters. Separation of mean was done by the Tukey test after the main effects were found to be significant at $p \leq 0.05$. The analysis was done for each of the land use types in nine combined treatments. Pearson's

correlation analysis was also computed to determine the relationships between the various physical and chemical parameters of the soil.

Results and discussion

Physical properties of soil

The results of the analysis of the physical properties of soil across the three land use types located within the considered geological settings (Figure 2) at different depths are shown in Table 1. The particle size distribution data showed very high sand contents. Sand, clay and silt values were the same at all depths in the sawmill. The percentages of clay content had no definite sequence and did not follow a definite pattern down the profiles in the dumpsite and market place, while the silt content decreased with depth in the dumpsite but was distributed in irregular patterns in the market. The values for bulk density increased with depth across the three land use types. The values for saturated hydraulic conductivity (K_{sat}) were generally low across the three land use types but with no definite pattern down the soil profiles. The moisture content increased with depth in the market place, while it had no definite sequence in the distribution down the profile at the sawmill and dumpsite.

The results of two-way ANOVA and the mean values for the physical properties of soil across the three land use types are shown in Tables 2 and 3, respectively.

Table 1: *Physical properties of soil in the different land use types*

Land use	Depth (cm)	Sand (%)	Clay (%)	Silt (%)	TC	K_{sat} (cm/h)	BD)	MC (%)
Sawmill	0–10	79.2	17.4	3.4	SL	0.901	0.69	6.20
	10–20	79.2	17.4	3.4	SL	1.102	0.71	8.16
	20–30	79.2	17.4	3.4	SL	0.987	0.76	4.96
Dumpsite	0–10	77.2	17.4	5.4	SL	1.104	0.69	3.92
	10–20	79.2	16.4	4.4	SL	0.796	0.74	3.97
	20–30	79.2	17.4	3.4	SL	0.876	0.77	3.47
Market	0–10	81.2	17.4	1.4	SL	1.750	0.74	7.26
	10–20	79.2	15.4	5.4	SL	0.570	0.75	8.40
	20–30	73.2	24.4	2.4	SCL	0.859	0.75	9.26

Notes: *K_{sat} = saturated hydraulic conductivity; TC = textural class; BD = bulk density; MC = moisture content; SL = sandy loam; SCL = sandy clay loam.*

Table 2: *Two-way ANOVA result for the physical properties of soil in the selected land use types*

		MS	*F*	*p*-value	Sig
Sand	Depth	1.333	0.182	0.840	No
	Land use	4.00	0.545	0.617	No
Clay	Depth	3.444	0.496	0.642	No
	Land use	8.778	1.264	0.375	No
Silt	Land use	1.444	0.743	0.532	No
	Depth	1.444	0.743	0.532	No
Bulk density	Depth	0.0005	1.280	0.372	No
	Land use	0.002	5.120	0.079	No
Moisture content	Depth	15.478	11.547	0.022	Yes
	Land use	1.005	0.750	0.529	No
Hydraulic conductivity	Depth	0.014	0.105	0.903	No
	Land use	0.155	1.195	0.392	No

Notes: *MS = mean square; F = calculated value; p = probability; sig = significance.*

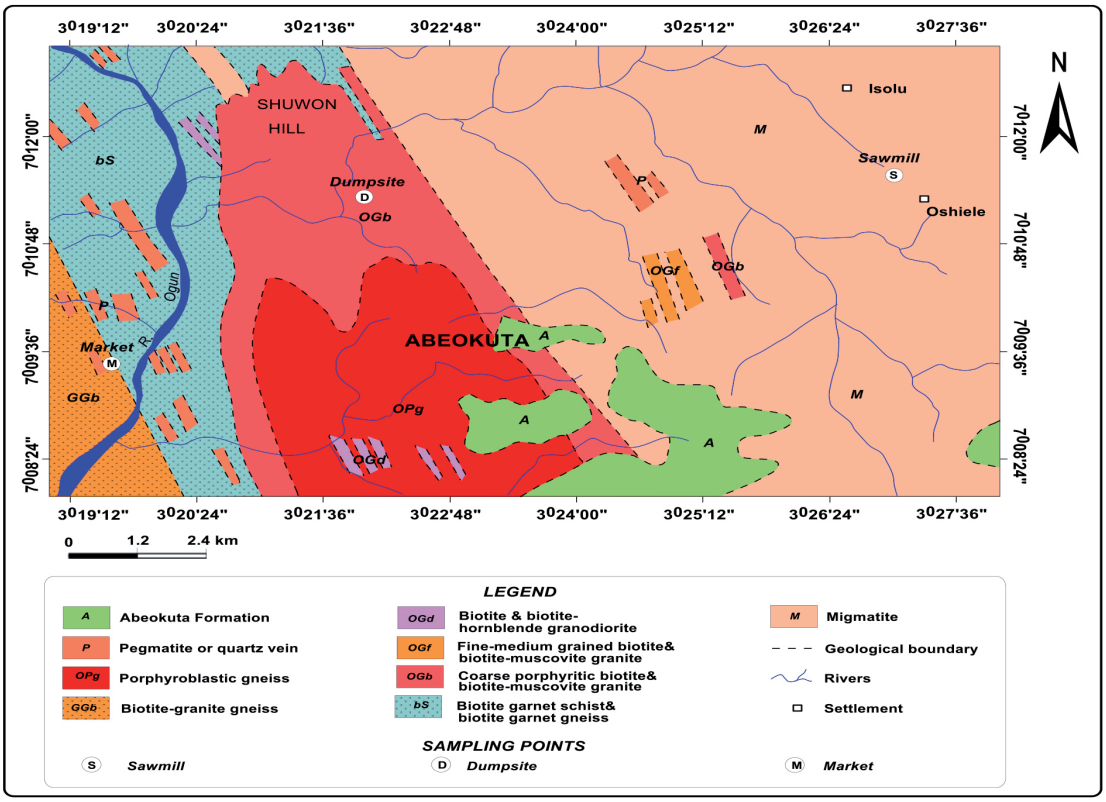

Figure 2: *Geological map showing the rock type that underlies the sampling point.*

Table 3: *Mean values of the physical properties of soils in the selected land use types*

Land use	Sand (%)	Silt (%)	Clay (%)	K_{sat} (cm/h)	BD (g/cm3)	MC (%)
Sawmill	79.200	3.400	17.400	0.997	0.720	6.440
Dumpsite	78.533	4.400	17.067	0.925	0.733	3.787
Market	77.867	3.067	19.067	1.060	0.747	8.307
SEM (±)	1.563	1.521	0.805	0.208	0.012	0.863

Notes: K_{sat} = *saturated hydraulic conductivity; BD = bulk density; MC = moisture content; SEM = standard error of the mean.*

The contents of sand, clay and silt were not significantly ($p > 0.05$) affected by land use and soil depths (Table 2). Considering the three land use types, the highest mean value of sand (79.20%) was recorded at the sawmill, while the lowest mean value of sand (77.87%) was observed at the market. This result is in agreement with previous findings [14] that soil with sand content >70% is highly permeable and allows large quantities of leachates to pass through. Silt fractions were the highest (4.40%) at the dumpsite, which may be due to the influence of organic waste, as stated by Elias and Gbadegesin [15], while its fractions were the lowest (3.07%) at the market. In contrast, the highest clay content (19.07%) was observed at the market place, whereas its lowest content (17.067%) was observed at the dumpsite (Table 3).

Bulk density was not significantly ($p > 0.05$) affected by land use and soil depth (Table 2). This may be due to differences in the organic matter content of the sites, as recorded by Olsen et al. [16]. Considering the mean values of the land uses, the highest bulk density (0.75 g/cm^3 was observed at the market. This may be because of the frequent movement of people during the market and normal days, which invariably lead to an increase in soil compaction; the low-

est value (0.72) was observed at the sawmill (Table 3).

Moisture content was significantly ($p \leq 0.05$) affected by land use but not by soil depth (Table 2), while K_{sat} was not significantly ($p > 0.05$) affected by land use and soil depth (Table 2). Considering the mean values of land use on hydraulic conductivity, the highest (1.06 cm/h) was recorded at the market place and the lowest (0.93 cm/h) was observed at the dumpsite (Table 3). This result is in agreement with the findings of Senjobi and Ogunkunle [1], who reported low and no definite sequence distribution within the profile in the investigated land use type.

Chemical properties of soil

The results from analysis of chemical properties of soils across the three land use types at different depths are shown in Tables 4 and 5.

The contents of organic carbon and organic matter followed no definite sequence down the profile across the three land use types. The AvP level decreased with depth across the three land use types. The pH of sawmill and market followed irregular patterns, while the pH for the dumpsite increased down the profile. This is in line with the study carried out by Mengistu et al. [4], who reported that the pH of soils in Warandhab area, Oromiya, Ethiopia, is affected by land use system and that it also increases with depth. Exchangeable acidity increased with depth in the market and dumpsite areas, while it decreased with depth in the sawmill. Total nitrogen decreased with depth in the sawmill, while it fluctuated irregularly with depth in the dumpsite and market place (Table 4). The effective CEC and exchangeable bases (Ca, Mg, Na and K) decreased with depth in all three land use types and were generally low in all land use types. Calcium and magnesium dominated the exchangeable complex in the three land use types (Table 5).

Soil pH was significantly ($p \leq 0.05$) affected by land use and not significantly ($p > 0.05$) affected by depth (Table 6). The soil pH was significantly higher (alkaline) in the dumpsite compared to that at other locations, which might be due to the presence of high inherent phosphorus contents of the parent material (the older granite). Considering the mean values of land use, the soil pH was observed to be the highest (9.23) at the dumpsite and lowest (7.37) at the sawmill (Table 7).

Exchangeable acidity was not significantly ($p > 0.05$) affected by land use and soil depth (Table 6). Considering the mean values of land use, the highest value (0.27 cmol/kg) for exchangeable acidity was recorded at the dumpsite, while its lowest value (0.13 cmol/kg) was recorded at the sawmill (Table 7).

Organic carbon was not significantly ($p > 0.05$) affected by either land or depth (Table 6). The mean values of land use on the variability of organic carbon were significantly higher (1.84%) in the market place and lower (1.42%) at the sawmill (Table 7). Organic carbon was generally low in all the three land use types, which may partly be due to the high temperature and high relative humidity, which favours rapid mineralisation.

Organic matter had values that ranged from 1.42% to 1.84%, considering the mean values of land use. Similar to organic carbon, organic matter was the highest in the market and lowest at the sawmill (Table 7). It was not significantly affected by land use and soil depth (Table 6).

AvP was significantly ($p \leq 0.05$) affected by land use and soil depth (Table 6). The mean values of land use on AvP were significantly higher (44.37 mg/kg) for the dumpsite than for other land use types. The lowest value (40.38 mg/kg) for AvP was recorded at the market place (Table 7). The content of phosphorus in all land use types was high when compared with the ratings for AvP [16]. The high phosphorus content in the three land use types might be due to the high phosphorus content of the parent material (the older granites).

Total nitrogen was significantly affected by land use ($p \leq 0.05$) but was not significantly ($p > 0.05$) affected by soil depth (Table 6). Nitrogen contents were medium at the sawmill and the market, but low in the dumpsite, when compared with the ratings for total nitrogen [17]. Intense mineralisation negatively affects the total nitrogen content in soils [18, 19], which may be the reason for the depletion of nitrogen content in the dumpsite.

Calcium was significantly ($p \leq 0.05$) affected by land use and soil depth (Table 8). Considering the mean values of land use, the calcium con-

Table 4: *Chemical properties of soils across the three land use types and depths*

Land use	Depth (cm)	OC (%)	OM (%)	AvP (mg/kg)	pH (H2O)	EA (cmol/kg)	TN (%)
Sawmill	0–10	1.756	3.027	45.21	7.2	0.2	0.199
	10–20	1.197	2.084	42.36	7.6	0.1	0.188
	20–30	1.317	2.269	38.45	7.3	0.1	0.170
Dumpsite	0–10	0.519	0.894	47.21	8.9	0.2	0.119
	10–20	3.471	5.985	45.67	9.3	0.3	0.109
	20–30	0.758	1.307	40.22	9.5	0.3	0.115
Market	0–10	1.317	2.269	44.58	8	0.1	0.123
	10–20	3.192	5.503	40.36	7.9	0.2	0.151
	20–30	0.998	1.719	36.21	7.7	0.3	0.144

Notes: *OC = organic carbon; OM = organic matter; AvP = available phosphorus; EA = exchangeable acidity; TN = total nitrogen.*

Table 5: *Chemical properties of soil across three land use types and depth*

Land use	Depth (cm)	Ca (cmol/kg)	Mg (cmol/kg)	Na (cmol/kg)	K (cmol/kg)	CEC (cmol/kg)
Sawmill	0–10	0.538	0.481	0.348	0.372	1.551
	10–20	0.518	0.446	0.283	0.321	1.939
	20–30	0.502	0.421	0.239	0.289	1.568
Dumpsite	0–10	0.524	0.469	0.370	0.449	1.551
	10–20	0.511	0.440	0.304	0.385	2.102
	20–30	0.489	0.412	0.261	0.295	1.940
Market	0–10	0.521	0.457	0.326	0.346	1.757
	10–20	0.503	0.423	0.283	0.308	1.750
	20–30	0.467	0.403	0.239	0.269	1.717

Note: *CEC = cation exchange capacity.*

Table 6: *Two-way ANOVA results of some chemical properties of soils in the selected land use types*

		MS	*F*	p-value	Sig
Soil pH	Depth	2.801111	47.12150	0.001658	Yes
	Land use	0.041111	0.691589	0.552132	No
Exchangeable acidity	Depth	0.013333	2.00000	0.250000	No
	Land use	0.003333	0.50000	0.640000	No
Organic carbon	Depth	0.129707	0.137959	0.875107	No
	Land use	2.300031	2.446357	0.202326	No
Organic matter	Depth	0.378277	0.136387	0.876395	No
	Land use	6.877982	2.479849	0.199312	No
Available phosphorus	Depth	12.03588	22.28408	0.006783	Yes
	Land use	41.44148	76.72769	0.000645	Yes
Total nitrogen	Depth	0.00393	18.66051	0.009371	Yes
	Land use	$3.08e^{-05}$	0.146136	0.868452	No

Notes: *ANOVA = analysis of variance; MS = mean square; F = calculated value; p = probability; Sig = significance.*

tents were the highest (0.52 cmol/kg) in the sawmill and the lowest (0.50 cmol/kg) at the market (Table 9). Magnesium was significantly ($p \leq 0.05$) affected by land use and soil depth (Table 8). The contents of magnesium in all the three land use types were significantly different from each other, which implies that the activities of the three land use types had significant effects on magnesium. This result is in line with a previous study [20], which stated that increase in calcium and magnesium contents in a sawmill is due to ashing from sawdust.

Table 7: *Mean values of some chemical properties of soils in the selected land use types*

Treatments	OC (%)	OM (%)	AvP (mg/kg)	pH (H2O)	EA (cmol/kg)	TN (%)
Sawmill	1.423	2.460	42.001	7.367	0.133	0.186
Dumpsite	1.583	2.729	44.367	9.233	0.267	0.114
Market	1.836	3.164	40.383	7.867	0.200	0.139
SEM (±)	0.560	0.962	0.424	0.141	0.047	0.008

Notes: *OC = organic carbon; OM = organic matter; AvP = available phosphorus; EA = exchangeable acidity; TN = total nitrogen; SEM = standard error of the mean.*

Table 8: *Two-way ANOVA result for the exchangeable bases (Ca, Mg, Na and K) and CEC*

		MS	*F*	*p*-value	Sig
Calcium	Depth	0.001317	33.95702	0.003094	Yes
	Land use	0.000374	9.647564	0.029484	Yes
Magnesium	Depth	0.002454	412.8411	2.32E-05	Yes
	Land use	0.000355	59.79439	0.001048	Yes
Sodium	Depth	0.007803	141.5948	0.000194	Yes
	Land use	0.000682	12.37702	0.019352	Yes
Potassium	Depth	0.008218	16.40523	0.011808	Yes
	Land use	0.003751	7.488743	0.044427	Yes
CEC	Depth	0.056972	5.132951	0.078618	No
	Land use	0.054687	4.927053	0.083361	No

Note: *MS = mean square; F = calculated value; p = probability; Sig = significance; CEC = cation exchange capacity.*

Table 9: *Mean values of the exchangeable bases and the CEC of soils in the selected land use type*

Treatments	Ca	Mg	Na	K	CEC
Sawmill	0.519	0.449	0.290	0.327	1.686
Dumpsite	0.508	0.440	0.312	0.376	1.933
Market	0.497	0.428	0.283	0.308	1.715
SEM (±)	0.004	0.001	0.004	0.013	0.061

Notes: *CEC = cation exchange capacity; SEM = standard error of the mean.*

Sodium was significantly ($p \leq 0.05$) affected by land use and soil depth (Table 8). The sodium content in the dumpsite was significantly different from that in other land use types, which implies that the activities at the dumpsite had a more significant effect on the sodium content than the activities in other land use types. Potassium was significantly ($p \leq 0.05$) affected by land use and soil depth (Table 8). The exchangeable bases were generally low in the three land use types when compared with the ratings for exchangeable bases [21, 22]. The depletion in exchangeable bases may be attributed to leaching of nutrients and weathering, which consequently leads to inherent low fertility status.

The effective CEC was not significantly ($p > 0.05$) affected by either land use or soil depth (Table 8). The result of this study is in line with the result of a previous study [23], which showed that the CEC was the highest in the dumpsites relative to the soils of fallow and cropped lands.

Pearson's correlation matrix for the various physical and chemical properties of soil

Table 10 shows that sand was significantly ($p \leq 0.01$) and negatively correlated with clay, with correlation coefficient $r = -0.861$, and significantly ($p \leq 0.01$) negatively correlated with clay, with correlation coefficient $r = -0.86$. Soil

Table 10: *Pearson's correlation and p-value matrix for the various physical and chemical properties of soil*

		P	Na	K	Ca	Mg	TN	PH	OC	OM	Sand	Clay	Silt	EA	K_{sat}	BD	MC	CEC
P	Pearson correlation	1	0.930**	0.937**	0.850**	0.880**	−0.182	0.319	0.137	0.137	0.469	−0.555	0.284	0.119	0.336	−0.704*	−0.443	0.253
	p-value		0.000	0.000	0.004	0.002	0.639	0.403	0.725	0.724	0.203	0.121	0.458	0.760	0.376	0.034	0.233	0.512
Na	Pearson correlation	0.930**	1	0.920**	0.826**	0.923**	−0.082	0.151	−0.002	−0.002	0.297	−0.397	0.268	0.041	0.336	−0.809**	−0.268	0.051
	p-value	0.000		0.000	0.006	0.000	0.834	0.699	0.996	0.995	0.437	0.290	0.485	0.917	0.377	0.008	0.486	0.897
K	Pearson correlation	0.937**	0.920**	1	0.727*	0.813**	−0.244	0.345	0.046	0.046	0.199	−0.401	0.445	0.172	0.211	−0.746*	−0.483	0.027
	p-value	0.000	0.000		0.027	0.008	0.526	0.363	0.906	0.907	0.608	0.285	0.230	0.659	0.586	0.021	0.188	0.946
Ca	Pearson correlation	0.850**	0.826**	0.727*	1	0.945**	0.300	−0.148	0.113	0.114	0.640	−0.653	0.182	−0.250	0.350	−0.752*	−0.236	0.165
	p-value	0.004	0.006	0.027		0.000	0.433	0.705	0.773	0.771	0.063	0.057	0.640	0.516	0.356	0.019	0.541	0.672
Mg	Pearson correlation	0.880**	0.923**	0.813**	0.945**	1	0.235	−0.130	−0.036	−0.035	0.406	−0.408	0.104	−0.198	0.411	−0.874**	−0.187	0.108
	p-value	0.002	0.000	0.008	0.000		0.542	0.739	0.927	0.928	0.279	0.276	0.790	0.610	0.272	0.002	0.629	0.781
TN	Pearson correlation	−0.182	−0.082	−0.244	0.300	0.235	1	−0.858**	−0.050	−0.048	0.038	0.017	−0.098	−0.534	−0.136	−0.377	0.452	0.027
	p-value	0.639	0.834	0.526	0.433	0.542		0.003	0.898	0.902	0.922	0.966	0.801	0.139	0.727	0.317	0.222	0.945
PH	Pearson correlation	0.319	0.151	0.345	−0.148	−0.130	−0.858**	1	0.061	0.060	0.061	−0.217	0.322	0.754*	−0.096	0.213	−0.668*	0.281
	p-value	0.403	0.699	0.363	0.705	0.739	0.003		0.877	0.878	0.877	0.574	0.397	0.019	0.806	0.582	0.049	0.465
OC	Pearson correlation	0.137	−0.002	0.046	0.113	−0.036	−0.050	0.061	1	10.000**	0.285	−0.439	0.373	0.310	−0.462	0.155	0.083	0.468
	p-value	0.725	0.996	0.906	0.773	0.927	0.898	0.877		0.000	0.457	0.237	0.323	0.417	0.211	0.690	0.831	0.204
OM	Pearson correlation	0.137	−0.002	0.046	0.114	−0.035	−0.048	0.060	10.000**	1	0.286	−0.440	0.373	0.309	−0.462	0.154	0.084	0.470
	p-value	0.724	0.995	0.907	0.771	0.928	0.902	0.878	0.000		0.456	0.236	0.322	0.419	0.211	0.692	0.829	0.202
Sand	Pearson correlation	0.469	0.297	0.199	0.640	0.406	0.038	0.061	0.285	0.286	1	−0.861**	−0.029	−0.191	0.359	0.000	−0.302	0.288
	p-value	0.203	0.437	0.608	0.063	0.279	0.922	0.877	0.457	0.456		0.003	0.942	0.623	0.342	10.000	0.430	0.452
Clay	Pearson correlation	−0.555	−0.397	−0.401	−0.653	−0.408	0.017	−0.217	−0.439	−0.440	−0.861**	1	−0.484	−0.035	0.015	0.127	0.432	−0.214
	p-value	0.121	0.290	0.285	0.057	0.276	0.966	0.574	0.237	0.236	0.003		0.186	0.929	0.969	0.745	0.245	0.581
Silt	Pearson correlation	0.284	0.268	0.445	0.182	0.104	−0.098	0.322	0.373	0.373	−0.029	−0.484	1	0.396	−0.647	−0.249	−0.330	−0.075
	p-value	0.458	0.485	0.230	0.640	0.790	0.801	0.397	0.323	0.322	0.942	0.186		0.292	0.060	0.518	0.386	0.847
EA	Pearson correlation	0.119	0.041	0.172	−0.250	−0.198	−0.534	0.754*	0.310	0.309	−0.191	−0.035	0.396	1	−0.574	0.180	−0.494	0.498
	p-value	0.760	0.917	0.659	0.516	0.610	0.139	0.019	0.417	0.419	0.623	0.929	0.292		0.106	0.643	0.176	0.172
K_{sat}	Pearson correlation	0.336	0.336	0.211	0.350	0.411	−0.136	−0.096	−0.462	−0.462	0.359	0.015	−0.647	−0.574	1	−0.173	0.033	−0.209
	p-value	0.376	0.377	0.586	0.356	0.272	0.727	0.806	0.211	0.211	0.342	0.969	0.060	0.106		0.657	0.933	0.590
BD	Pearson correlation	−0.704*	−0.809**	−0.746*	−0.752*	−0.874**	−0.377	0.213	0.155	0.154	0.000	0.127	−0.249	0.180	−0.173	1	0.000	−0.031
	p-value	0.034	0.008	0.021	0.019	0.002	0.317	0.582	0.690	0.692	10.000	0.745	0.518	0.643	0.657		0.999	0.938
MC	Pearson correlation	−0.443	−0.268	−0.483	−0.236	−0.187	0.452	−0.668*	0.083	0.084	−0.302	0.432	−0.330	−0.494	0.033	0.000	1	−0.101
	p-value	0.233	0.486	0.188	0.541	0.629	0.222	0.049	0.831	0.829	0.430	0.245	0.386	0.176	0.933	0.999		0.795
CEC	Pearson correlation	0.253	0.051	0.027	0.165	0.108	0.027	0.281	0.468	0.470	0.288	−0.214	−0.075	0.498	−0.209	−0.031	−0.101	1
	p-value	0.512	0.897	0.946	0.672	0.781	0.945	0.465	0.204	0.202	0.452	0.581	0.847	0.172	0.590	0.938	0.795	

Notes: *K_{sat} = saturated hydraulic conductivity; BD = bulk density; MC = moisture content; CEC = cation exchange capacity; OC = organic carbon; OM = organic matter; AvP = available phosphorus; EA = exchangeable acidity; TN = total nitrogen. **Correlation is significant at the 0.01 level (two tailed); *correlation is significant at the 0.05 level (two tailed). Others are not significant at the 0.01 and 0.05 levels (two tailed).*

bulk density was significantly ($p \leq 0.05$) negatively correlated with AvP. Moisture content was moderately ($p \leq 0.05$) negatively correlated with soil pH, with $r = -0.67$. Soil pH was significantly ($p \leq 0.01$) negatively correlated with total nitrogen, with r=–0.86. AvP was significantly ($p \leq 0.01$) and strongly positively correlated with potassium, calcium, magnesium and sodium, with $r = 0.94$, 0.85, 0.88 and 0.93, respectively. AvP was also significantly ($p \leq 0.05$) positively correlated with the CEC, with $r = 0.77$, which implies that as the AvP increases, the contents of sodium, potassium, calcium and magnesium in the soil increase, as does the effective CEC.

Conclusion

It was observed that soil nutrients vary from one land use type to another. The results of this study suggest that the three land use types have high sand contents. Findings from the study revealed that soil properties, such as pH, AvP, Ca, Na, K and TN, are influenced by land use at the different depths considered. Soil nutrient depletion was also observed to be very prominent across all the three land use types. AvP and exchangeable bases (such as Ca, Mg, Na and K) were observed to be significantly affected by land use with respect to soil depth. It was observed that the pH of the dumpsite was very high/strongly alkaline compared to that at the other land use types; this may be attributed to the high content of AvP in the dumpsite. Nitrogen contents were generally low in the dumpsite and the market place but were found in medium quantities at the sawmill. Soil nutrient depletion was observed to be predominant in all the three land use types. Therefore, ameliorative land management practices must be put in place to help prevent nutrient loss and land degradation.

Acknowledgement

The authors are grateful to the Department of Civil Engineering, Federal University of Agriculture Abeokuta, Ogun State, Nigeria, for permitting the use of their laboratory to carry out this study.

References

[1] Senjobi, B.A and Ogunkunle, A. O. (2011). Effect of Different Land Use Types and Their Implication on Land Degradation and Productivity in Ogun, Nigeria. *Journal of Agricultural Biotechnology and Sustainable Development,* 3(1): 7–18.

[2] Ufot, U.O., Iren, O.B. and Chikere Njoku, C.U. (2016). Effects of Land Use on Soil Physical and Chemical Properties in Akokwa Area of Imo State, Nigeria. *International Journal of Life Science and Scientific Resources,* 2(3): 273–278.

[3] Gol (2009). Effects of Land Use Change on Soil Properties and Organic Carbon at Dagdami River Catchment in Turkey. *Journal of Environmental Biology*, 30: 825–830.

[4] Mengistu, C., Kibebew, K., Tarekegn, F. (2017). Influence of Different Land Use Types and Soil Depths on Selected Soil Properties Related to Soil Fertility in Warandhab Area, Horo Guduru Wallaga Zone, Oromiya, Ethiopia. *International Journal of Environmental Sciences and Natural Resources,* 4(2): 001–011.

[5] Ágota H., Eszter T., Györgyi G., Ilona K., Zsófia B., and Csilla F.(2015). Effects of Land Use and Management on Soil Hydraulic Properties. De Gruyter Open Geoscience, 1:742–754.

[6] Offiong, I. (2009). Effects of Land Use Change on Soil Physico-Chemical Properties in a South-Southern Nigeria. *African Journal of Environmental Pollution and Health,* 7: 47–51.

[7] Deekor, T.N., Iwara, A.I., Ogundele, F.O., Amiolemen, S.O. and Ita, A. E. (2012). Changes in Soil Properties under Different Land Use Covers in Parts of Odukpani, Cross River State, Nigeria. *Journal of Environmental and Ecology,* 3 (1): 86–99. 3 (1).

[8] Olurin, O.T., Ganiyu, S.A., Hammed, O.S. and Aluko, T.J. (2016). Interpretation of Aeromagnetic Data over Abeokuta and its Environs, Southwest Nigeria, using Spectral Analysis (Fourier Transform Technique). *RMZ – Materials and Geoenvironment*, (63): 199– 212. *RMZ – M&G*,

[9] Bouyoucos (1951). A Recalibration of the Hydrometer Method for Making Mechanical Analysis of Soils. *Agronomy Journal*, 43: 434–438.

[10] Dane, J.H and Topp, G.C. (2002). Methods of Soil Analysis. Part 4: Physical Methods. *Soil Science Society of America*, 51: 980–1115.

[11] Walkley, A. and Black, C.A. (1934): An Examination of the Degtjareff Method for Determining Soil Organic Matter and a Proposed Modification of the Chromic Acid Titration Method. Soil Science, 37: 2938.

[12] Bray, R.H. and Kurtz, L.T. (1945): Determination of Total, Organic and Available Forms of Phosphorus in Soils. *Soil Science*, 59: 39–45.

[13] Bremner (1996). Nitrogen-total in Sparks, D., Page, A., Helmke, P., Loeppert, R., Soltanpour, P., Tabatabai, M., Johnston, C., and Sumner, M. Methods of Soil Analysis, Part 3- Chemical Methods. Soil Science Society of America, USA, pp. 1085–1121.

[14] Anikwe, M.A.N. and Nwobodo, K.C.A. (2002). Long Term Effect of Municipal Waste Disposal on Soil Properties and Productivity of Sites used for Urban Agriculture in Abakaliki, Nigeria. *Bioresources Technology*, 83: 241–250.

[15] Elias, P. and Gbadegesin, A. (2011). Spatial Relationships of Urban Land Use, Soils and Heavy Metal Concentrations in Lagos Mainland Area. *Journal of Applied Science and Environmental Manage*ment, 15 (2): 391–399.

[16] Olsen, S.R., Cole, C.V., Watanable, F.S. and Dean, L.A. (1954). Estimation of Available Phosphorus in Soil by Extraction with Sodium Bicarbonate. *USDA Circular*, 939: 1–19.

[17] Berhanu D (1980). The Physical Criteria and Their Rating Proposed for Land Evaluation in the Highland Region of Ethiopia. Land Use Planning and Regulatory Department, MoA, Addis Ababa, Ethiopia 8(3): 1990–6145.

[18] Senjobi, B.A. (2007). Comparative Assessment of the Effect of Land Use and Land Type on Soil Degradation and Productivity in Ogun State, Nigeria. Published Ph.D. Thesis submitted to the Department of Agronomy, University of Ibadan, Ibadan, Nigeria. pp. 161. Ibadan,

[19] Senjobi, B.A. and Ogunkunle, O.A. (2010). Effect of Land Use on Soil Degradation and Soil Productivity Decline on Alfisols and Ultisols in Ogun State in Southern Western Nigeria. *Journal of Agricultural Conspectus Science*, 75(1): 9–19.

[20] Owolabi, O., Adeleye, A., Oladeje, B.T. and Ojeniyi, S.O. (2003). Effect of Wood Ash on Soil Fertility and Crop Yield in Southwest Nigeria. *Nigeria Journal of Soil Science*, 13: 55–60.

[21] R. N. Roy, A. Finck, G. J. Blair, and H. L. S. Tandon, FAO Fertilizer and Plant Nutrition Bulletin 16. Plant Nutrition for Food Security. A Guide for Integrated Nutrient Management, FAO, Rome, Italy, 2006 Rome, Italy.

[22] Landon, J.R. (1991). Booker Tropical Soil Manual. Longman Scientific and Technical Essex, UK. pp. 474.

[23] Okonkwo, C.I., Arinzechukwu, P. and Njoku, C. (2013). Changes in Physical and Chemical Properties of Soil in Timber Sawmill Dumpsite in Abakaliki, Abakaliki Southeastern, Nigeria. *British Journal of Environment and Climate Change,* 3(2): 215–228.

Original scientific paper

Received: May 27, 2017
Accepted: Apr 09, 2018
DOI: 10.2478/rmzmag-2018-0020

High resolution airborne radiometric and magnetic studies of ilesha and its environs, southwestern Nigeria

Visokoločljivostna aeroradiometrična in aeromagnetna raziskava območja ilesha in okolice v jugozahodni nigeriji

Okeyode I. C.[1], Olurin O. T.*[,1], Ganiyu S. A. and Olowofela J. A.[1]

[1] Department of Physics, Federal University of Agriculture, P. M. B. 2240, Abeokuta Ogun State Nigeria

* stolurin@yahoo.com

Abstract

The study of the nature of distribution of natural radioelements in Ilesha and its environs with its geological structure has been studied using aeroradiometric data. Aeromagnetic data have also been subjected to three automated gradient techniques to delineate the subsurface structure of the study area. From the study, it can be found that maximum values of "eU" (ppm) and "eTh" (ppm) fall within the branded gneiss, whereas the maximum value of K (%) falls within porphyritic granite regions. eTh had the highest radioactive content. The environmental dose rate of Ilesha was between 0.1817 and 3.9296 msv/yr. Although there were extreme values, but the mean dose rate was 0.522 ± 0.310 msv/yr (within acceptable safe limit of 1.0 msv/yr). eU/K, eU/eTh and eTh/K ratios were analysed for enrichment or depletion of radioisotopes. eU/eTh >1 showed uranium depletion, while eTh >2 showed eTh enrichment. The magnetic intensity values ranged from -79.41 to 140.93 nT. The horizontal gradient method (HGM) and analytic signal amplitude (ASA) revealed that depth to magnetic sources ranged from 0.478 to 4.112 km and 0.348 to 2.551 km, respectively, whereas local wavenumber (LWN) depth ranged from 0.478 to 5.48 km, which overestimated those compared using HGM and ASA functions. The apparent susceptibility ranged from -0.00325 to 0.00323 SI, showing that ferromagnetic and diamagnetic mineral ranges control apparent susceptibility in Ilesha.

Key words: Aeromagnetic data, Apparent Susceptibility, Background Radiation Doses, Ilesha, Radiometric Data

Povzetek

Lastnosti porazdelitve naravnih radioaktivnih prvin in geološko zgradbo na območju Ilesha in okolice so proučevali z aeroradiometričnimi podatki. Za raziskavo globinske geološke zgradbe proučevnega ozemlja so uporabili tudi aeromagnetne meritve po treh avtomatskih gradientnih metodah. Iz študije sledi, da izkazujejo najvišje vrednosti "eU" (ppm) in "eTh" (ppm) območja izdankov gnajsa, največje vrednosti K (%) pa območja porfiritnega granita. Najvišje so vrednosti radioaktivnega eTh. Radioaktivna doza ozadja v Ileshiu se giblje med 0,1817 in 3,9296 mSv/a. Nastopajo ekstremne vrednosti, toda povprečna doza ozadja znaša 0,522 ± 0,310 mSv/a (znotraj sprejemljive meje 1,0 mSv/a). Z analizo razmerij eU/K, eU/eTh in eTh/K so ugotavljali obogatitve ali osiromašenja radioaktivnih izotopov; vrednost eU/eTh >1 nakazuje osiromašenje z uranom, eTh, ki je večja od 2, pa obogatitev z eTh. Vrednosti magnetne intenzitete se gibljejo med -79,1 in – 140.93 nT. Metodi horizontalnega gradienta (HGM) in amplitude analitskega signala (ASA) nakazujeta globine do virov magnetizma v razponih 0,478–4,112 km in ustrezno 0,348–2,551 km, medtem ko je razpon globin z metodo Local Wavenumber (LWN) od 0,478 do 5.48 km, kar je precenjeno glede na rezultate HGM in ASA. Navidezna susceptibilnost se giblje v razponu od -0.00325 do – 0.00323 SI, kar kaže, da je susceptibilnost v Ileshu odvisna od feromagnetnih in diamagnetnih mineralov.

Ključne besede: aeromagnetni podatki, navidezna susceptibilnost, radiacijske doze ozadja, Ilesha, radiometrični podatki

Introduction

Since the time radioactivity has been discovered, more efforts have been put into the study of the environmental natural radiation [1]. Calculations of equivalent doses from natural environments have recently been possible through ground and airborne gamma-ray surveys [2–4]. Air-borne gamma ray spectrometry measures natural emission of gamma radiation from the surface of the earth. Thorium-232 and uranium-238 decay series as well as potassium-40 are the natural radionuclides that are used for estimating the abundance of thorium, uranium and potassium in airborne radiometric surveys. Having the image of gamma rays emanating from the surface of the earth is as good as having the surface geochemical map that shows how radionuclides in rocks, soil, etc. spread [5]. Airborne geophysical survey has been a very useful tool available to Earth scientists in interpreting geology of difficult terrain [6]. The broad view of the Earth that the airborne geophysics perspective provides has been well recognised since the early days of balloon photography and military reconnaissance [7]. Aeromagnetic survey has proved essential in displaying the spatial distribution and relative abundance of magnetic minerals and nonmagnetic minerals in the upper levels of the crust, which can help in the visualisation of the geology and geological structures of the upper crust of the earth [6]. The aim of this study was to use high-resolution airborne radiometric data of Ilesha to assess and quantify naturally occurring radioactive materials in order to estimate background radiological doses of the area and correlate the data with the geological map of the area to show the distribution of the radioelements with geology. In addition, the aim of this study was to use aeromagnetic data to estimate source parameters (source location, depth and apparent magnetic susceptibility contrast) from the grid in conjunction with the local geomagnetic field parameters associated with the area under consideration using automated magnetic gradient techniques in accordance with [8].

Description and Geology of the Study Area

Ilesha is a popular town in Osun State, south western Nigeria. This city serves as a major linked way to the northern, southern and eastern parts of Nigeria. The area has remarkable agricultural potentials with production of major food crops, which include but are not limited to oil palm, cocoa, pumpkin, cotton and cola nut. Different minerals and most especially gold in commercial quantities are also available. Gold mining is one of the occupations of some artisans in Ilesha and its environs. This kind of activity has been identified with high concentrations of uranium [9]. The study cover area located between latitude 7°30´N to 8°00´N and longitude 4°30´E to 5°00´E. Ilesha and its environs lie within the basement complex (schist belt) of southwest Nigeria, which is of Precambrian age [10,11]. In 1947 and 1957, [12] and [13], respectively, suggested that the Nigerian basement complex is polycyclic. This was confirmed by Hurley [14] who used radiometric method to determine the age of the rocks. The uniqueness of this terrain is evident by complex coexistences of basement and sedimentary rock, and the contact between the two rock types is often poorly defined. The basement complex rocks of Pre-Cambrian age are made up of older and younger granites, with the younger and older sedimentary rocks (formation) of both tertiary and secondary ages. The formation is pre-drift sequence of continental sands, grits and silts (Figure 1).

In terms of structural features, lithology and mineralisation, the schist belts of Nigeria show considerable similarities to the Achaean greenstone belts. However, the latter usually contain much larger proportions of mafic and ultramafic bodies and assemblages of lower metamorphic grade [11,15]. Rocks in this area are structurally divided into two main segments by two major fracture zones often called the Iwaraja faults in the eastern part and the Ifewara faults in the western part [16,17]. The western part of the fault comprises mostly amphibolites, amphiboles schists, metaultramafites and metapelites. Extensive psammitic units with minor metapelites constitute the eastern segment. These are found as quartzites and quartz schists. All these assemblages are associated with migmatitic gneisses and are cut by a variety of granitic bodies [11]. The rocks of Ilesha district is broadly grouped into gneiss–migmatite complex, mafic–ultramafic suite (or

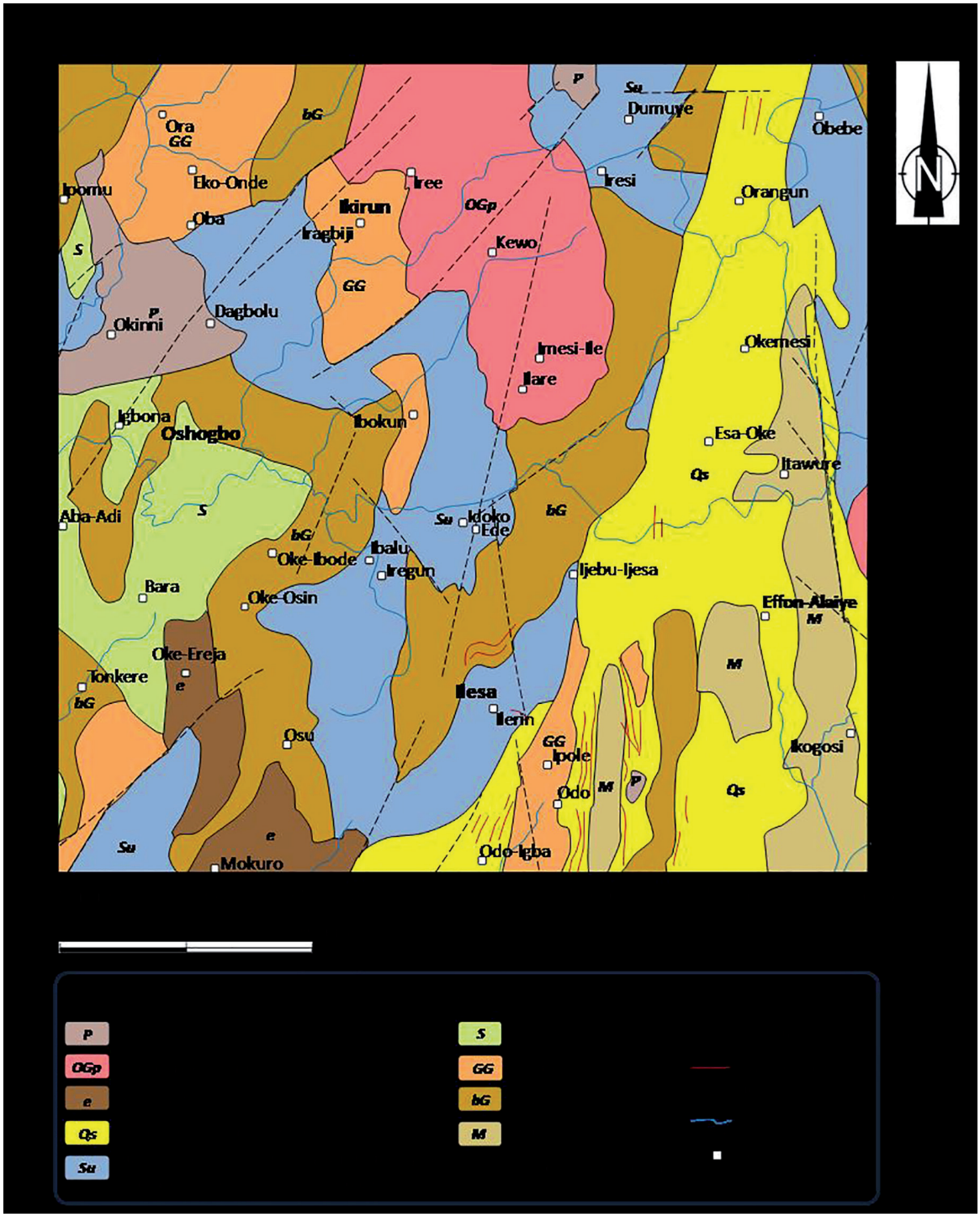

Figure 1: *Geological map of Ilesha and its environs.*

amphibolite complex), meta-sedimentary assemblages and intrusive suite of granitic rocks. A variety of minor rock types are also related to these units. The gneiss–migmatite complex comprises migmatitic and granitic, calcareous and granulitic rocks. The mafic–ultramafic suite is mainly composed of amphibolites, amphibole schists and minor meta-ultramafites made up of anthophyllite–tremolite–chlorite and talc schists. The meta-sedimentary assemblages,

chiefly metapelites and psammitic units, are found as quartzites and quartz schists. The intrusive suite consists essentially of Pan-African granitic units. The minor rocks include garnet–quartz–chlorite bodies, biotite–garnet rock, syenitic bodies and dolerites [11,16,18].

Instrumentation and Data Collection

The airborne radiospectrometric and magnetic data of Ilesha sheet number 243 on scale 1:50,000 were surveyed by the Nigerian Geological Survey Agency in 2009. The airborne potential field data were acquired at a mean altitude of 80 m with flight line separation of 400 m along the northwest–southeast direction. The aircraft travelled at the airspeed between 150 and 250 km/h, which covered the entire area under consideration. The flight line direction was in the direction 135° azimuths, while the tie line direction was in 45°. The average magnetic inclination and declination across the survey were -9.67° and -2.52°, respectively. The geomagnetic gradient was removed from the data using International Geomagnetic Reference Field (IGRF) of Epoch 2009. The flight path was generally followed by the pilot of the aircraft using a real-time differential Global Positioning System, which was also used to recover the positions of each measurement and allow the precise and accurate positioning of the survey data and integration with other spatial data. These data had been prepared for subsequent processing by digitising the maps in a numeric format that permits the application of interpolation (gridding) technique. Therefore, they had been subjected to different techniques of processing [19].

Airborne Radiometric Analysis

The distributions of the three natural radionuclides (equivalent concentrations of thorium (eTh), equivalent concentrations of uranium (eU) and equivalent concentrations of potassium (K)) present in the study area have been obtained using the surveyed radiometric data (Figures 2–4, respectively). When weathering occurs, it modifies the distribution and the concentrations of radioelements when compared to the original bedrock [20]. These gamma rays emitted from the surface are related to the weathered materials and geochemistry as well as the mineralogy of the bedrock. The plots of the radioelement ratios (eU/K, eU/Th and eTh/K) are shown in Figures 5–7, respectively. The composite image of the radioelements combines all the three data, K (%), eU and eTh, as shown in Figure 11. In order to verify the environmental effects due to these natural radionuclides, the exposure rates, E ($\mu R/hr$), and the equivalent dose rates, D(mSv/yr), were calculated using the following equations, respectively [19–22]:

$$E\ (\mu R/hr) = 1.505\ \text{K}\ (\%) + 0.287\text{eTh}\ (\text{ppm}) + 0.653\ \text{eU}\ (\text{ppm}) \quad (1)$$

$$D(mSv/yr) = 0.0833 \quad (2)$$

where eTh, eU and K are the equivalent concentrations of thorium, uranium and potassium in part per million and K (%) is potassium in percentage. The plot of the environmental radioactivity dose rates is presented in Figure 9. In order to assess the trend of uranium migration in the study area, uranium migration index was calculated using Equation (3) as stated by [19] and [23] and is plotted in Figure 10.

$$eU - \frac{eTh}{3.5} \quad (3)$$

The radiometric data have been statistically treated, and the results are summarised in Table 1.

Qualitative interpretation of airborne radiometric data

The thorium equivalent concentration contour map

The study area is enriched with some level of thorium radioactivity, most especially the northern through the southern central parts. In Figure 2, these levels can be seen to be from 0.11 to 5.22 (ppm), characterised by pegmatite/schist geological formation, 5.22–9.14 ppm, and quartzite/quartz schist geological formation, 9.14–18.59 ppm Undifferentiated schist amphibolite meta volcanic with pegmatite complex and 18.59–76.49 (ppm) characterised by Branded Gneiss. There is a high anomaly in this last range. The average value was found to

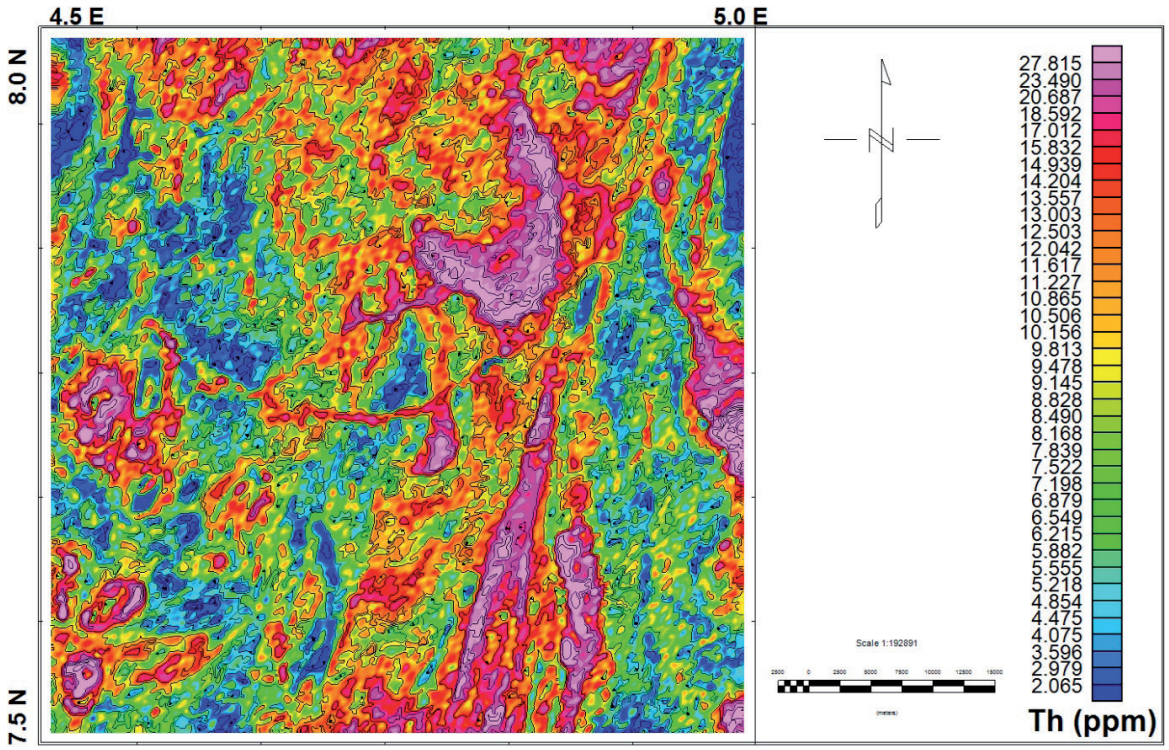

Figure 2: *Airborne radiometric thorium anomalies of the study area.*

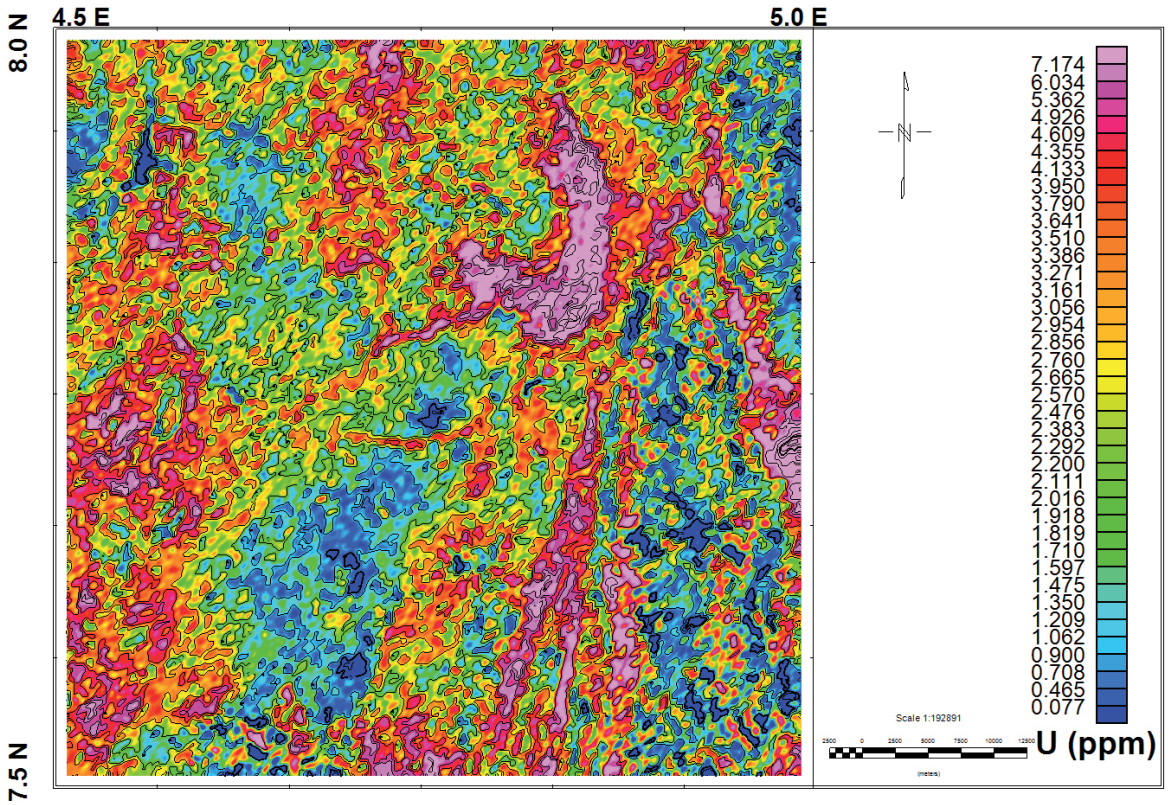

Figure 3: *Airborne radiometric uranium anomalies of the study area.*

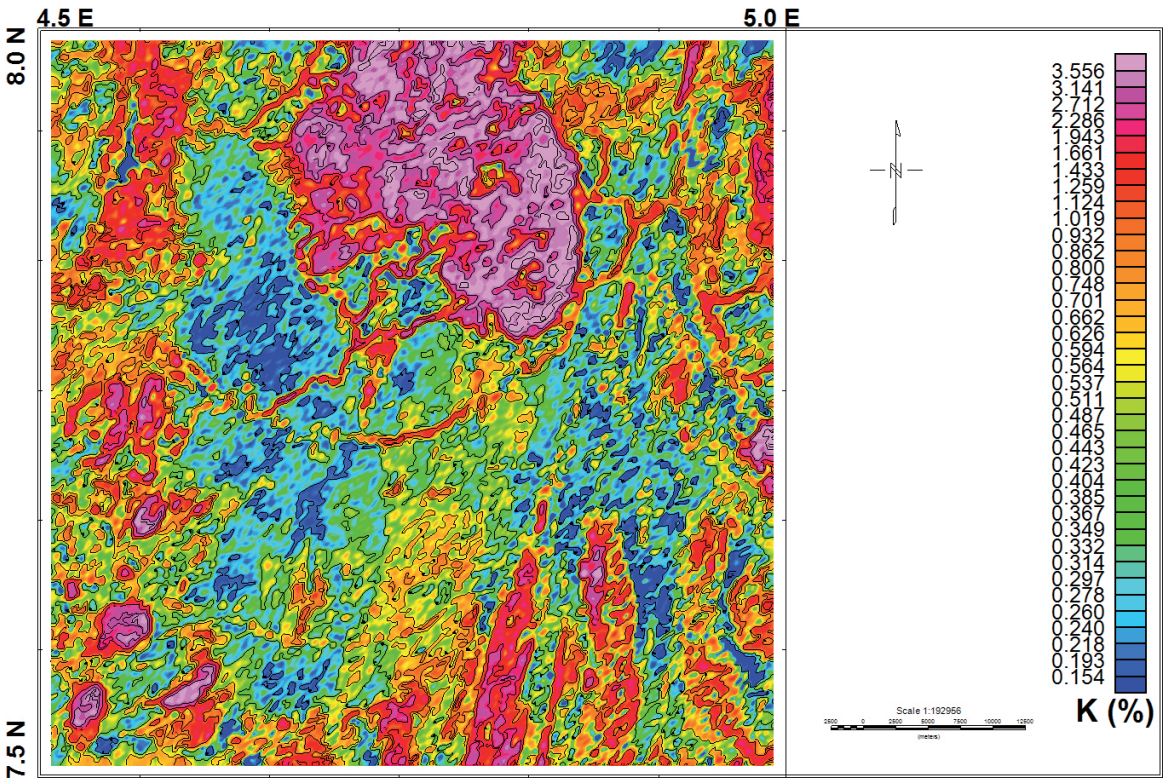

Figure 4: *Airborne radiometric potassium anomalies of the study area.*

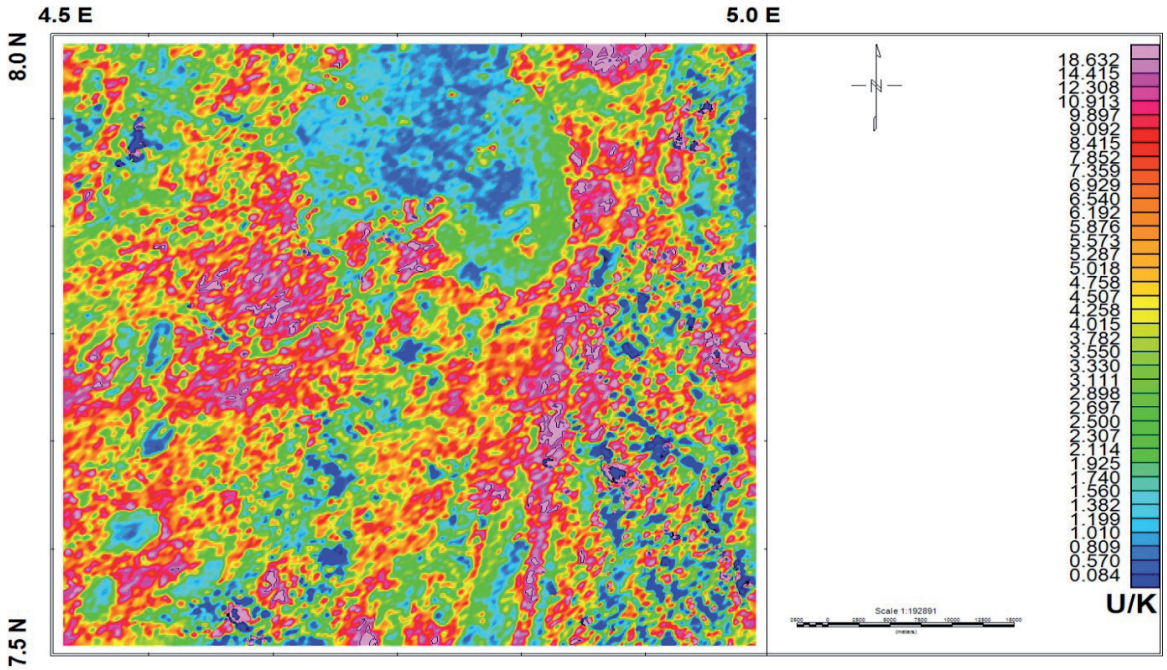

Figure 5: *Airborne radiometric ratio of uranium to potassium (U/K) anomalies of the study area.*

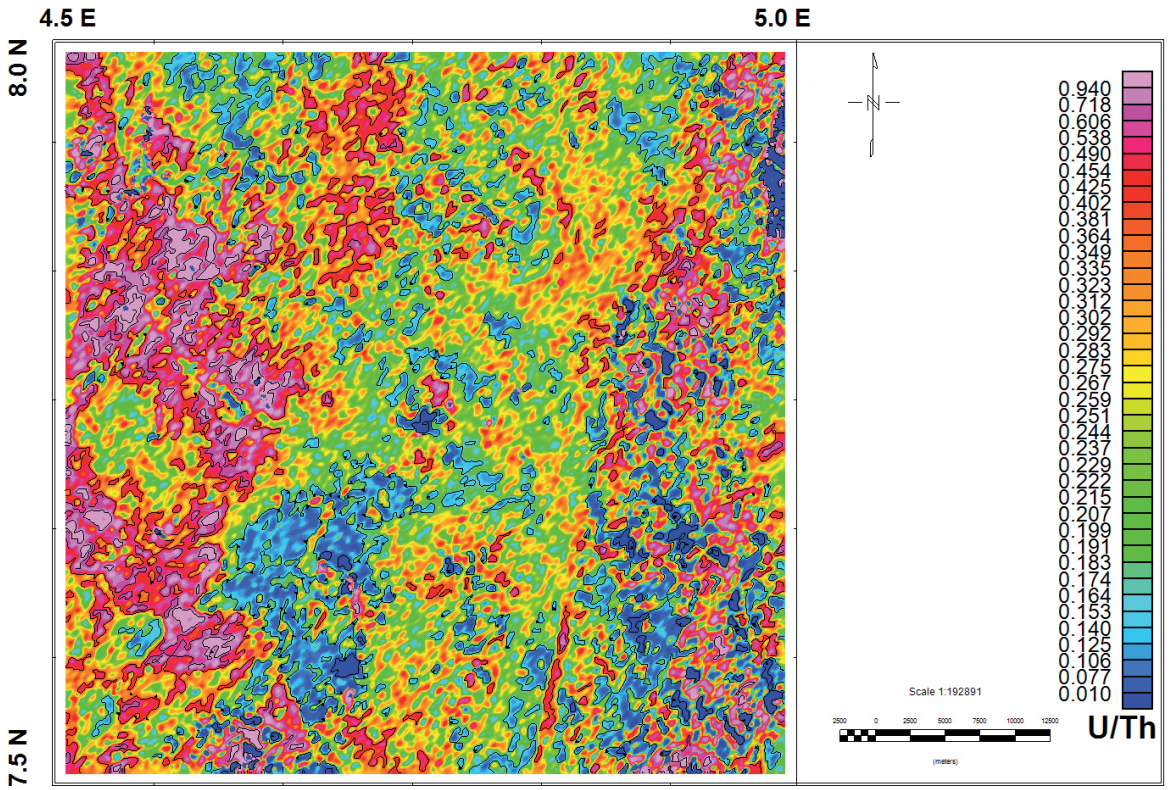

Figure 6: *Airborne radiometric ratio of uranium to thorium (U/Th) anomalies of the study area.*

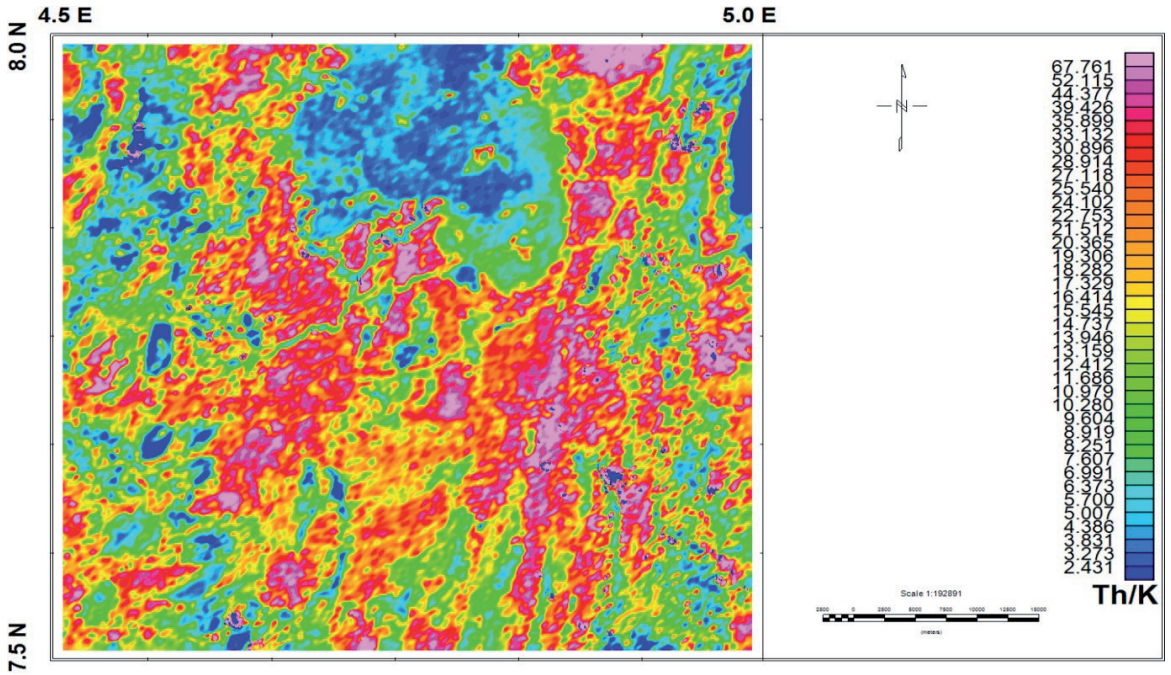

Figure 7: *Airborne radiometric ratio of thorium to potassium (Th/K) anomalies of the study area.*

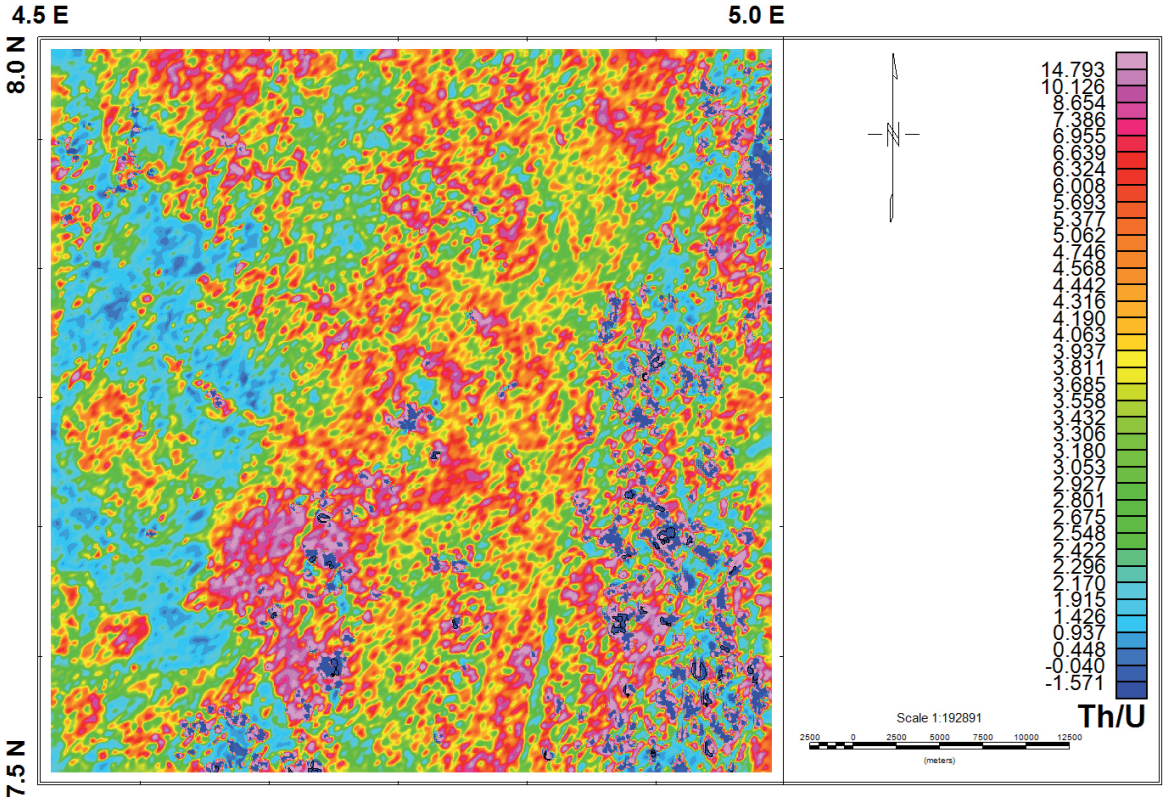

Figure 8: *Airborne radiometric ratio of thorium to uranium (Th/U) anomalies of the study area.*

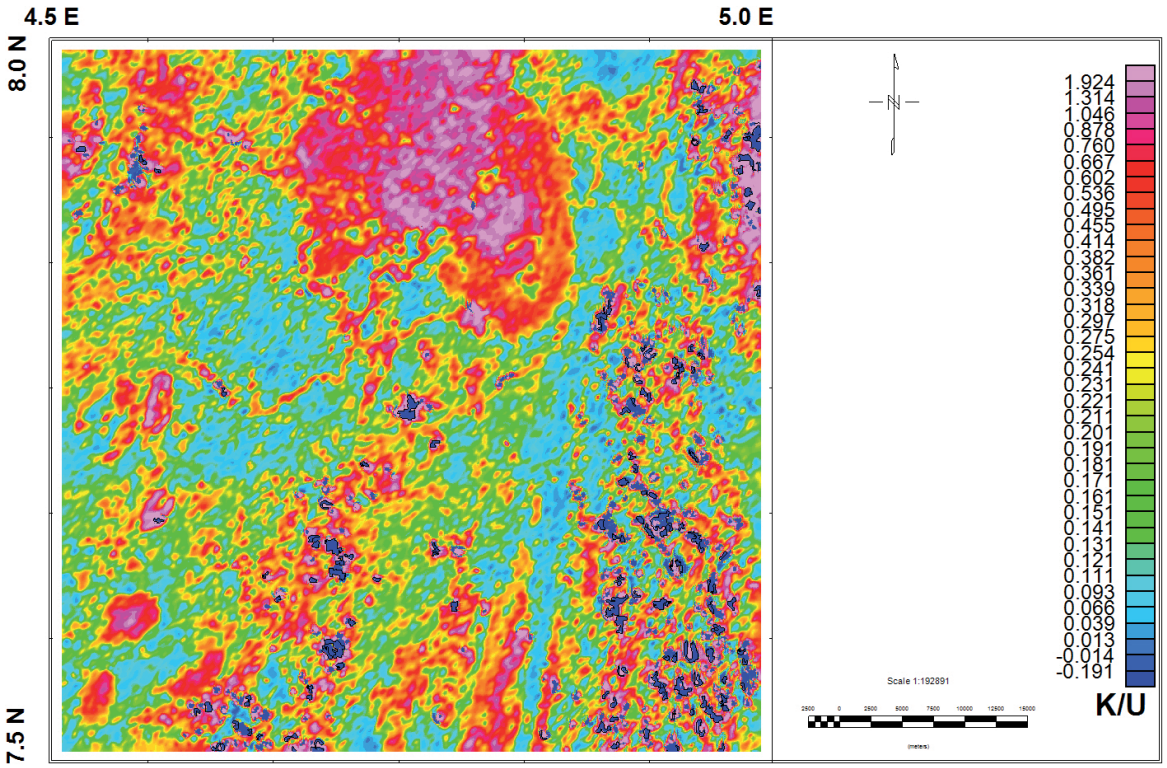

Figure 9: *Airborne radiometric ratio of potassium to uranium (K/eU) anomalies of the study area.*

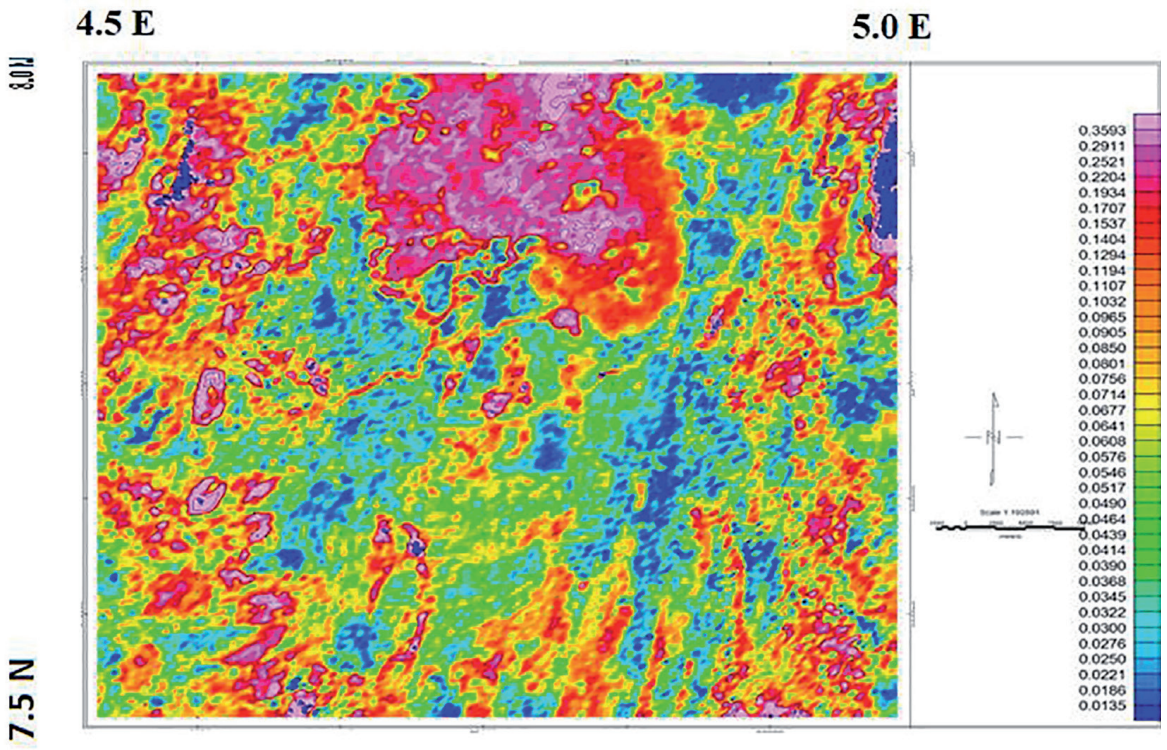

Figure 10: *Airborne radiometric ratio of potassium to thorium (K/Th) anomalies of the study area.*

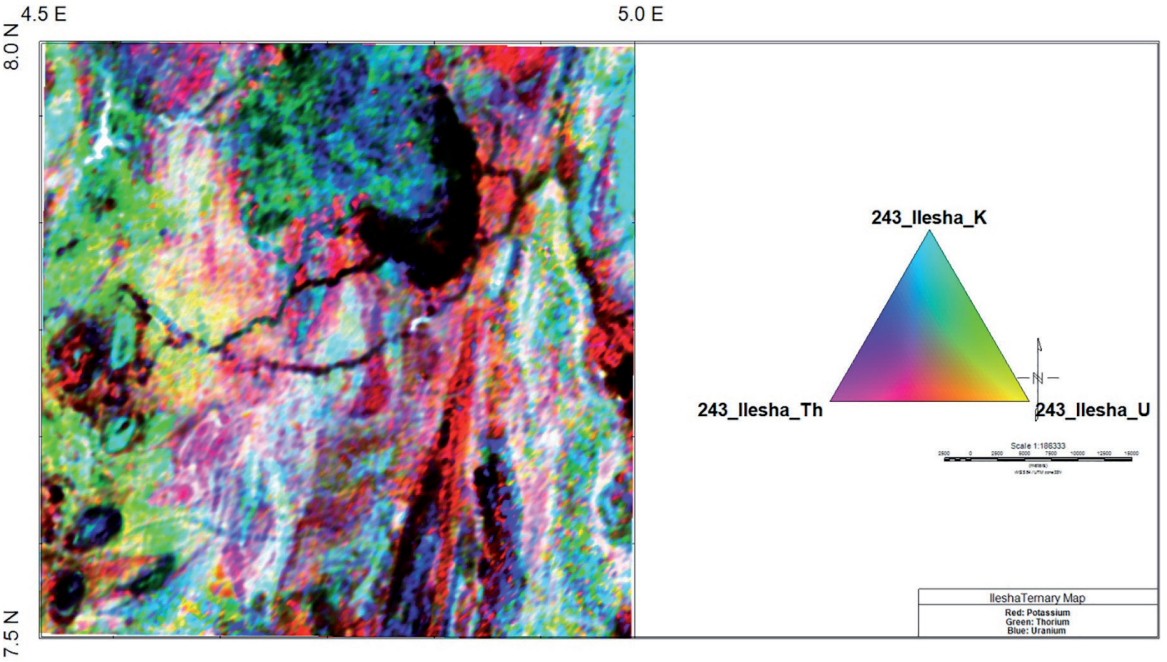

Figure 11: *Airborne radiometric of thorium (Th), uranium (U) and potassium (K) in RGB ternary image of the study area.*

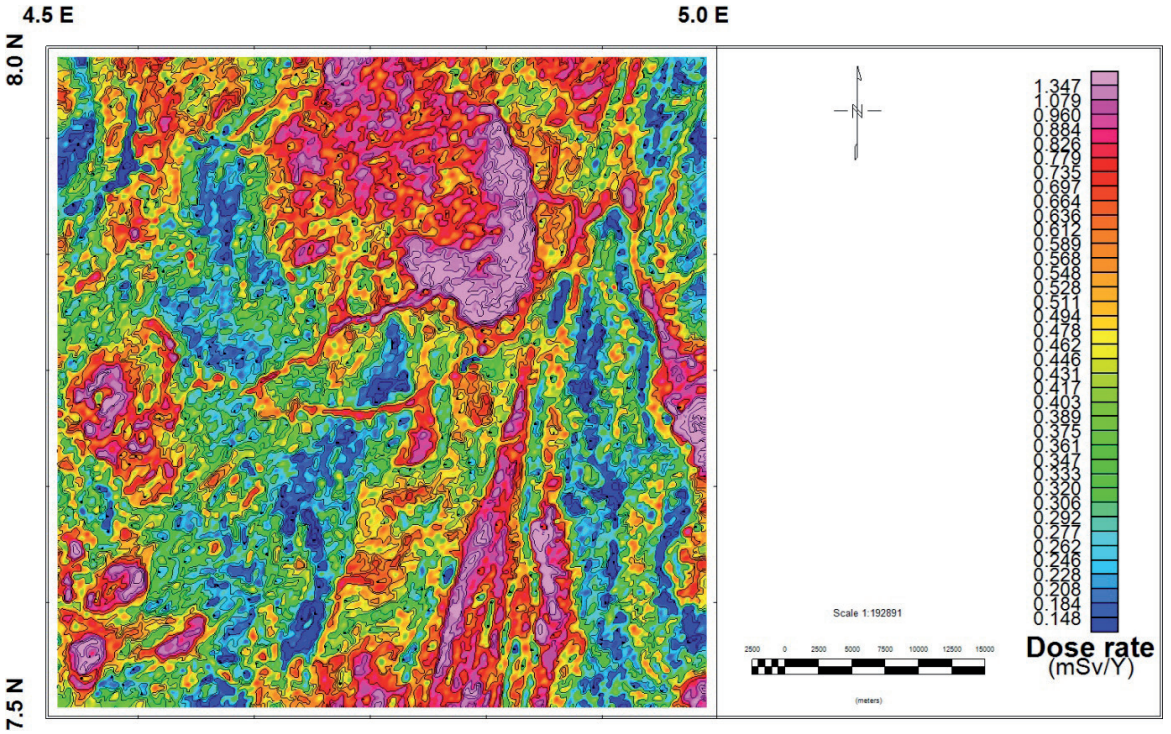

Figure 12: *Radioactivity dose rate contour map of the study area.*

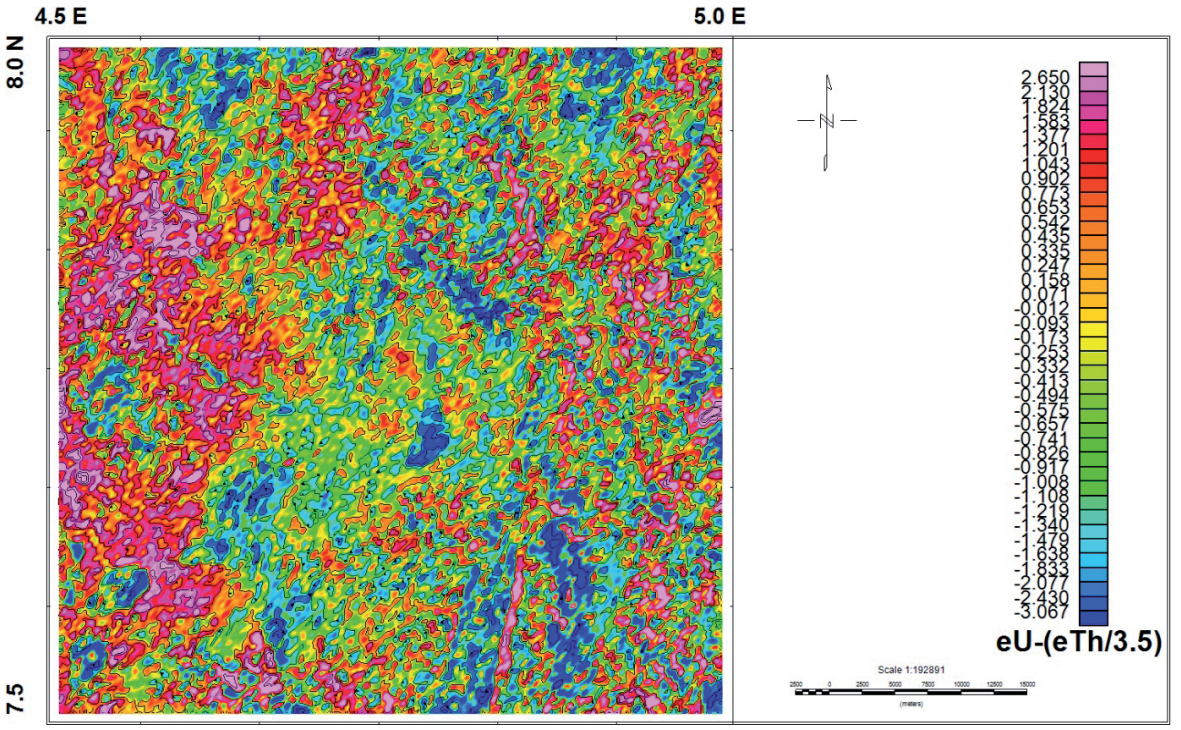

Figure 13: *Uranium migration index contour map of the study area.*

Table 1: *Summary of statistical results.*

	eTh (ppm)	eU (ppm)	K (%)	Dose rate (mSv/yr)	Composite/total counts (Ur)
Average	10.6	2.85	0.91	0.522	14.52
Minimum	0.11	0.1	0.15	0.182	2.27
Maximum	76.49	37.79	3.56	3.93	26.72
Standard deviations	6.8	1.91	0.90	0.31	8.60

be 10.60 ± 6.80, having the minimum value of 0.11 ppm and the maximum value of 76.49 ppm (Table 1); one of the stable thorium minerals was monazite, which could be assumed to be present [19].

The equivalent concentration uranium contour map

From the equivalent concentration uranium contour map in Figure 3, it can be found that there were relatively four levels of radioactivity with characteristic geological representation of undifferentiated schist amphibolite meta-volcanic with pegmatite complex and quartzite/quartz schist for levels between 0.08 and 1.35, granite gneiss/porphyritic granite for levels between 0.10 and 2.57, schist/branded gneiss for levels between 2.57 and 4.93 and lastly, branded gneiss for the level with the highest value of equivalent uranium radioactivity between 4.93 and 37.79 ppm, which was in agreement with the earlier work by [19]. There is a high difference in this last range. The average value of equivalent uranium concentrations in the study area from Table 1 is 2.85 ± 1.91, ranging from 0.10 to 37.79 ppm; it could be assumed that zircon mineral may be present in these areas since it is a stable uranium mineral.

The potassium % contour map

The plot of the distribution of potassium (%) in the study area shows that the area is enriched with potassium (%), which corresponds to porphyritic granites in the geological map of the area. Some parts such as the northwest, northeast and south are also relatively rich in it.

The levels of this radioactivity from the contour map in Figure 4 were shown to be from 0.15 to 0.30, 0.30 to 0.54, 0.54 to 1.94 and 1.94 to 3.56, which corresponded to geological representations of banded gneiss, undifferentiated schist amphibolite meta-volcanic with pegmatite complex, granite gneiss and pegmatite/quartz vein and the highest porphyritic granite formations, respectively. The average value of potassium (%) in the study area found from Table 1 is 0.91 ± 0.90%, having a minimum value of 0.15% and a maximum value of 3.56%.

The contour map of eU/K ratio

The contour map of eU/K ratio shown in Figure 5 reveals that the area has eU/K ratio >1 in almost all the study areas except at porphyritic granite areas where the values are ≤ 0.8.

The contour map of eU/eTh ratio

Looking at the contour map of eU/eTh ratio (Figure 6), it was noticed that the radioactive level of eTh was higher than that of eU, as the ratios are less than 1. eU/eTh ratio dominates the western part with characteristic geology of pegmatite/quartz vein, granite gneiss, metadiorite and some parts of schist zones and also a few places in the eastern part with characteristic feature of migmatite representations. The ratios of eU/eTh are lowest around the central parts (undifferentiated schist amphibolite meta-volcanic with pegmatite complex).

The contour map of eTh/K ratio

Figure 7 shows that there are more eTh contents than potassium contents. It can be seen that the values decrease where there are highest contents of potassium at the porphyritic granite areas, whereas the ratios are high at granite gneiss, banded gneiss, undifferentiated schist amphibolite meta-volcanic with pegmatite complex and some parts of quartzite/

quartz schist geological representations. These areas are enriched in thorium.

The contour maps of K/eU, K/eTh and eTh/eU ratios

The ratios of eTh/eU, K/eU and K/eTh are shown in Figures 8–10, respectively. In Figure 8, the theoretically expected ratio of thorium to uranium for normal continental crust is approximately 3.0, which shows that no significant fractionalisation occurs during weathering and there is no involvement in metasomatic activity of the radioelement. Figure 8 also shows that uranium leaching occurs. Potassium abundance is measured directly as gamma rays are emitted when ^{20}K decays to argon, uranium and thorium and cannot be measured directly. The granitic rocks with little soil cover could be easily identifiable with high concentrations of K and Th, whereas the same granitic bodies with thick soil cover show negative anomalies than the granitic terrain. The value of the ratios of eTh/eU, K/eU and K/eTh ranges between -1.571 and 14.793, -0.191 and 1.924 and 0.0135 and 0.3593, respectively.

The composite (total count) contour map of the radioelements (Ur)

The composite image of the radioelements combines all the three data, K (%), eU and eTh, in Figure 11; this is also the total count contour map. At the lower part of the porphyritic granite around Imesi Ile and Ilare, a high concentration of the three radioelements is shown. eU, K and eTh occur at high concentrations in fresh granite soil and in granite soil where clay layers are close to or exposed at the surface [24].

The northwestern region through southwestern parts shows more thorium, the northeastern region through the middle region shows more potassium contents and towards the extreme northwest and some parts of the south-south, uranium contents are dominated.

The average total count in the study area is 14.52 ± 8.60, with the minimum value of 2.27 and the maximum total count (Ur) of 26.76.

Equivalent dose rates of the study area

The study to determine environmental dose rates in Ilesha was carried out using Equations (1) and (2) in order to quantify the radiological relevant doses to ascertain that the environment of the study area does not pose any harm to the public. Figure 12 shows the contour map. The areas with high environmental dose rates fall within the granite gneiss, banded gneiss and some migmatite areas with some relatively high dose rate areas around the porphyritic lithological areas. The areas with low environmental doses fall within undifferentiated schist amphibolite meta-volcanic with pegmatite complex and some parts of quartzite/quartz schist areas. It has been known from studies that igneous rocks of granite compositions are really enriched in thorium and uranium contents compared to rocks of ultramafic or basaltic composition [25]. Some shales and phosphate rocks too are exceptions [26].

The range of the dose rates calculated in the study is between 0.1817 and 3.9296, having an average value of 0.5222 ± 0.3106 mSv/yr. Places like Imesi Ile, Ilare, Idi-Aba, Tonkere, Ipole, Kewo, Iree, Odo-Igba, Boluwaduro and Ikogosi are around the high dose rate areas. This could be attributed to the outcrops in the area since outcrop areas are known to have high background radiations as a result of the basement complex rock formation. These areas are still comparable with places that are known to have high background radiations such as Abeokuta and Jos in Nigeria [27,28]. The average dose rate for the study area is still below the recommended safe limit of 1 mSv/yr for natural radiation sources in the environment [26]. The areas with anomalies should be subjected to further studies using other techniques.

The contour map of uranium migration index (ppm)

The uranium migration index was calculated to study the migration of uranium into and out of the different geological regions' migration index. There was depletion of uranium along the fault line of undifferentiated schist amphibolite meta-volcanic with pegmatite complex around Dumuye village as shown in Figure 13 and also mostly around the centre of the study area with characteristic geology of quartzite/quartz schist. The areas with negative values of uranium trends from northwest to southwest within the area under consideration majorly have uranium deposition as these regions have pos-

itive values of the index. Schist, granite gneiss, branded gneiss and few parts of undifferentiated schist amphibolite meta-volcanic with pegmatite complex fall under these regions, with places such as Ora, Igbona, Idi-Aba, Tonkere, Bara, etc.

Magnetic data processing

Airborne magnetic data were subjected to magnetic automated gradient technique in order to emphasise magnetic features from sources in both shallow and deep geologic environments. The purpose of the enhancements was to transform anomalies into forms that can be directly compared with important rock mineralogical properties. This process correctly positioned anomalies over their causative sources, increased the resolution of small-scale anomalies related to near-surface magnetic sources and converted data to a model of magnetic susceptibilities for comparison with rock mineralogical properties.

Horizontal Gradient

The horizontal gradient method (HGM) is in many ways the simplest approach to estimating contact locations and depths. It requires the greatest number of assumptions about the sources but is the least susceptible to noise in the data, because it only requires calculation of the first-order horizontal derivatives of the magnetic field. If *T(x, y)* is the magnetic field, then the horizontal gradient magnitude *HG(x, y)* is given as follows:

$$HG(x,y) = \sqrt{\left(\frac{dT}{dx}\right)^2 + \left(\frac{dT}{dy}\right)^2 + \left(\frac{dT}{dz}\right)} \qquad (4)$$

This function peaks over magnetic contacts under the following assumptions: (1) the regional magnetic field is vertical, (2) the source magnetisations are vertical, (3) the contacts are vertical, (4) the contacts are isolated and (5) the sources are thick. Violations of the first four assumptions can lead to shifts in the peaks away from the contacts. Violations of the fifth assumption can lead to secondary peaks parallel to the contacts. In order to partially satisfy the first two assumptions, it is usually necessary to perform transformation known as pseudo-gravity on the observed magnetic field. Crests in the horizontal gradient magnitude can be located by passing a small 3 × 3 window over the HGM grid and searching for maxima [29]. The 1997 programme HDEP [30] used a similar approach within a 5 × 5 window to both locate the crests and determine their strike direction. Once a crest is located and the strike direction is known, data within the window and within a belt perpendicular to the strike can be used to determine the depth of the contact by performing the least-squares fit method to the theoretical shape of the HGM over a contact. If h is the horizontal distance to the contact, d is the depth to the top of the contact and k is a constant, then the theoretical curve is given by the following equation [31]:

$$HG(h) = \frac{k}{h^2 + d^2} \qquad (5)$$

The least-squares fit method gives an estimate of both the depth and its standard error, which can be expressed as a percentage of the depth. Typically, only depth estimates with standard errors of 15% or better are retained in the final interpretation. The HGM is relatively insensitive to noise in the data and interference effects between nearby sources.

Analytic signal amplitude (ASA)

Analytic signal (AS) is a transform formed through the combination of horizontal and vertical gradients of a magnetic anomaly. In 1972 and 1974, Nabighian [32,33] involved the concept of the AS for magnetic interpretation and showed that its amplitude yields a bell-shaped function over each corner of a 2D body with polygonal cross-section.

AS is defined as

$$A(x,y) = \frac{dT}{dx}i + \frac{dT}{dy}j + \frac{dT}{dz}k \qquad (6)$$

where i, j and k are unit vectors in x, y and z directions, respectively. The real and imaginary parts of its Fourier transform are horizontal and vertical derivatives of T.

In the frequency domain, the amplitude of the AS of the total magnetic field T is calculated from the three orthogonal derivatives of the field [34]. The absolute value or amplitude A

of the simple AS is given by the following equation:

$$|A(x,y)| = \left[\left(\frac{dT}{dx}\right)^2 + \left(\frac{dT}{dy}\right)^2 + \left(\frac{dT}{dz}\right)^2\right]^{1/2} \quad (7)$$

Equation 7 shows that the location of the source in the horizontal plane can be deduced from the peak position of the amplitude of the AS and the source depth can be estimated as the half width of the half maximum of the amplitude of the AS. This function acts as envelope of all possible phase shifts of an observed anomaly and peaks over magnetic contacts, regardless of the regional magnetic field direction, the source magnetisation and the dip of the contact. It was pointed out by Roest et al. [35] that depth can be estimated from the shape of the AS based on non-linear curve fitting; solving the non-linear problem is always difficult. The contact depth model can therefore be calculated from the AS using the 2D expression of the AS magnitude for a model given by the following equation [36]:

$$AS(x) = \frac{k}{(x^2 + z^2)^{\frac{1}{2}}} \quad (8)$$

where k is the magnetisation constant and z the depth to the top of contact.

Local wavenumber (LWN) method

The phase angle is defined as the angle between the vertical derivative and the absolute value of the total horizontal derivative of the potential field data, which in edge detection context is termed as tilt angle [37]. In this study, we analysed depth estimates derived using the LWN. The determination of the local phase (LP) and LWN for grid-based data have been made easier using the methods reported by Fairhead et al. [38] and Verduzco et al. [39]. In 1965, Bracewell [40] defined f (the local frequency) as the rate of change of LP with respect to x. Thus, f can be expressed mathematically as given in the following equation:

$$f = \frac{1}{2\pi}\frac{\partial}{\partial x}\tan^{-1}\left[\frac{\frac{\partial T}{\partial z}}{\frac{\partial T}{\partial x}}\right] \quad (9)$$

Defining the LWN in terms of frequency,

$$k = 2\pi f \quad (9)$$

Substituting Equation (9) into Equation (10) leads to the following equation:

$$k = \frac{1}{|A|^2}\left(\frac{\partial^2 T}{\partial x \partial z}\frac{\partial T}{\partial x} - \frac{\partial T}{\partial x^2}\frac{\partial T}{dz}\right) \quad (10)$$

For gridded data, it has been shown by Huang and Versnel [41] that the wavenumber is given by

$$k = \frac{1}{T_x^2 + T_y^2 + T_z^2}$$

$$\times \left\{T_x\left[T_{xx} - \frac{T_z}{T_x^2 + T_y^2}\left(T_x \,.\, T_{xx} + T_y \,.\, T_{xy}\right)\right]\right. \quad (11)$$

$$\left. + T_y\left[T_{xy} - \frac{T_z}{T_x^2 + T_y^2}\left(T_x \,.*\, T_{xy} + T_y \;*.\, T_{yy}\right)\right]\right\}$$

By considering a sloping contact, the expressions for the vertical and horizontal gradients as defined by Nabighian [32] are given by

$$\frac{\partial T}{\partial z} = 2sFc\sin d$$

$$\frac{x\cos(2I - d - 90) - h\sin(2I - d - 90)}{h^2 + x^2} \quad (12)$$

$$\frac{\partial T}{\partial x} = 2sFc\sin d$$

$$\frac{h\cos(2I - d - 90) - x\sin(2I - d - 90)}{h^2 + x^2} \quad (13)$$

where s is the susceptibility contrast, F the magnitude of the ambient field, , a the ambient field declination, I the inclination of the ambient field, d the angle of dip of the body and h the depth to the top of the contact.

Substituting Equations (12) and (13) into Equation (10), we have Equations (14), (15) and (16), which are the required source parameters, namely, magnetic contact depth, local dip and local susceptibility, respectively.

$$k = \frac{h}{h^2 + x^2} \quad (14)$$

Let $x = 0$ and the peaks coincide with the edges of the bodies, then local depth can be written as

$$h = \frac{1}{k} \quad [8] \ (15)$$

and

$$K = \frac{|A|}{k2kcSind} \quad (16)$$

Magnetic data interpretation

According to Poirier [42], the main use of high-resolution airborne magnetic maps and their derivatives in mineral prospecting is to make geological deduction from them. The total magnetic intensity grid was created using a minimum curvature gridding algorithm with a grid cell size of 50 m. The grid values fit the profile data to within 1 nT for 99.98% of the profile data points. The average gridding error is well below 0.1 nT. The total magnetic intensity map of the gridding of sheet number 243 is shown in Figure 12.

From the range of magnetic intensity values of these data, information on subsurface lithology, trend and geological structures can be obtained. Quantitative interpretation approach was adopted for the mapping of basement topography around Ilesha, southwestern Nigeria, with the aim of establishing depth to basement in the basement complex. The total magnetic field intensity map of Ilesha and its environs is presented in Figure 14. The total magnetic field intensity map indicates high magnetic intensity values in the north, west, northwestern, southeastern and the central part of the area under consideration (Imesi Ile, Ilare, Idi-Aba, Tonkere, Ipole, Odo, Odo Ibga and Ikogosi). The total magnetic intensity value of the field ranged from –79.41 to 140.93 nT with a range of 220.34 nT between the lowest and highest intensity points, suggesting contrasting rock type in the study area. Regions of magnetic lows (low-amplitude magnetic anomaly) and highs (high-amplitude magnetic anomaly) are apparently revealed on the magnetic map (Figure 15). The northern and western regions of this map are characterised by relatively high-amplitude magnetic intensity values (16.93–140.93 nT) with intrusion of low magnetic intensity signature that coincides with ferruginous quartzite and the Precambrian crystalline basement rocks of southwestern Nigeria on the surface geological map (Figure 1), whereas the southeastern area with relatively low-amplitude magnetic intensity values (–79.41–2.58 nT) coincides with relatively thick sedimentary cover, where the effect of the thick weakly susceptible materials masks the high magnetic susceptibility from relatively deep basement rocks.

Figure 15 shows the effect of the application of reduction to the magnetic equator filter operation, the filtering attempts to centre some of the wrongly horizontally elongated anomalies due to low latitude effects. The reduction to equator (RTE) map shows that the correction in the asymmetries of the observed anomalies had been minimised, and it centres the anomalies directly over the causative elongated bodies. The reduction in magnetic intensity values of the equator map ranged from –64.62 to 133.09 nT. The reduction to the equator map is characterised by high frequency, short wavelength, small size, weak intensity, sharp low amplitude and nearly irregular-shaped anomalies, which may be due to near-surface sources, such as shallow geologic units and cultural features.

The second vertical derivative filter was applied to the airborne magnetic data of the study area to improve local anomalies obscured by broader regional trends. It accentuates short-wavelength components of the anomaly field, while de-emphasising long-wavelength components. The output of its application in the study area is shown in Figure 16.

AS map of Ilesa (Figure 17) was derived from AS grid computed from 1st-order vertical derivative values of two horizontal gradients and one vertical gradient of the magnetic intensity of the sheet number 243. AS map of the study area (sheet number 243) shows the amplitudes of the magnetic signature. Prominent high-amplitude AS anomalies are apparent on the AS map. The analytic function acts as the envelope of possible phase shift of the observed anomaly

and peaks over magnetic contacts. The AS map also shows the attenuation of shallow sources. Some regions in the map are characterised by very high amplitude, which reflects lithological variation in magnetic basement, while some parts of the study area is dominated by low amplitude and indicates presence of thick sediment covering the weathered basement. The magnitude of amplitude of magnetic gradient intensity ranges from 0 to 2.8 nT/km.

The sources' location and magnetic contact depth solutions were computed by HGM of RTE grid, ASA of total magnetic intensity grid, and local wavenumber (LWN) of total magnetic intensity grid using a maximum standard error of 15%. Depths on sheet number 243 (Ilesha) are shown in Figures 18–20, respectively, for HGM of RTE grid, ASA, and LWN.

The HGM assumes that the sources are isolated vertical contacts separating thick geologic units and that the magnetisation vectors are collinear with the geomagnetic field vector. Peaks in the horizontal gradient magnitude of the RTE magnetic field indicate the location of the contacts and estimate their strike directions in the depth map as shown in Figures 18–20. In addition, peaks in the ASA and LWN, which is derived from the first horizontal and vertical derivatives of the observed magnetic field, indicate the location of the contacts and estimate their strike directions.

The results obtained indicate that HGM records the highest number of contacts with 113 solutions at comparatively deeper depths than other methods. The results obtained from the HGM revealed depth range limit of 0.478–4.112 km, while the AS gave an estimated depth to the magnetic sources ranging from 0.348 to 2.551 km. The LWN method revealed an estimated depth ranging from 0.478 to 5.48 km. The solutions from HGM and analytical ASA functions are comparable and better than the solutions from the LWN. In each diagram (Figures 18–20), the centre of each circle coincides with the location of maximum for that function and the diameter of the circle is proportional to the depth estimate for the source point of the anomalies. The direction of the diameter indicates the strike direction of the lineament. LWN overestimates the source depths relative to other methods; otherwise, the three results contain similar features, which is in agreement with earlier works by [43] and [44].

A close examination of the maps of HGM, ASA and LWN in Figures 18, 19 and 20, respectively, reveals the differences in the diagnostic attributes of these functions. The resolution of HGM and ASA is comparable, while that of the LWN map is least. The apparent magnetic susceptibility values were estimated using the filter operator in Oasis montaj™ [45], a software package for potential data processing. The apparent susceptibility values of the study area (sheet number 243) ranged from -0.00325 to 0.00323

Table 2: *Magnetic susceptibility values of minerals [46].*

Minerals	Magnetic susceptibility (10^{-6}) SI
Andradite	2,280–4,320
Staurolite	790–1,590
Cordierite	200–1,100
Tourmaline	39–1,520
Beryl	23
Epidote	1,010
Orthite	970–960
Zircon	–15–386
Opal	–12.9
Orthoclase	–13.7
Halite	–10.3
Calcite	–10–100
Quartzite schist	140–220
Pegmatite	90–370
Muscovite tourmaline	10–120
Gneiss	164–260
Limestone	4–20
Sandstone	0.2–5
Gabbro	200–420
Augite	17–100
Haematite	2,150–5,100
Schist	213–469
Tourmaline	20–79
Sphene	264
Actinolite	100–990
Hornblende	764–1368
Pyrite	-6.3–63
Galena	-33–9.3
Dolomite	14–23
Garnet	10–56
Quartz	-6.3
Graphite	-4–76
Biotite	100–307

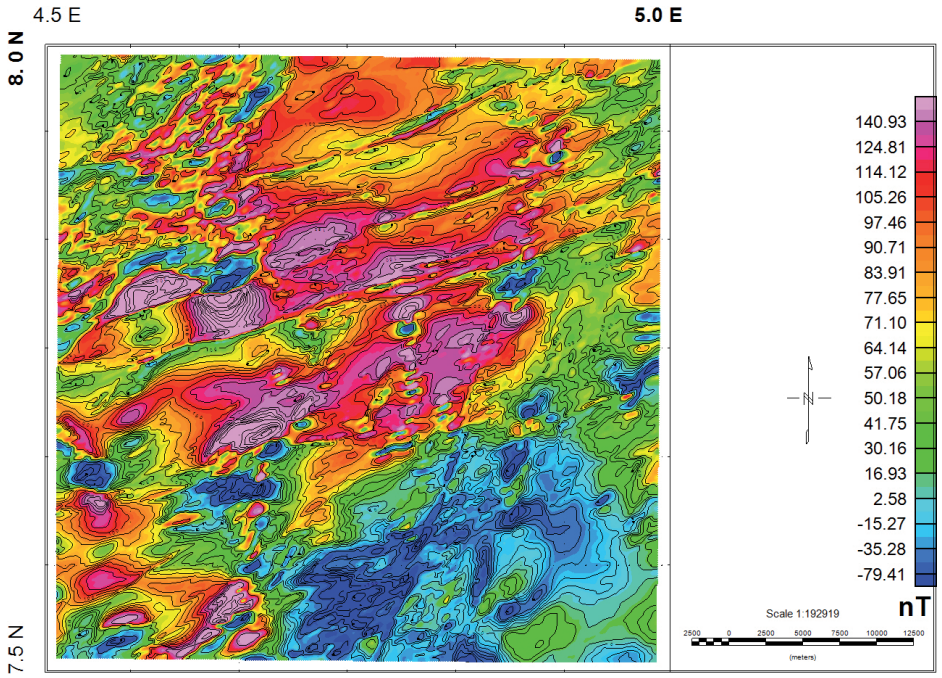

Figure 14: *Total magnetic intensity map of Ilesha and its environs.*

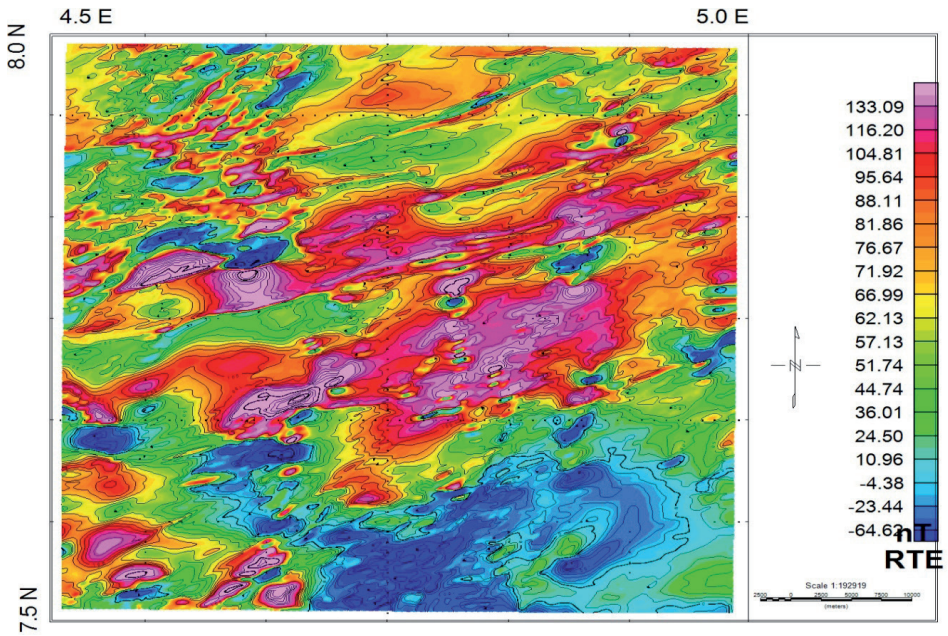

Figure 15: *Total magnetic intensity map of study area after reduction to equator.*

as shown in Figure 21 suggesting contrasting rock types. The northern, southern, southeastern and northwestern regions of this map are characterised by relatively high susceptibility values ranging from 0.00061 to 0.00323, which could be inferred as areas where the fibre-grained quartzite schist, muscovite, tourmaline gneiss and pegmatite are concentrated in the deposit, whereas the southwestern region is characterised by relatively low apparent susceptibility values ranging from -0.0004 to 0.00058, which could be inferred as a weathered and fresh basement area.

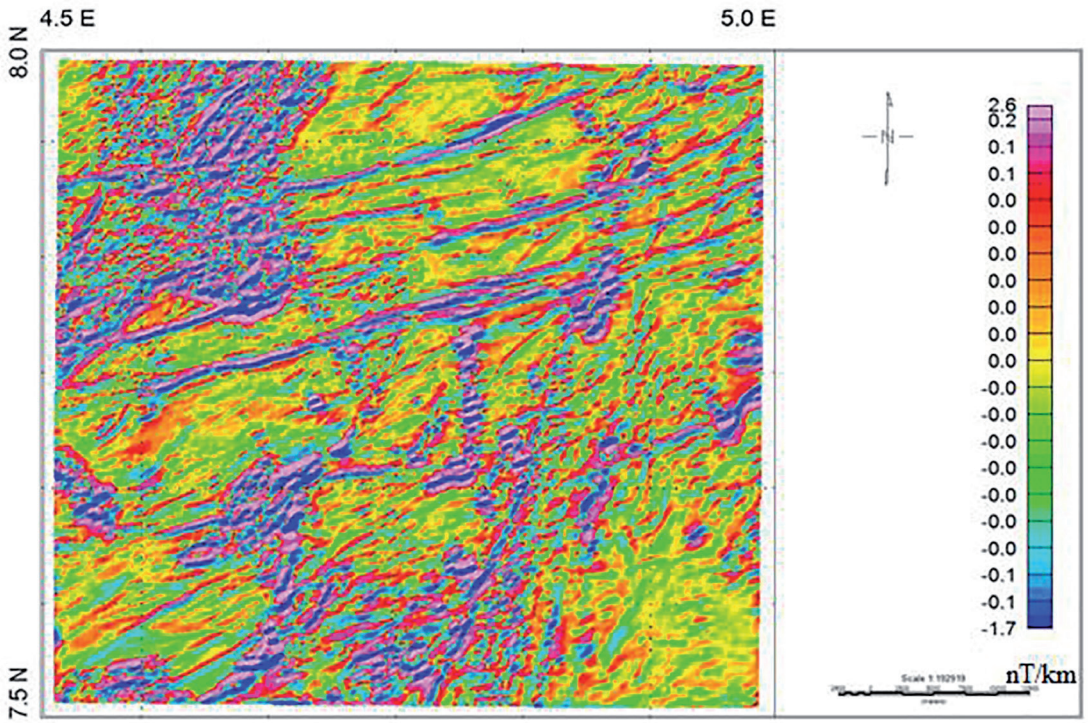

Figure 16: *Vertical gradient map of the study area.*

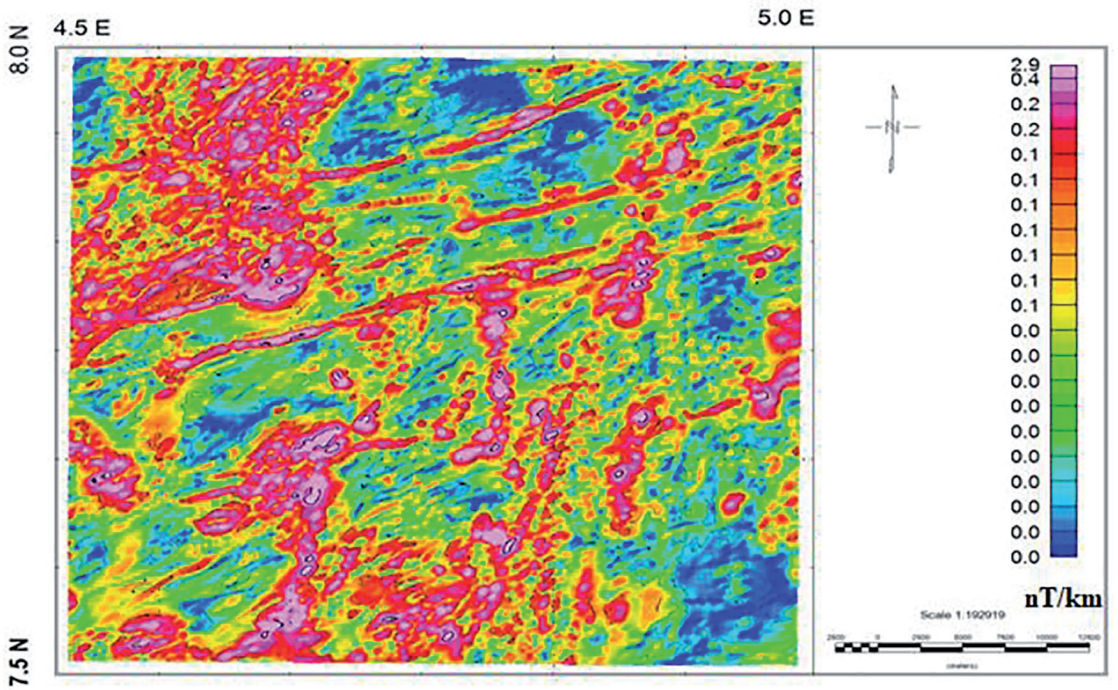

Figure 17: *Analytical map of the study area.*

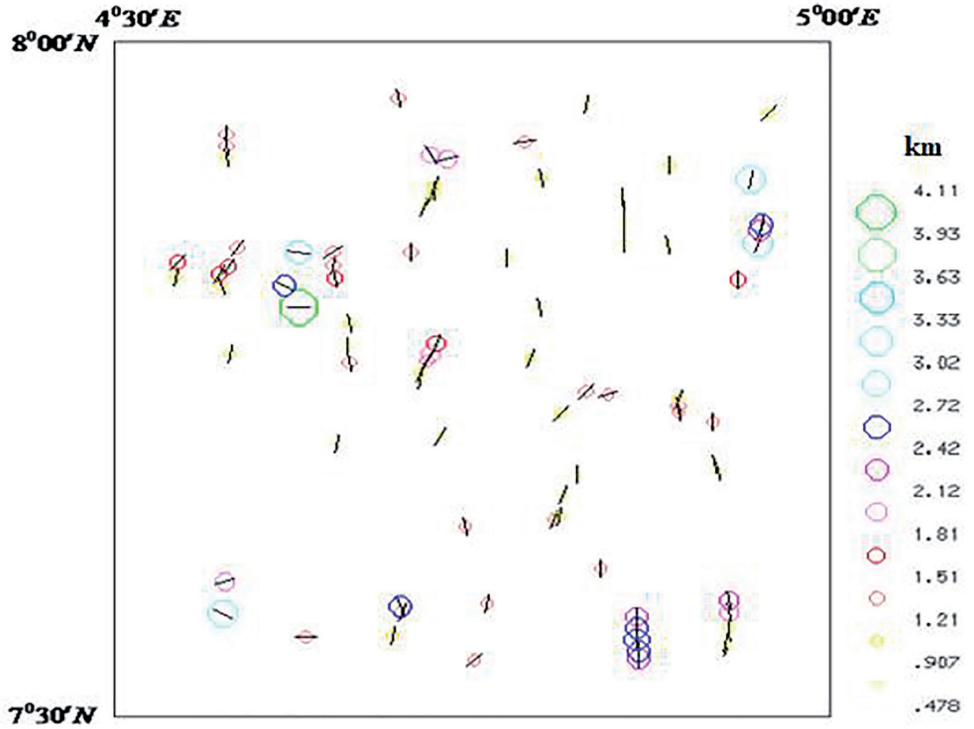

Figure 18: *Horizontal gradient depth map of Ilesha and its environs.*

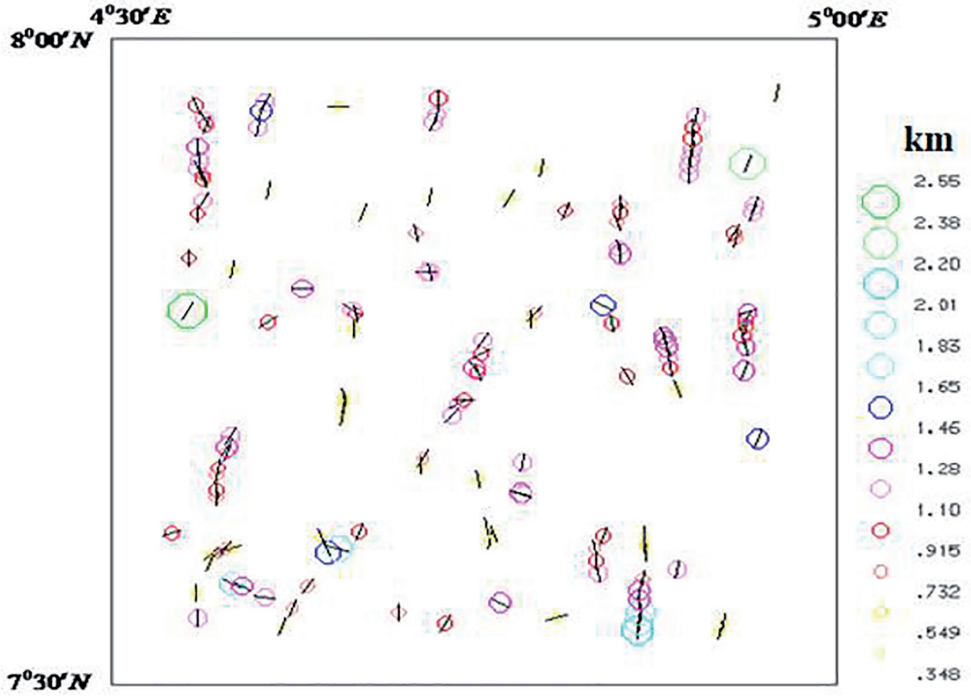

Figure 19: *AS magnitude depth map of the study area.*

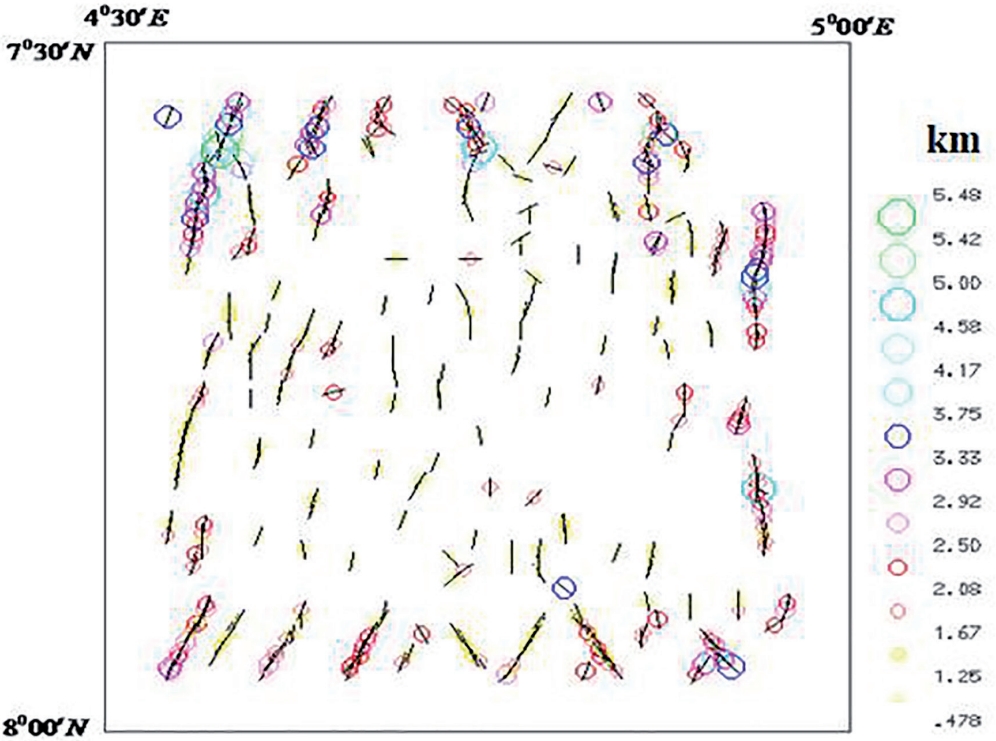

Figure 20: *LWN depth map of Ilesha and its environs.*

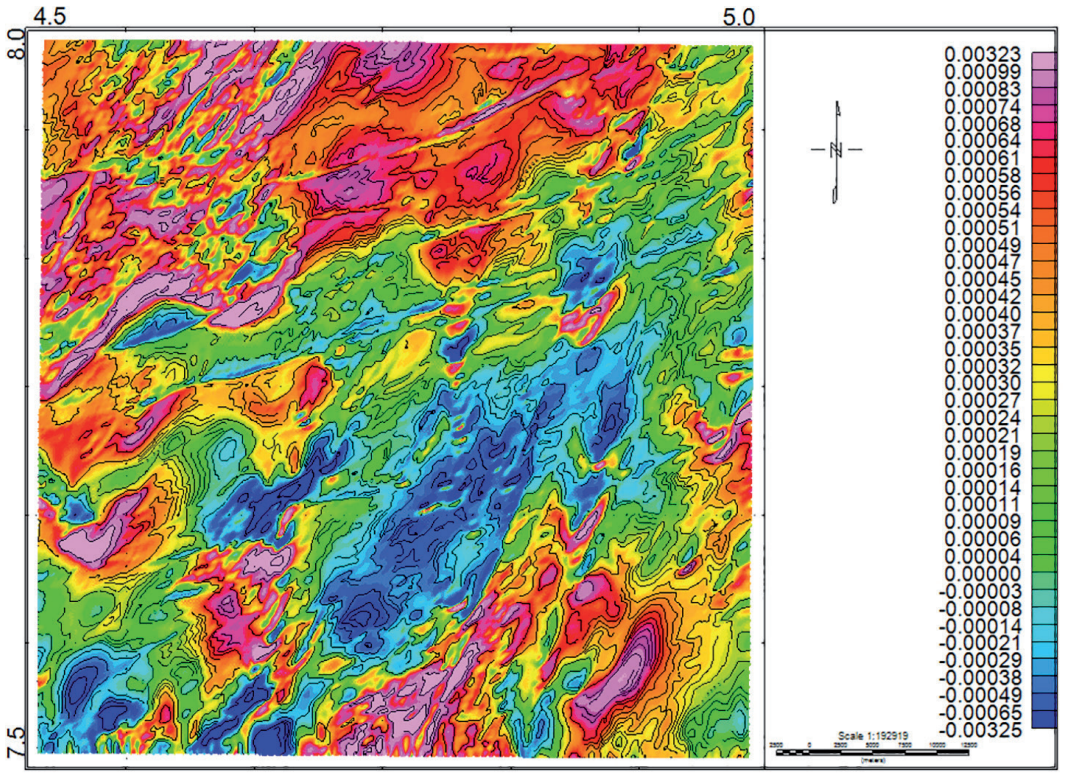

Figure 21: *Apparent susceptibility map of Ilesha and its environs.*

Conclusion

The study of the nature of the distribution of the three radioelements has been carried out using radiometric data. The distribution of the three radioelements with the geological structures of the area has been studied, and it was noted that the maximum values of eU and eTh (ppm) fall within the branded gneiss regions, while the maximum values of K (%) fall within the porphyritic granite region. Equivalent thorium has the highest radioactive content. The mean environmental radioactivity dose rates of the study area were found to fall within the acceptable safe limit of 1.0 mSv/yr, although there are places with high values. Ratios of the radioelements (eU/K, eU/eTh and eTh/K) have been analysed to check whether there was an enrichment or depletion of radioisotopes [25] in the area, and it was found that eU/eTh is less than 1 since eTh is higher than eU, indicating depletion in uranium, whereas eTh/K is greater than 2, indicating equivalent thorium enrichment.

The airborne magnetic data have been analysed using three automated gradient techniques, namely, HGM, ASA and LWN. In addition, the apparent susceptibility filtering technique was used to estimate apparent magnetic susceptibility of the anomaly within the area under consideration. These techniques have been adopted to delineate Ilesha area in order to gain understanding and interpretations. The value of magnetic intensity distribution in the field ranged from -79.41 to 140.93 nT, and it was found to depend on the size, depth of burial and the thickness of the low susceptibility superficial material overlying the magnetite crystalline rocks within the study area. High magnetic intensity values characterised the basement rocks, whereas lower magnetic intensity values distinguished metasedimentary rocks and fresh basement. The results revealed that a basement rock occurs in all parts of the study area. The location and depth to magnetic contacts have been estimated from the peak of the HGM, LWN and ASA functions of the total intensity magnetic data. The results of this study have shown that the estimates of depth limit to shallow magnetic contact by HGM and ASA methods are relatively close and comparable.

The LWN method overestimated the depth to the shallow sources and revealed a smaller depth for the shallow sources. The shallower depth, ranging from 0.382 to 0.478 km, may refer to some major magnetic units, uplifted basement surface and some local magnetic features. These results therefore demonstrate the applicability of the three gradient techniques of magnetic interpretation in estimating depths to the surface of magnetic basement in a basement complex. The obtained apparent susceptibility of the entire Ilesha and its environs ranged from -0.00325 to 0.00323 SI. This study has shown that the apparent susceptibility within the study area is controlled mainly by ferromagnetic and diamagnetic minerals. The integration of airborne radiometric and magnetic results shows that the northwestern, southeastern and central parts of the study area are dominated by high dose rates and high magnetic intensity values. These high values were observed directly in radiometric and magnetic patterns.

Acknowledgement:

The authors acknowledge Nigeria Geological Survey Agency of Nigeria for releasing airborne magnetic and spectrometric data.

References

[1] El-Sadek, M.A., Ammar, A.A., Sabry, A.R. (2002): Aeroradiospectrometry in the Lithological Mapping and Environmental Monitoring of Wadi Araba Area. *The Arabian Journal for Science and Engineering*, 27(2A), pp. 131–148.

[2] Grasty, R.L., Carson, J.M., Charbonneau, B.W., Holman, P.B (1984): Natural Background Radiation in Canada. *Geological Survey of Canada Bulletin*, 360, pp. 39–60.

[3] Linden, A., Melander, A. (1986): Airborne Measurement in Sweden of the Radioactive Fallout After the Nuclear Reactor Accident in Chernobyl, USSR, Preliminary Report SGAB TFRAP 8606, 1986.

[4] Akerblom, G. (1987): Investigation and Mapping of Radon Risk Areas. In: Proceedings of the International Symposium, Geological Mapping in Service of Environmental Planning, 6–9 August 1986, F.C. Wolff (ed.), 1987.

[5] Wilford, J., Minty, B. (2006): The use of Airborne Gamma Ray Imagery for Mapping Soils and Understanding Landscape Processes. *Developments in Soil Science*, 31, pp. 207–218.

[6] Gun, P.J. (1975): Linear transformation of gravity and magnetic fields. *Geophysical Prospecting*, 23(2), pp. 300–312.

[7] Dobrin, M.B. (1976): *Introduction to geophysical prospecting*. New York: McGraw-Hill Book Company, 630 p.

[8] Thurston, J.B., Smith, R.S. (1997): Automatic conversion of magnetic data to depth, dip, and susceptibility contrast using the SPI™ method. *Geophysics*, 62(3), pp. 807–813.

[9] Coetzee, H., Larkin, K. (2011): Airborne Radiometric Surveying for the Management of Health, Safety and the Environment in the Uranium Mining Industry: Potential Applications and Limitations. B. Merkel, M. Schipek, The New Uranium Mining Boom, 483–492.

[10] De Swardt, A.J. (1953): The geology of the country around Ilesa. *Geological Survey of Nigeria Bulletin*, 23, 55 p.

[11] Rahaman, M.A. (1976): *Review of the basement geology of south western Nigeria*. In: Geology of Nigeria, Kogbe, C.A (ed.). Elizabethan: Publishing Lagos.

[12] DeSwardt, A.M.J. (1947): The Ife-Ilesa goldfield (Interim report number 2). Geology of Survey of Nigeria annual report, pp. 14–19.

[13] Russ, P. (1957): Airborne electromagnetics in review. *Geophysics*, 22, pp. 691–713.

[14] Hurley, S. (1970): Radar propagation in rock salt. *Geophysical Prospecting*, 18(2), pp. 312–328.

[15] Ajayi, T.R. (1981). On the geochemistry and origin of the amphibolites of Ife Ilesha area south west Nigeria. *Journal of Mining and Geolology*, 17, pp. 176–179.

[16] Folami, S.L. (1992): Interpretation of aeromagnetic anomalies in Iwaraja area, south western Nigeria. *Journal of Mining and Geology*, 28(2), pp. 391–396.

[17] Elueze, A.A. (1986): *Geology of the Precambranian Nigeria*. Geological Survey of Nigeria, pp. 77–82.

[18] Kayode, J.S. (2009): Vertical component of the ground magnetic study of Ijebu-Ijesa, southwestern Nigeria. A paper presented at the International Association of Seismologist and Physics of the Earth Interior (IASPEI), conference at Cape Town, South Africa; Jan 10th-16th 2009.

[19] Helmy, S.O.A., Monsour, A. Al Garni (2015): Airborne Gamma-ray Spectrometric and Magnetic Studies of Wadi Um Gehig- Wadi Abu Eligam area, Central Eastern Desert, Egypt. *Arabian Journal of Geoscience*, 8(10), pp. 8811–8833.

[20] Wilford, J.R., Bierwirth, P.N., Craig, M.A. (1997): Application of airborne gamma-ray spectrometry. *AGSO Journal Australian Geology and Geophysics*, 17(2), pp. 201–206.

[21] International Atomic Energy Agency (2003): Guidelines for radioelement mapping using gamma ray spectrometry. Vienna: International Atomic Energy Agency, 173 p.

[22] Grasty, R.L., Holman, P.B., Blanchard, Y.B. (1991): Transportable calibration pads for ground and airborne gamma –rays spectrometers. *Geology Survey of Canada*, 90, pp. 23–24.

[23] Clarke, S.P., Peterman, Z.E., Heier, K.S. (1966): Abundances in Uranium, Thorium and Potassium. In: Handbook of Physical Constants. Geological Society of America, 97: 521–541.

[24] Ramadass, G., Subbash Babu, A., Udaya Laxmi, A. (2015): Structural Analysis of Airborne Radiometric. Data for Identification of Kimberlites in Parts of Eastern Dharwar Craton. *International Journal of Science and Research*, 4(4), pp. 2375–2380.

[25] Tzortzis, M., Tsertos, H. (2004): Determination of thorium, uranium and potassium elemental concentrations in surface soils in Cyprus. *Journal of Environmental Radioactivity*, 77(3), pp. 325–328.

[26] UNSCEAR, (2000): Sources and Effects of ionizing radiation. Report to General Assembly, With Scientific Annexes, New York: United Nations.

[27] Farai, I.P., Jibiri, N.N. (2000): Baseline studies of terrestrial outdoor Gamma Dose Rate level in Nigeria. *Radiation Protection Dosimetry*, 88, pp. 247–254.

[28] Okeyode, I.C., Rabiu, J.A., Alatise, O.O., Makinde, V., Akinboro, F.G., Alhazim, D., Mustapha, A.O. (2016): Area monitoring ambient dose rate in part of southwestern Nigeria using GPS-Integrated radiation survey meter. *Radiation Protection Dosimetery*, 173(1), pp. 263–267.

[29] Blakely, R.J., Simpson, R.W. (1986): Approximating edges of source bodies from magnetic or gravity anomalies. *Geophysics*, 51(7), pp. 1494–1498.

[30] Phillips, J.D. (1997): Potential field geophysical software for P.C version 2.2. Open file report 97–725.

[31] Roest, W.R., Pilkington, M. (1993): Identifying remanent magnetization effects in magnetic data. *Geophysics*, 58 (5), pp. 653–659.

[32] Nabighian, M.N. (1972): The Analytic signal of two dimensional bodies with polygonal cross section-its properties and use for automated anomaly interpretation. *Geophysics*, 37, pp. 507–517.

[33] Nabighian, M.N. (1974): Addition comment on the analytic signal of two dimensional bodies with polyg-

onal cross section-its properties and use for automated anomaly interpretation. *Geophysics*, 39, pp. 85–92.

[34] Purucker, M. (2006): Crustal Magnetism: Geophysics, 5, Version 2.5

[35] Roest, W.R., Verhoef, J., Pilkington, M. (1992): Magnetic interpretation using the 3-D analytic signal. *Geophysics,* 57(1), pp. 116–125.

[36] MacLeod, I.N., Jones, K., Dai, T.F. (1993): Analytic signal in the interpretation of total magnetic field data at low magnetic latitudes. *Exploration Geophysics*, 24, pp. 679–688.

[37] Miller, H.G., Singh, V. (1994): Potential field tilt- A new concept for location of potential field sources. *Journal of Applied Geophysics*, 32, pp. 213–217.

[38] Fairhead, J.D., Green, C.M., Verduzco, B., MacKenzie, C. (2004): A new set of magnetic field derivatives for mapping minerals prospects. SEG 17th Geophysics (2004).

[39] Verduzco, B., Fairhead, J.D. Green, C.M., MacKenzie, C. (2004): New insights into magnetic derivatives for structural mapping: *The Leading Edge*, 23, pp. 116–119.

[40] Bracewell, R. (1965): *The Fourier transform and its applications*. New York: McGraw – Hill Book Co., 474 p.

[41] Huang, D., Versnel, P.A. (2000). Depth estimation algorithm applied to FTG data. Society of Exploration Geophysics. Expanded Abstract, pp. 394–397.

[42] Poirier, J.P. (2000): *Introduction to Physics of the earth interior*. Cambridge: Cambridge University press, 312 p.

[43] Phillips, J.D. (2010): Locating magnetic contacts; A comparison of the horizontal gradient, analytic signal, and local wavenumber methods, Society of Exploration Geophysics Annual General Meeting, Calgary, Alberta, Expanded Abstracts.

[44] Olowofela, J.A., Badmus, B.S., Ganiyu, S.A., Olurin, O.T., Babatunde, P. (2011): Source location and depth estimation from digitised aeromagnetic data acquired from the basement complex formation. *Earth Science India*, 4, pp. 136–142.

[45] Geosoft INC. (2010). Geosoft INC. 85 Richmond Street, 8th Floor, Toronto, Ontario, Canada.

[46] Frantisek, H., Jiri, P., Jazek, J. Chadina, M. (2009): Out – of- Phase Magnetic Susceptibility of rocks and soil rapid tool for magnetic granulometry. *Geophysical Journal International,* 194, pp. 170–181.

Instructions for Authors

RMZ – MATERIALS & GEOENVIRONMENT (RMZ – Materiali in geookolje) is a periodical publication with four issues per year (established in 1952 and renamed to RMZ – M&G in 1998). The main topics are Mining and Geotechnology, Metallurgy and Materials, Geology and Geoenvironment.
RMZ – M&G publishes original scientific articles, review papers, preliminary notes, and professional papers in English. Only professional papers will exceptionally be published in Slovene. In addition, evaluations of other publications (books, monographs, etc.), in memoriam, presentation of a scientific or a professional event, short communications, professional remarks and reviews published in RMZ – M&G can be written in English or Slovene. These contributions should be short and clear.
Authors are responsible for the originality of the presented data, ideas and conclusions, as well as for the correct citation of the data adopted from other sources. The publication in RMZ – M&G obligates the authors not to publish the article anywhere else in the same form.

Specification of the Contributions

Optimal number of pages is 7 to 15; longer articles should be discussed with the Editor-in-Chief prior to submission. All contributions should be written using the ISO 80000.

- Original scientific papers represent unpublished results of original research.
- Review papers summarize previously published scientific, research and/or expertise articles on a new scientific level and can contain other cited sources which are not mainly the result of the author(s).
- Preliminary notes represent preliminary research findings, which should be published rapidly (up to 7 pages).
- Professional papers are the result of technological research achievements, application research results and information on achievements in practice and industry.
- Publication notes contain the author's opinion on newly published books, monographs, textbooks, etc. (up to 2 pages). A figure of the cover page is expected, as well as a short citation of basic data.
- In memoriam (up to 2 pages), a photo is expected.
- Discussion of papers (Comments) where only professional disagreements of the articles published in previous issues of RMZ – M&G can be discussed. Normally the source author(s) reply to the remarks in the same issue.
- Event notes in which descriptions of a scientific or a professional event are given (up to 2 pages).

Review Process

All manuscripts will be supervised shall undergo a review process. The reviewers evaluate the manuscripts and can ask the authors to change particular segments, and propose to the Editor-in-Chief the acceptability of the submitted articles. Authors are requested to identify three reviewers and may also exclude specific individuals from reviewing their manuscript. The Editor-in-Chief has the right to choose other reviewers. The name of the reviewer remains anonymous. The technical corrections will also be done and the authors can be asked to correct the missing items. The final decision on the publication of the manuscript is made by the Editor-in-Chief.

Form of the Manuscript

All papers must be submitted via the online system.
The original file of the Template is available on RMZ – Materials and Geoenvironment Home page address: **www.rmz-mg.com**.

The contribution should be submitted in Microsoft Word. Manuscript should be written in Arial font and 12 pt font with 1.5 line spacing and should contain all figures, tables and formulas. Headings should be written in Arial bold font and shuold not be numbered. Subheadings should be written in Arial italic font. The electronic version should be simple, without complex formatting, hyphenation, and underlining. For highlighting, only bold and italic types should be used.

Annexes

Annexes are images, spreadsheets, tables, and mathematical and chemical formulas. Math formulas should be included in article as editable text and not as images.
Annexes should be included in the text at the appropriate place, and they should also be submitted as a separate document, i.e. separated from the text in the article.
Annexes should be originals, made in an electronic form (Microsoft Excel, Adobe Illustrator, Inkscape, AutoCad, etc.) and in .eps, .tif or .jpg format with a resolution of at least 300 dpi.
The width of the annex should be at least 152 mm. They should be named the same as in the article (Figure 1, Table 1). The text in the annexes should be written in typeface Arial Regular (6 pt).
The title of the image (also schemes, charts and graphs) should be indicated in the description of the image.
When formatting spreadsheets and tables in text editors, tabs, and not spaces, should be used to separate columns.
Each formula should have its number written in round brackets on its right side.
References of the annexes in the text should be as follows: “Figure 1…” and not “as shown below:”. This is due to the fact that for technical reasons the annex cannot always be placed at the exact specific place in the article.

Composition of the Manuscript

Title
The title of the article should be precise, informative and not longer that 100 characters. The author should also indicate the short version of the title. The title should be written in English as well as in Slovene..

Information on the Authors
Information on the authors should include the first and last name of the authors, the address of the institution and the e-mail address of the corresponding author.

Abstract
The abstract presenting the purpose of the article and the main results and conclusions should contain no more than 180 words. It should be written in Slovene and English.

Key words
A list of up to 5 key words (3 to 5) that will be useful for indexing or searching. They should be written in Slovene and English.

Introduction

Materials and methods

Results and discussion

Conclusions

Acknowledgements

References

The references should be cited in the same order as they appear in the article. **Where possible the DOI for the reference should be included at the end of the reference.** They should be numbered in square brackets. References should be cited according SIST ISO 690:1996 standards.

Book:
[1] Reynolds, J.M. (2011). *An introduction to Applied and Environmental Geophysics*. New York: Wiley, 710 p.

Unpublished Master thesis or PhD dissertation:
[2] Trček, B. (2001): *Solute transport monitoring in the unsaturated zone of the karst aquifer by natural tracers*. Ph. D. Thesis. Ljubljana: University of Ljubljana 2001; 125 p.

Chapter in an edited book:
[3] Blindow, N., Eisenburger, D., Illich, B., Petzold, H., Richer, T. (2007): *Ground Penetrating Radar*. In: Environmental Geology: Handbook of Field Methods and Case Studies, Knödel, K., Lange, G., Voigt, H.J. (eds.). Springer: Berlin; pp. 283–335.

Journal article : Journal title should be complete and not abbreviated.
[4] Higashitani, K., Iseri, H., Okuhara, K., Hatade, S. (1995): Magnetic Effects on Zeta Potential and Diffusivity of Nonmagnetic Particles. *Journal of Colloid and Interface Science*, 172, pp. 383–388.
[5] Mcmechan, G.A, Loucks, R.G, Mescher, P.A, Xiaoxian, Z. (2002): Characterization of a coalesced, collapsed paleocave reservoir analog using GPR and well-core data. *Geophysics*, 67, pp. 1148–1158. doi: 10.1190/1.1500376

Proceedings Paper:
[6] Benac, Č., Gržančić, Ž., Šišić, S., Ružić, I. (2008): Submerged Karst Phenomena in the Kvarner Area. In: Proceedings of the 5th International ProGEO Symposium on Conservation of the Geological Heritage, Rab, Croatia, Marjanac, T (ed.). Pro GEO Croatia: Zagreb; pp. 12–13.

Electronic source:
[7] CASREACT – Chemical reactions database [online]. Chemical Abstracts Service, 2000, renewed 2/15/2000 [cited 2/25/2000]. Available on: <http://www.cas.org/casreact.html>.

Scientific articles, review papers, preliminary notes and professional papers are published in English. Only professional papers will exceptionally be published in Slovene.

Units

SI System should be used for units. Physical quantities should be written in Italics (e.g. m, l, v, T). Symbols for units should be in plain text with spaces (e.g. 10 m, 5.2 kg/s, 2 s-1, 50 kPa). All abreviations should be spelt out in full on first appearance.

Manuscript Submission

Please submit your article via RMZ-M&G Editorial Manager System. You can find it on the address:
http://edmgr.editool.com/rmzmag/default.htm

Log in as an author and submit your article.
You can follow the status of your submission in the system manager and your e-mail.

Information on RMZ – M&G

— Assistant editor
  Jože Žarn
  E-mail address: joze.zarn@ntf.uni-lj.si

— Secretary
  Vukič Nivesč
  Telephone: +386 01 47 04 610
  E-mail address: nives.vukic@ntf.uni-lj.si

These instructions are valid from April 2017.

ISSN 1408-7073